NASA MEMO 4-15-59L

NASA

MEMORANDUM

CHARTS OF THE INDUCED VELOCITIES NEAR A LIFTING ROTOR

By Joseph W. Jewel, Jr., and Harry H. Heyson

Langley Research Center
Langley Field, Va.

NATIONAL AERONAUTICS AND SPACE ADMINISTRATION
WASHINGTON
May 1959

NATIONAL AERONAUTICS AND SPACE ADMINISTRATION

MEMORANDUM 4-15-59L

CHARTS OF THE INDUCED VELOCITIES NEAR A LIFTING ROTOR

By Joseph W. Jewel, Jr., and Harry H. Heyson

SUMMARY

A compilation of charts of the induced velocities near a lifting rotor is presented. The charts cover uniform as well as various non-uniform distributions of disk loading and should be applicable to many aerodynamic interference problems involving rotors.

INTRODUCTION

Many problems of helicopters and convertiplanes originate in the action of the rotor flow field on different portions of the machine. A few of these problems (see refs. 1 and 2) are the mutual interference between the rotors of multirotor helicopters, the interference between the wing and the rotor of a convertiplane, and the effect on stability of the rotor downwash acting on the tail.

In order that the designer may cope with these problems, a knowledge of the induced velocities in the vicinity of the rotor is necessary. Several theoretical investigations have dealt with this subject. The results of the most basic studies are given in references 3 and 4. These papers are, however, of limited usefulness to the designer because of the restricted locations for which the induced velocities were calculated. References 5 and 6 use methods of numerical integration to obtain induced velocities throughout the longitudinal and lateral planes of a uniformly loaded rotor. The results of these investigations are presented in simple, easy-to-use, chart form. This work has recently been extended (ref. 7) by means of an electromagnetic analog to obtain induced velocities throughout almost the entire field of the rotor for one case representing a high-speed flight condition.

Experimental results from a comprehensive rotor-downwash investigation are presented in references 8 and 9. A preliminary analysis of these results (ref. 8) indicated that the average of the induced velocities across the span of a rotor is approximated rather well by the calculated induced velocities in the longitudinal plane of a uniformly loaded rotor (ref. 5). However, more complete analysis (ref. 9) indicated that the actual local velocities differ greatly from the average across

the span. Thus, there is a distinct possibility that large errors may result from the use of the uniformly loaded rotor calculations to obtain the interference velocities for surfaces of short span such as the usual helicopter horizontal tail.

The actual local induced velocities are largely a function of the distribution of load upon the rotor disk. Reference 9 gives a numerical method for converting the uniformly loaded rotor flow to correspond to that for a rotor with an arbitrary, nonuniform, axisymmetric, disk-load distribution. In addition, reference 9 gives charts of induced velocity for two different reasonable distributions of disk load for the longitudinal plane of symmetry of the rotor. These charts were limited to this one plane because only reference 5 was available at that time.

The more recent appearance of references 6 and 7 has made it possible to extend these calculations to many additional areas near the rotor. The actual numerical work required to obtain the induced velocities for nonuniformly loaded rotors is quite tedious. It is, therefore, desirable for design purposes to have these velocities available in a simple chart form.

The purpose of this paper is to provide induced-velocity charts for several appropriate nonuniform disk loadings and for a number of wake skew angles. In order to increase the utility of the calculated results, induced-velocity charts previously published in references 5, 6, 7, and 9 are also included in this report to provide, under one cover, a compilation of almost all available rotor-induced-velocity calculations. Details of the method of calculations and of the extent of the correlation with experiment are not presented herein inasmuch as the present work is intended to supplement rather than to supplant the more basic references.

SYMBOLS

All symbols are defined with respect to the control axis.

a_1 longitudinal first-harmonic blade flapping angle, deg

C_T rotor thrust coefficient, $\frac{T}{\rho\pi R^2(\Omega R)^2}$

R rotor radius, ft

r radial distance from Z-axis, ft

T thrust, lb

V forward velocity of rotor, ft/sec

v local induced velocity, ft/sec

v_o momentum-theory value of rotor induced velocity, $\frac{C_T \Omega R}{2\sqrt{\mu^2 + \lambda^2}}$, ft/sec

X,Y,Z Cartesian coordinates centered in rotor plane (see fig. 1), ft

α rotor control-axis angle of attack, deg

λ rotor inflow ratio, $\frac{V \sin \alpha - v_o}{\Omega R}$

μ rotor tip-speed ratio, $\frac{V \cos \alpha}{\Omega R}$

ρ mass density of air, slugs/cu ft

χ wake skew angle, angle between Z-axis and axis of wake (see fig. 1), $\tan^{-1}\left(-\frac{\mu}{\lambda}\right) + a_1$, deg

ψ rotor azimuth angle, measured from X-axis in direction of rotation, deg

Ω rotor rotational speed, radians/sec

RESULTS

General Considerations

A uniformly loaded rotor has the simplest possible loading. The circulation along the blade is constant, and vortices are shed only at the tip; thus the wake may be considered as a single vortex cylinder. Numerical methods for calculating the induced velocities directly from this comparatively simple vortex system are given in references 5 and 6.

If, however, the loading is nonuniform, the circulation will vary along the length of the blade, and vortices must be shed all along the blade instead of only at the tip. Thus, the wake may be considered as a series of concentric vortex cylinders. To calculate the induced velocities directly from this vortex wake would be a particularly arduous

task. The direct calculation may be avoided, however, since the field of each of the vortex cylinders is, except for dimensions, the same as that of the uniformly loaded rotor of references 5 to 7. Thus, superposition may be used to develop the field of a nonuniformly loaded rotor from that of the uniformly loaded rotor. The entire process is exactly analogous to the use of the horseshoe vortex in developing the field of a nonuniformly loaded wing. Details of the treatment for a rotor are given in reference 9 and the results are presented rather compactly in chart form. In the present paper, all the charts are presented with reference to the axis system shown in figure 1.

Loadings Considered

The disk-load distributions considered in the present paper are shown in figure 2. Note that the disk loading varies as $1/r$ times the blade loading (ref. 9). The calculated-flow charts are presented in figures 3 to 20. Table I has been prepared to facilitate reference to these charts. A few remarks appropriate to the choice of each loading are presented in the following sections.

Uniform loading.- As pointed out previously, the induced-flow field of the uniformly loaded rotor is calculated directly from the wake-vortex system. No new uniformly loaded rotor calculations have been made for this paper, the charts having been collected from references 5 to 7. They are included in the present report since they are fundamental in the calculation of the fields of nonuniformly loaded rotors.

Triangular loading.- The triangular loading was chosen because it is the simplest possible loading which is representative of an actual helicopter rotor in all flight conditions. This loading is zero at the rotor center representing the presence of a nonlifting hub. The load increases linearly toward the rotor tips; thus the elementary considerations of increasing blade-section velocity along the blade are satisfied.

Typical loading.- The typical load distribution is similar to the average radial load distribution measured during wind-tunnel tests of a rotor having untapered, untwisted blades. These blades were equipped with instrumentation for measuring the actual pressure distribution. (See ref. 10.) The loading used herein represents a typical cruising condition for a lightly loaded rotor.

Uniform loading with cutout.- Helicopter rotor blades are often tapered and twisted in order to approximate the optimum condition of uniform loading in hovering. This condition is, of course, not realizable in the region of the hub; thus the actual loading will be similar to that called "uniform with cutout" in this paper. The charts for this

loading are limited to two skew angles of $\tan^{-1} 0$ and $\tan^{-1} \frac{1}{4}$ since, in practice, this loading can be achieved only at very low speeds. Several charts for this type of loading have also been prepared for the plane of the rotor at one high skew angle ($\chi = \tan^{-1} 10$). These charts are not intended to represent any practical case but are presented only to illustrate the magnitude of the effect of a cutout on the induced-velocity distribution.

DISCUSSION

The discussion of the calculated results will be very brief in this paper since many of the charts show the same characteristics that have been discussed in reference 9. The reader's attention is directed to that paper for a more complete discussion of the results and to references 1, 8, and 9 for a discussion of the extent to which the calculated induced velocities correlate with measurements.

Longitudinal Plane

A comparison of the charts for the various loadings in the longitudinal (XZ) plane indicates that the near field of the uniformly loaded rotor is considerably different from that of the nonuniformly loaded rotors. This difference is particularly noticeable near the center of the rotor, where the induced-velocity ratio is 1.0 for uniform loading but zero for the nonuniform loadings. In general, the triangular and typical loadings result in very similar fields in this plane. At least for the low skew angles considered, however, the uniform loading with cutout results in a flow field which, except near the center of the wake, is very nearly like the flow field for a completely uniform loading. At greater distances from the wake and rotor, only very small differences in the flow are observed for widely different loadings.

Lateral Plane

The flow field in the lateral (YZ) plane is very sensitive to the details of the actual loading. A comparison between the charts corresponding to the various disk-load distributions reveals significant differences in each case. The calculated flow is symmetrical with respect to the longitudinal center plane as a result of the assumption in the analysis that the loading and the corresponding wake vorticity are symmetrical. In practice, however, as the tip-speed ratio μ is increased the loading becomes more unsymmetrical because of the different velocities on the opposite sides of the rotor. No complete theoretical

treatment of this effect is available as yet, but estimates of the dissymmetry can be made from the experimental results of reference 9.

A point worthy of notice is the small lateral extent of the upwash region below the center of the rotor. This trend should also be evident farther rearward. (See, for example, the flow-survey data of ref. 9.) The practical aspect of this type of flow distribution is that the charts for the longitudinal plane are strictly applicable only to tail surfaces of zero span. There may be a large gradient of induced velocity across a tail of large span, and the average induced velocity across the tail will be correspondingly different. (See refs. 1 and 8.)

Plane of Rotor

The usefulness of the charts for the plane of the rotor is somewhat restricted since reference 1 has already shown that these charts represent only the time-averaged induced velocities which are useful for calculating interference effects. Thus, these are not the effective or instantaneous induced velocities which are actually sensed by the blades and which are required for vibration studies. Several qualitative trends are, however, emphasized by a brief examination of the calculated flow in the plane of the rotor. Figures 18(a), 18(b), and 18(c), indicate that the loading gradient in the outer portion of the blades has no large effect on the induced-velocity distribution over the front half of the rotor. This is shown in particular by the similarity of the induced velocities within the three-quarter-radius point in figures 18(b) and 18(c). Notice also the corresponding similarity in the disk loadings shown in figure 2.

The predominant feature of the flow in the rear half of the plane of the rotor is the presence of a region of upwash (negative induced-velocity ratios) just behind the center of all the nonuniformly loaded rotors and the uniformly loaded rotors with cutout. The extent and magnitude of this upwash is primarily a function of the size of the cutout (figs. 18(d), 18(e), and 18(f)). Notice the large effect caused by even an extremely small cutout in an otherwise uniformly loaded rotor (fig. 18(d)).

As mentioned previously, although these time-averaged induced velocities are applicable to performance and stability studies they are not directly applicable to detailed blade-loading and vibration studies. There remains, however, a possibility that the time-averaged induced velocities may yield qualitative trends with regard to these problems. If such should prove to be the case, figure 18 would indicate that blade twist, which increases the loading gradient near the hub cutout, might tend to aggravate rather than to relieve rotor blade vibration.

CONCLUDING REMARKS

This report presents an extensive compilation of charts of the induced velocities near a lifting rotor. Both uniform and nonuniform disk-load distributions are considered. These charts may be conveniently applied to calculations of the interference between the rotor and wings, tails, or other rotors in its vicinity, but they are probably not applicable to studies of blade vibrations.

Langley Research Center,
National Aeronautics and Space Administration,
Langley Field, Va., January 21, 1959.

REFERENCES

1. Heyson, Harry H.: Induced Velocity Near a Rotor and Its Application to Helicopter Problems. Proc. Fourteenth Annual National Forum, Am. Helicopter Soc., Inc., April 16-19, 1958, pp. 63-71. (Also available as: Induced Flow Near a Helicopter Rotor. Aircraft Engineering, vol. 31, no. 360, Feb. 1959, pp. 40-44.)

2. Tapscott, Robert J.: Some Static Longitudinal Stability Characteristics of an Overlapped-Type Tandem-Rotor Helicopter at Low Airspeeds. NACA TN 4393, 1958.

3. Coleman, Robert P., Feingold, Arnold M., and Stempin, Carl W.: Evaluation of the Induced-Velocity Field of an Idealized Helicopter Rotor. NACA WR L-126, 1945. (Formerly NACA ARR L5E10.)

4. Mangler, K. W., and Squire, H. B.: The Induced Velocity Field of a Rotor. R. & M. No. 2642, British A.R.C., May 1950.

5. Castles, Walter, Jr., and De Leeuw, Jacob Henri: The Normal Component of the Induced Velocity in the Vicinity of a Lifting Rotor and Some Examples of Its Application. NACA Rep. 1184, 1954. (Supersedes NACA TN 2912.)

6. Castles, Walter, Jr., and Durham, Howard L.: Distribution of Normal Component of Induced Velocity in Lateral Plane of a Lifting Rotor. NACA TN 3841, 1956.

7. Castles, Walter, Jr., Durham, Howard L., Jr., and Kevorkian, Jirair: Normal Component of Induced Velocity for Entire Field of a Uniformly Loaded Lifting Rotor With Highly Swept Wake as Determined by Electromagnetic Analog. NACA TN 4238, 1958.

8. Heyson, Harry H.: Preliminary Results From Flow-Field Measurements Around Single and Tandem Rotors in the Langley Full-Scale Tunnel. NACA TN 3242, 1954.

9. Heyson, Harry H., and Katzoff, S.: Induced Velocities Near a Lifting Rotor With Nonuniform Disk Loading. NACA Rep. 1319, 1957. (Supersedes NACA TN 3690 by Heyson and Katzoff and NACA TN 3691 by Heyson.)

10. Rabbott, John P., Jr., and Churchill, Gary B.: Experimental Investigation of the Aerodynamic Loading on a Helicopter Rotor Blade in Forward Flight. NACA RM L56I07, 1956.

TABLE I.- DIRECTORY OF INDUCED-VELOCITY CHARTS

χ	Plane of chart	Distribution of disk loading			
		Uniform	Triangular	Typical	Uniform with cutout
$\tan^{-1} 0$ (0°)	Longitudinal	3(a)	3(b)	-----	3(c) (15% R)
$\tan^{-1} \frac{1}{4}$ (14.04°)	Longitudinal	4(a)	4(b)	-----	4(c) (15% R)
$\tan^{-1} \frac{1}{2}$ (26.56°)	Longitudinal	5(a)	5(b)	-----	----------
$\tan^{-1} 1$ (45.00°)	Longitudinal Lateral	6(a) 7(a)	6(b) 7(b)	6(c) 7(c)	---------- ----------
$\tan^{-1} 2$ (63.43°)	Longitudinal Lateral	8(a) 9(a)	8(b) 9(b)	8(c) 9(c)	---------- ----------
$\tan^{-1} 4$ (75.97°)	Longitudinal Lateral	10(a) 11(a)	10(b) 11(b)	10(c) 11(c)	---------- ----------
$\tan^{-1} 10$ (84.29°)	$\psi = 0^\circ, 180^\circ$ $\psi = 30^\circ, 150^\circ, 210^\circ, 330^\circ$ $\psi = 60^\circ, 120^\circ, 240^\circ, 300^\circ$ $\psi = 90^\circ, 270^\circ$	12(a) 13(a) 14(a) 15(a)	12(b) 13(b) 14(b) 15(b)	12(c) 13(c) 14(c) 15(c)	---------- ---------- ---------- ----------
	Plane of rotor	18(a)	18(b)	18(c)	18(d) (5% R) 18(e) (15% R) 18(f) (25% R)
$\tan^{-1} \infty$ (90.00°)	Longitudinal Lateral	16(a) 17(a)	16(b) 17(b)	16(c) 17(c)	---------- ----------
$\tan^{-1} 0$ to $\tan^{-1} \infty$ (0° to 90°)	Longitudinal axis only Lateral axis only	19(a) 20(a)	19(b) 20(b)	19(c) 20(c)	---------- ----------

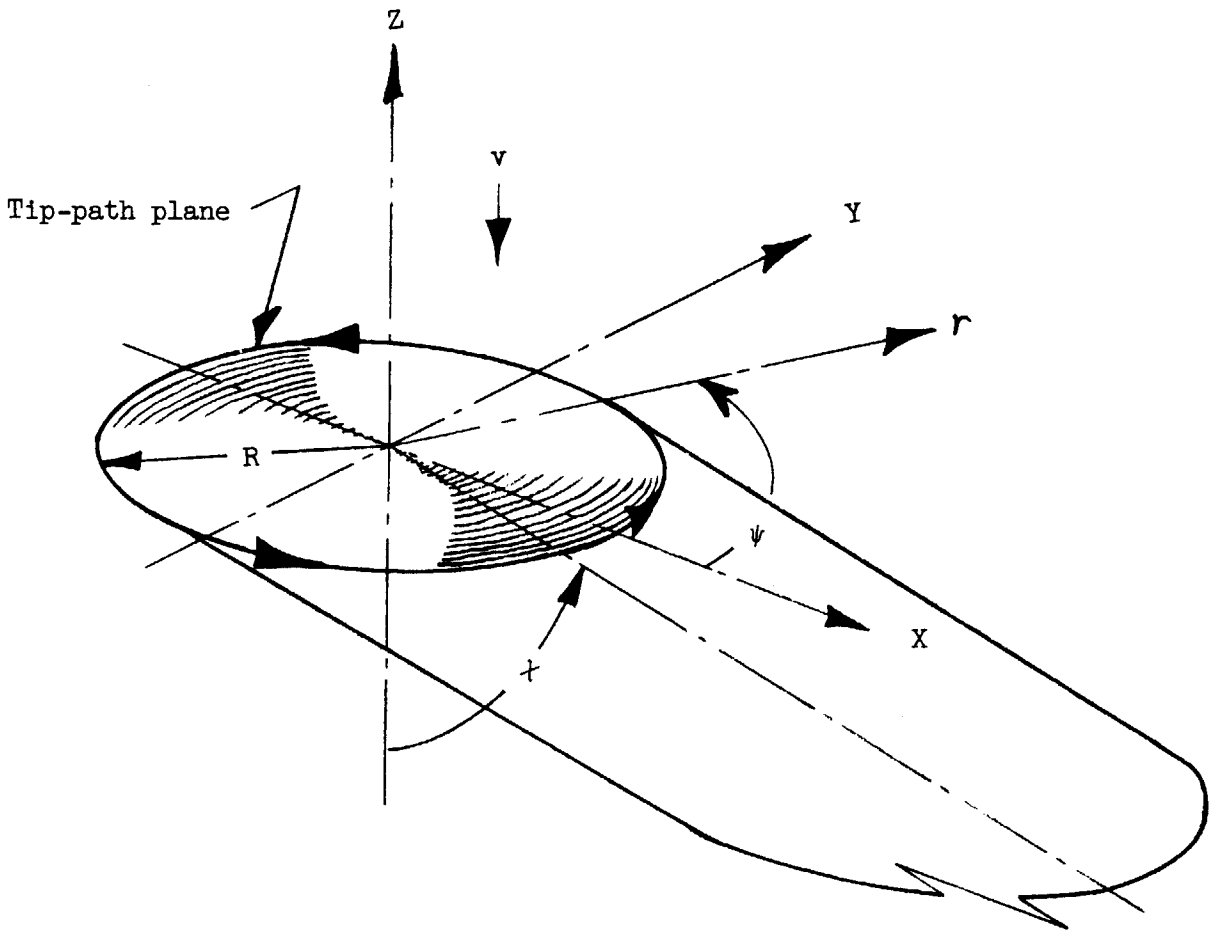

Figure 1.- Coordinate system of rotor and wake. Arrows denote positive direction.

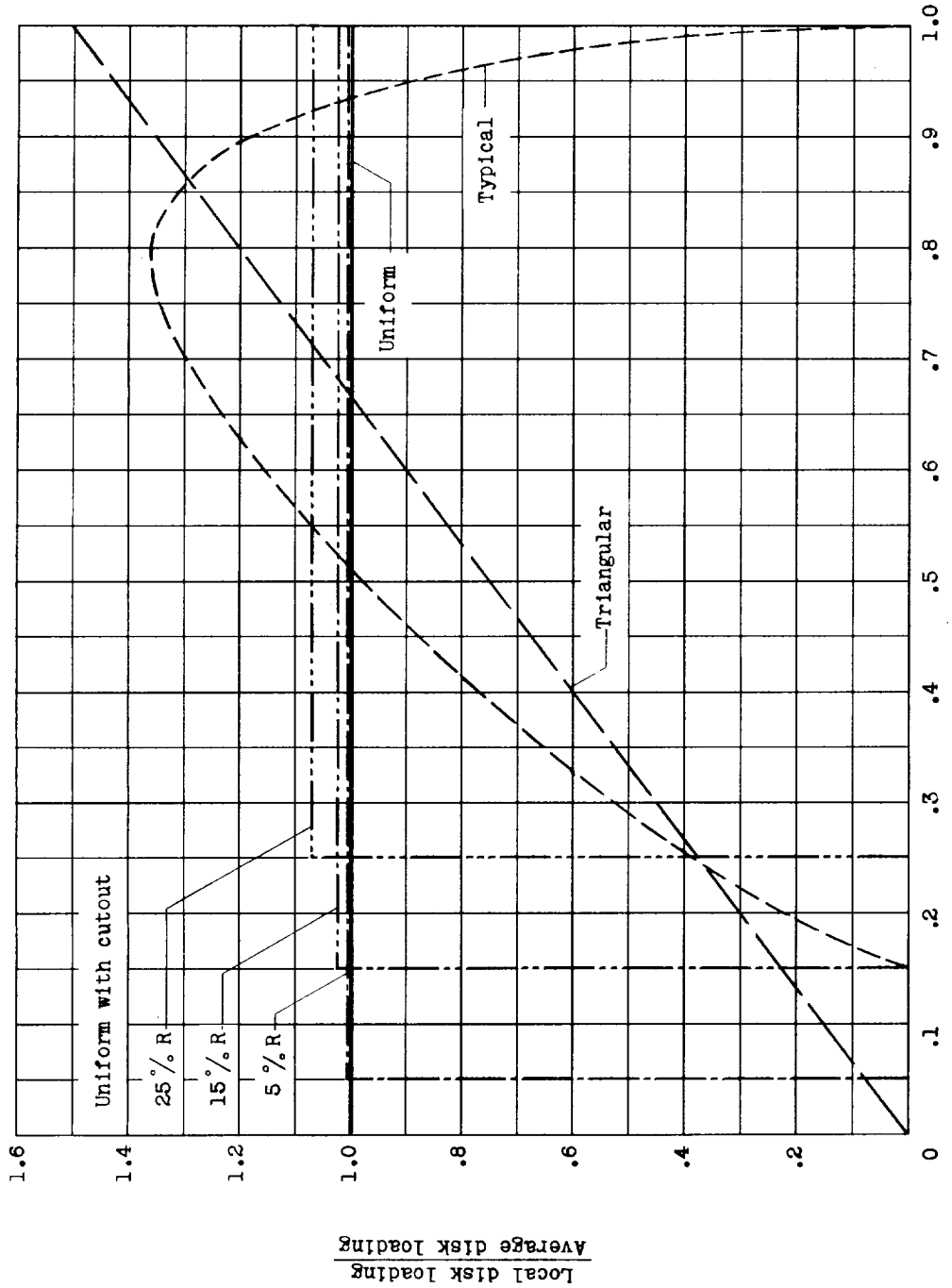

Figure 2.- Disk loadings considered in calculations.

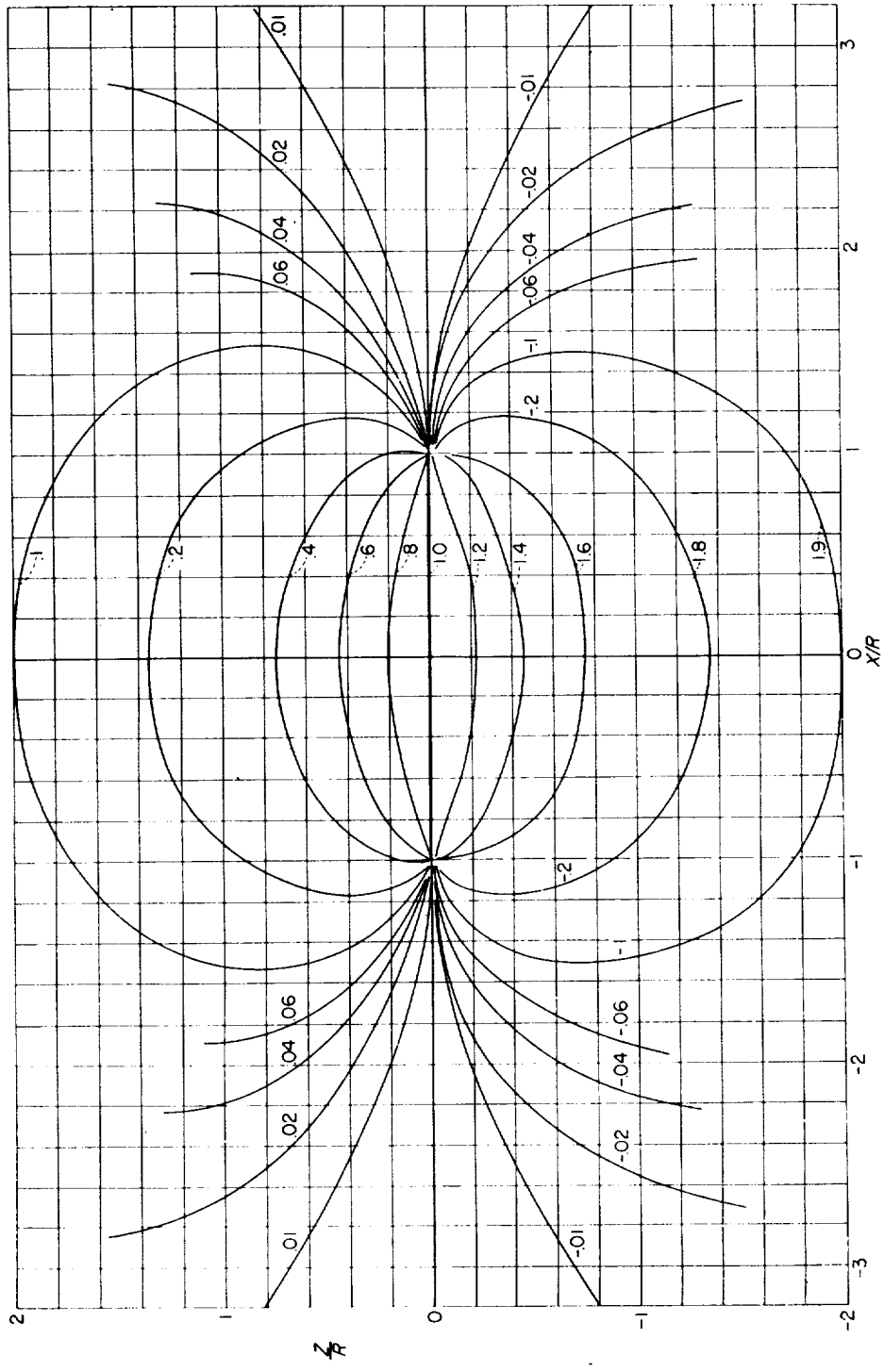

(a) Uniform disk loading (from ref. 5).

Figure 3.- Contours of induced-velocity ratio v/v_o in the longitudinal plane of the rotor for $\chi = \tan^{-1} 0 = 0^o$.

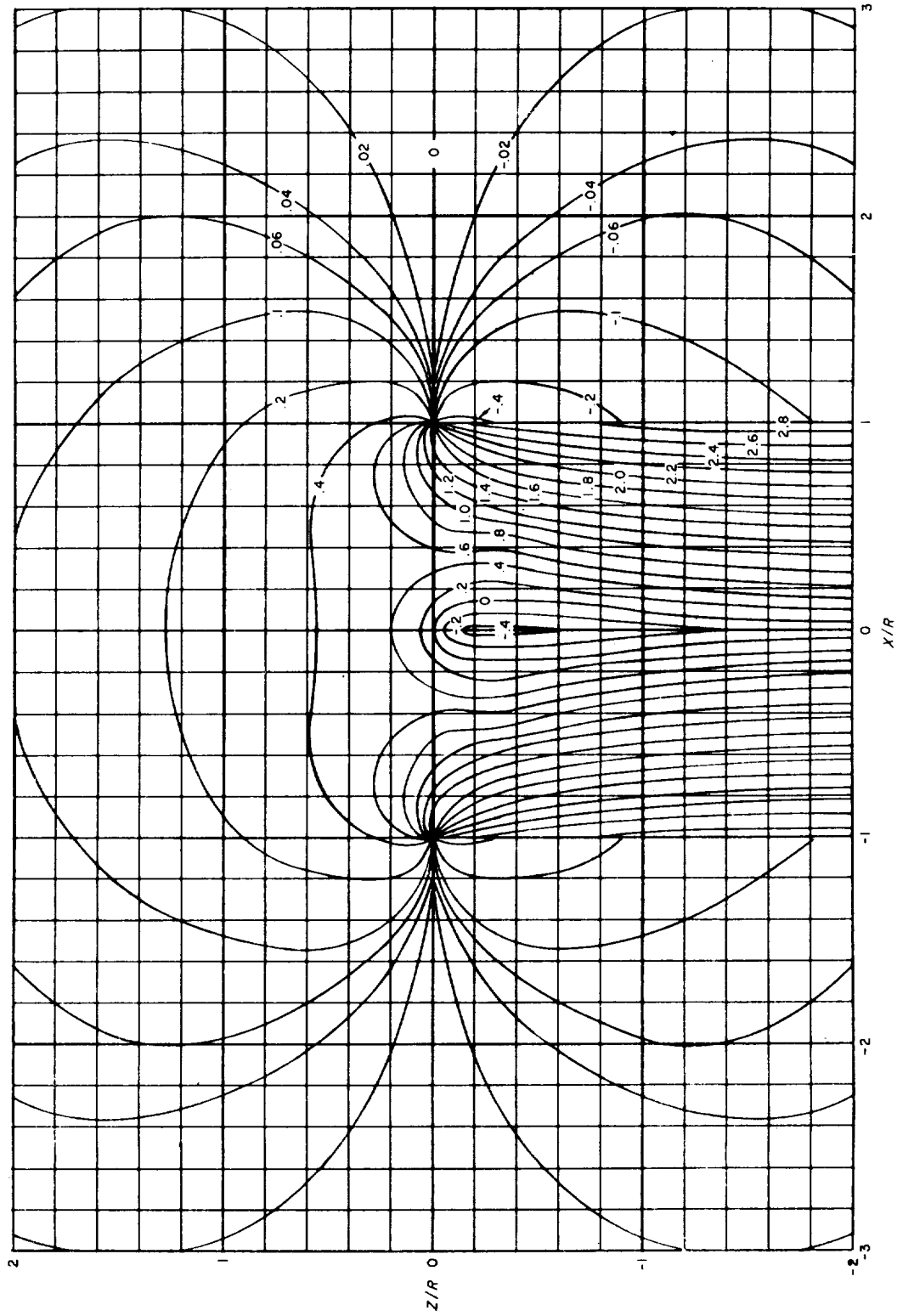

(b) Triangular disk loading (from ref. 9).

Figure 3.- Continued.

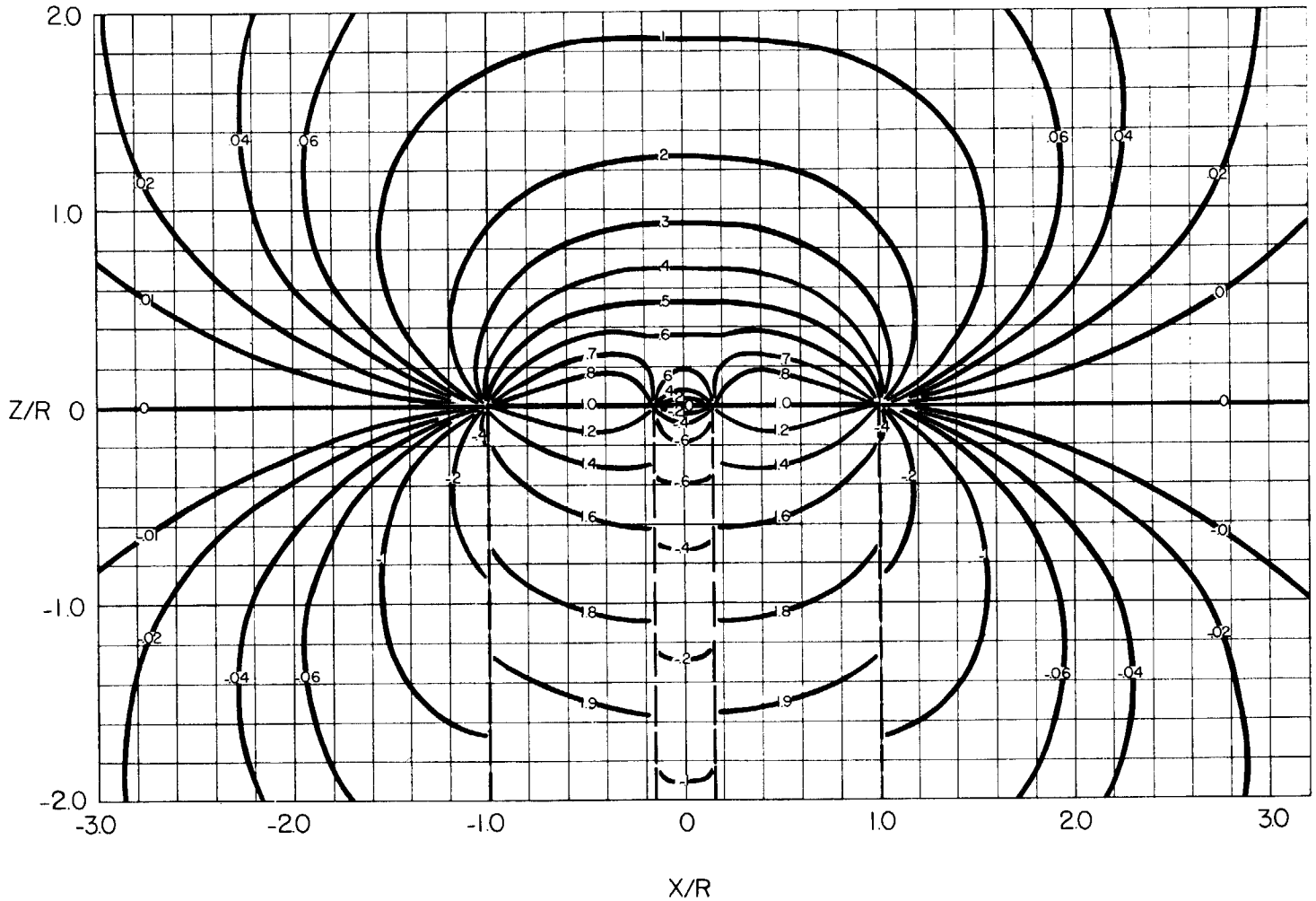

(c) Uniform disk loading with cutout of 15 percent R.

Figure 3.- Concluded.

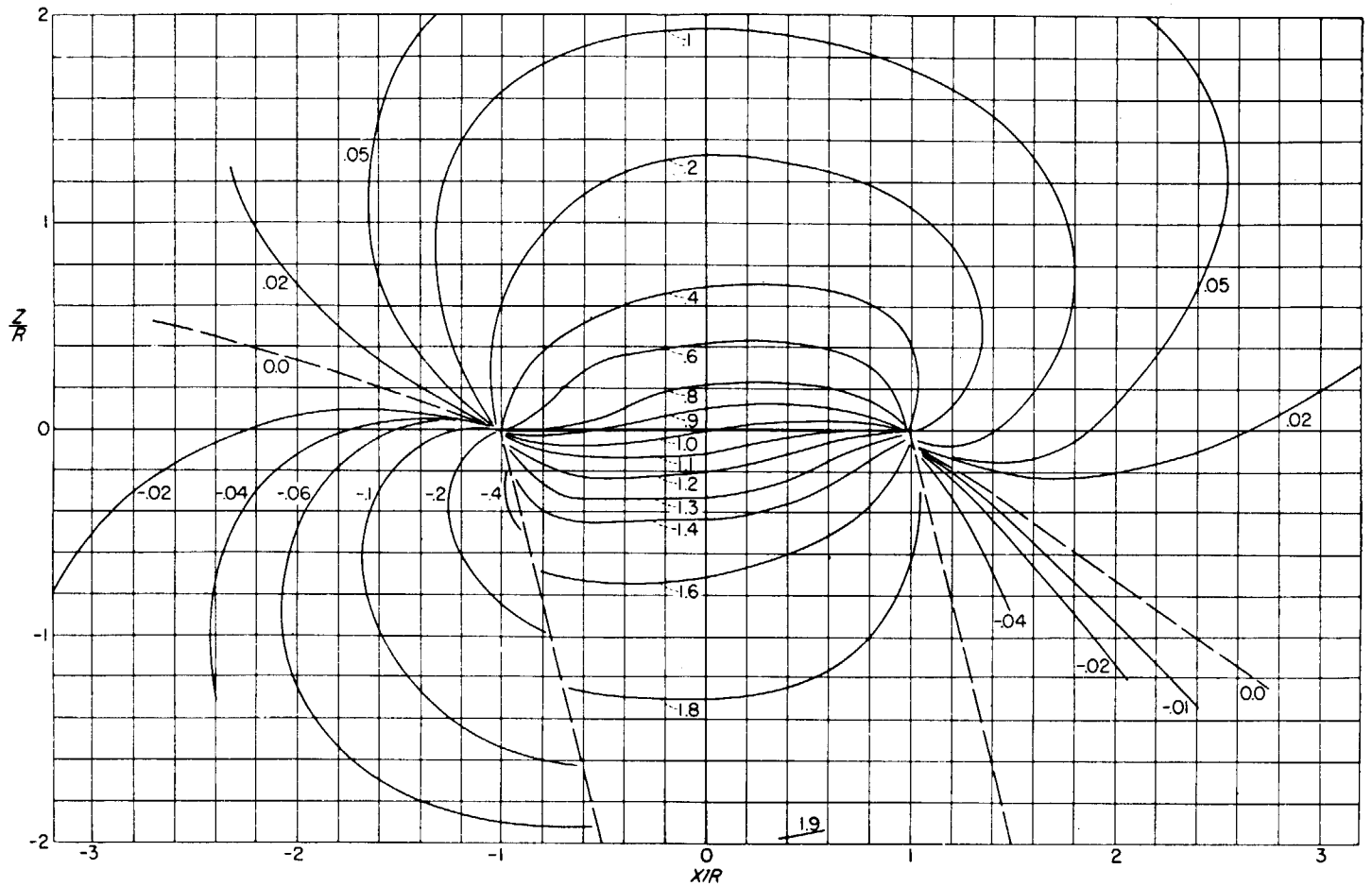

(a) Uniform disk loading (from ref. 5).

Figure 4.- Contours of induced-velocity ratio v/v_o in the longitudinal plane of the rotor for $\chi = \tan^{-1}\frac{1}{4} = 14.04^{\circ}$.

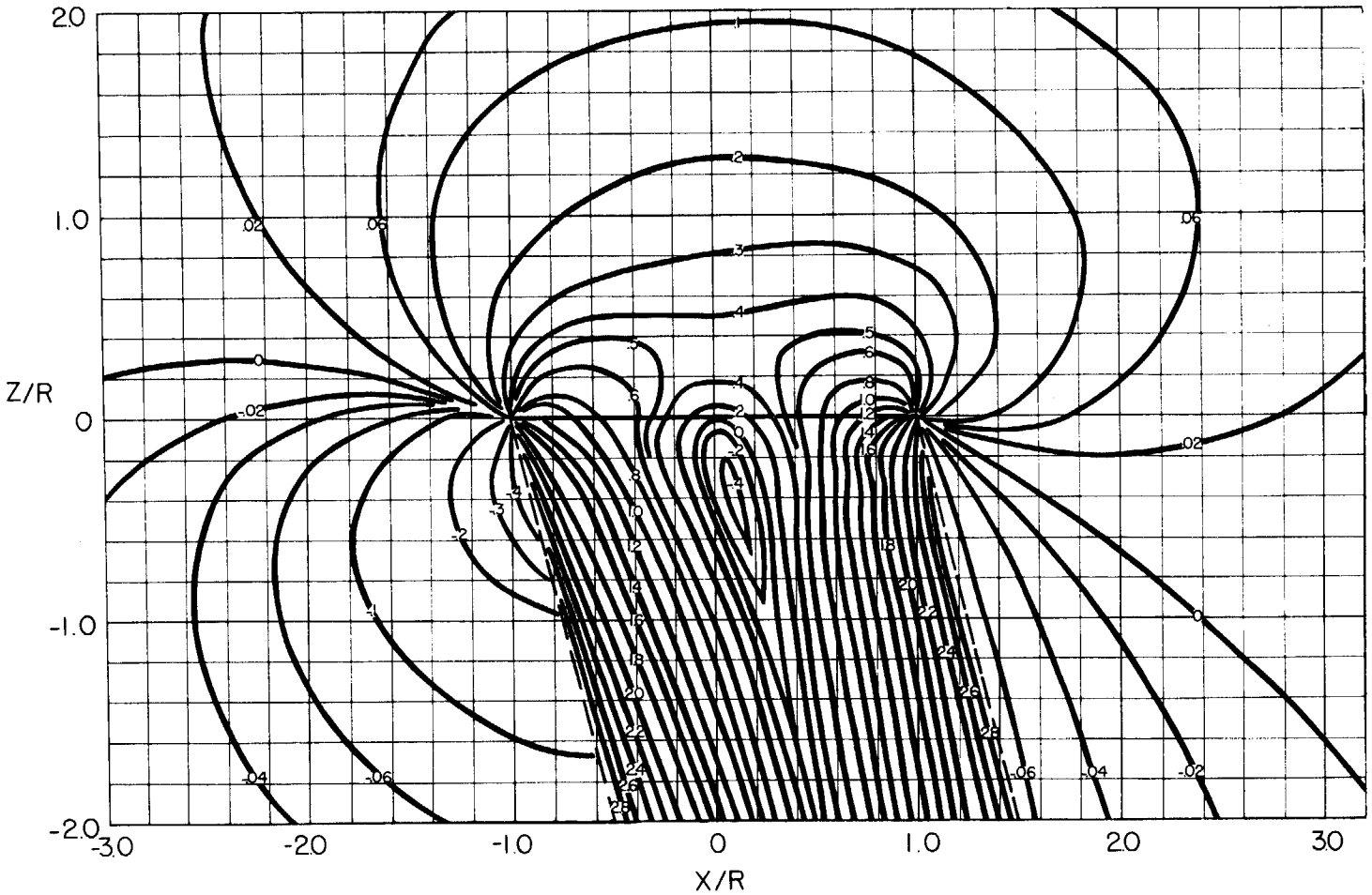

(b) Triangular disk loading.

Figure 4.- Continued.

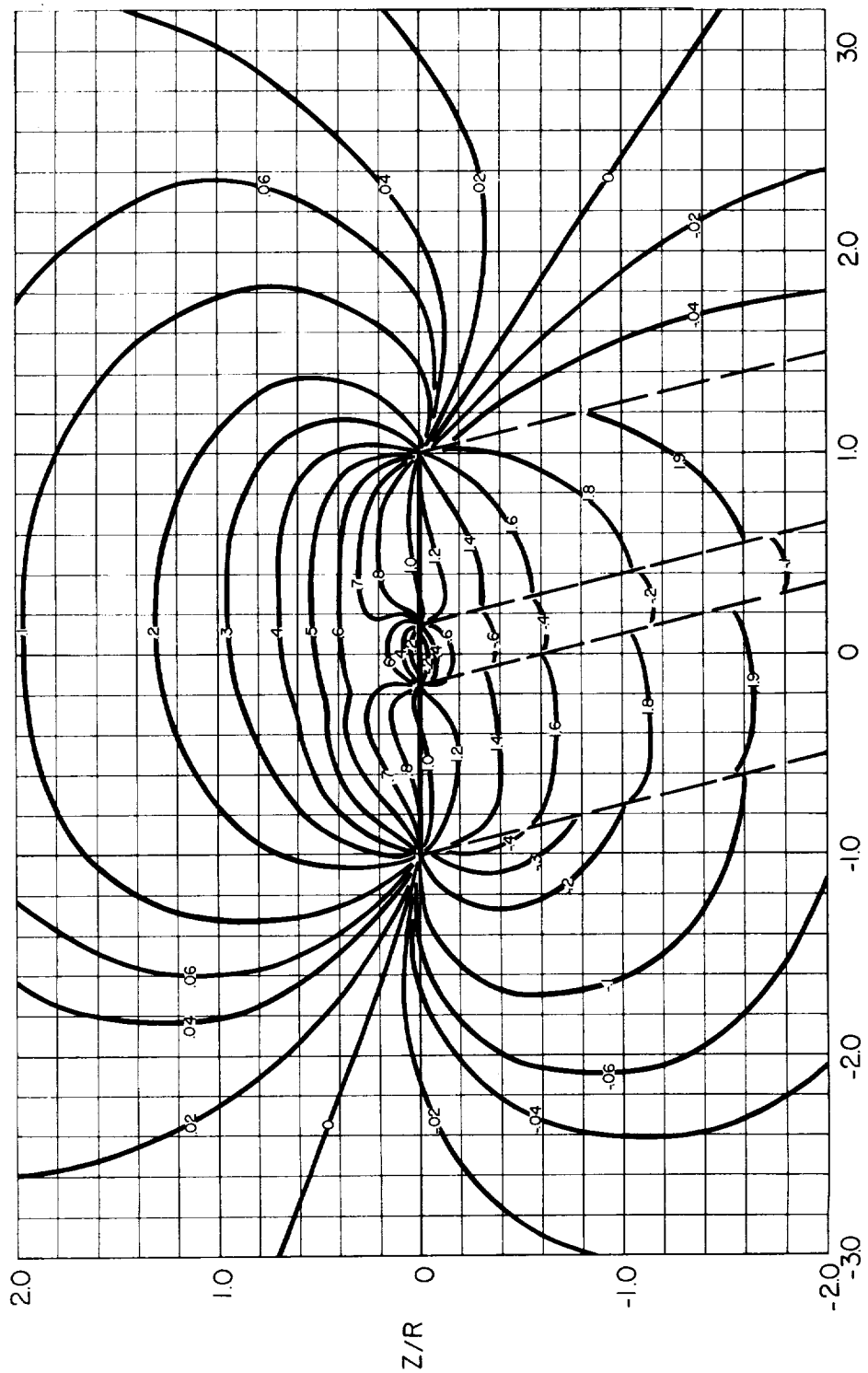

(c) Uniform disk loading with cutout of 15 percent R.

Figure 4.- Concluded.

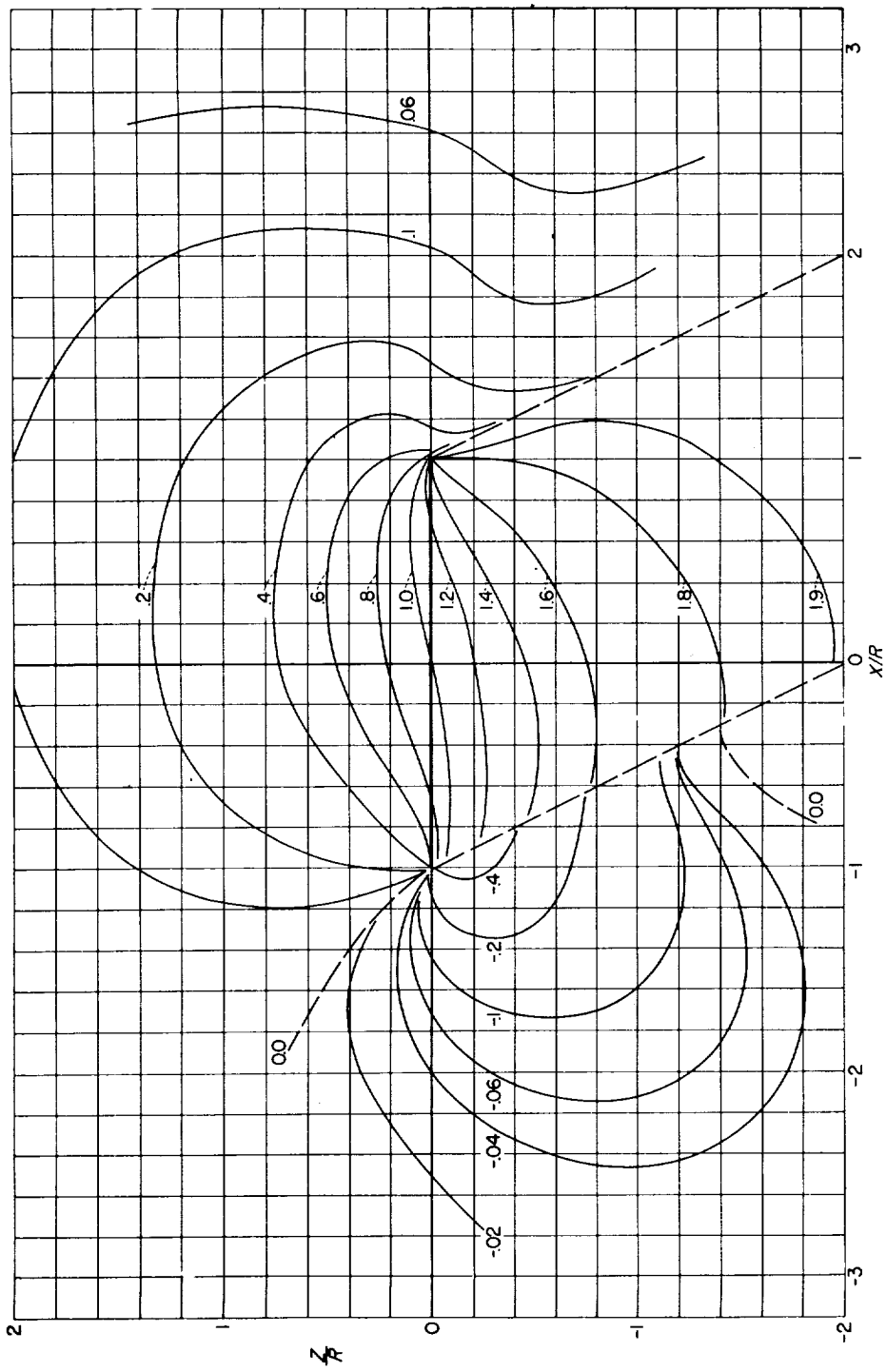

(a) Uniform disk loading (from ref. 5).

Figure 5.- Contours of induced-velocity ratio v/v_o in the longitudinal plane of the rotor for $\chi = \tan^{-1}\frac{1}{2} = 26.56^{\circ}$.

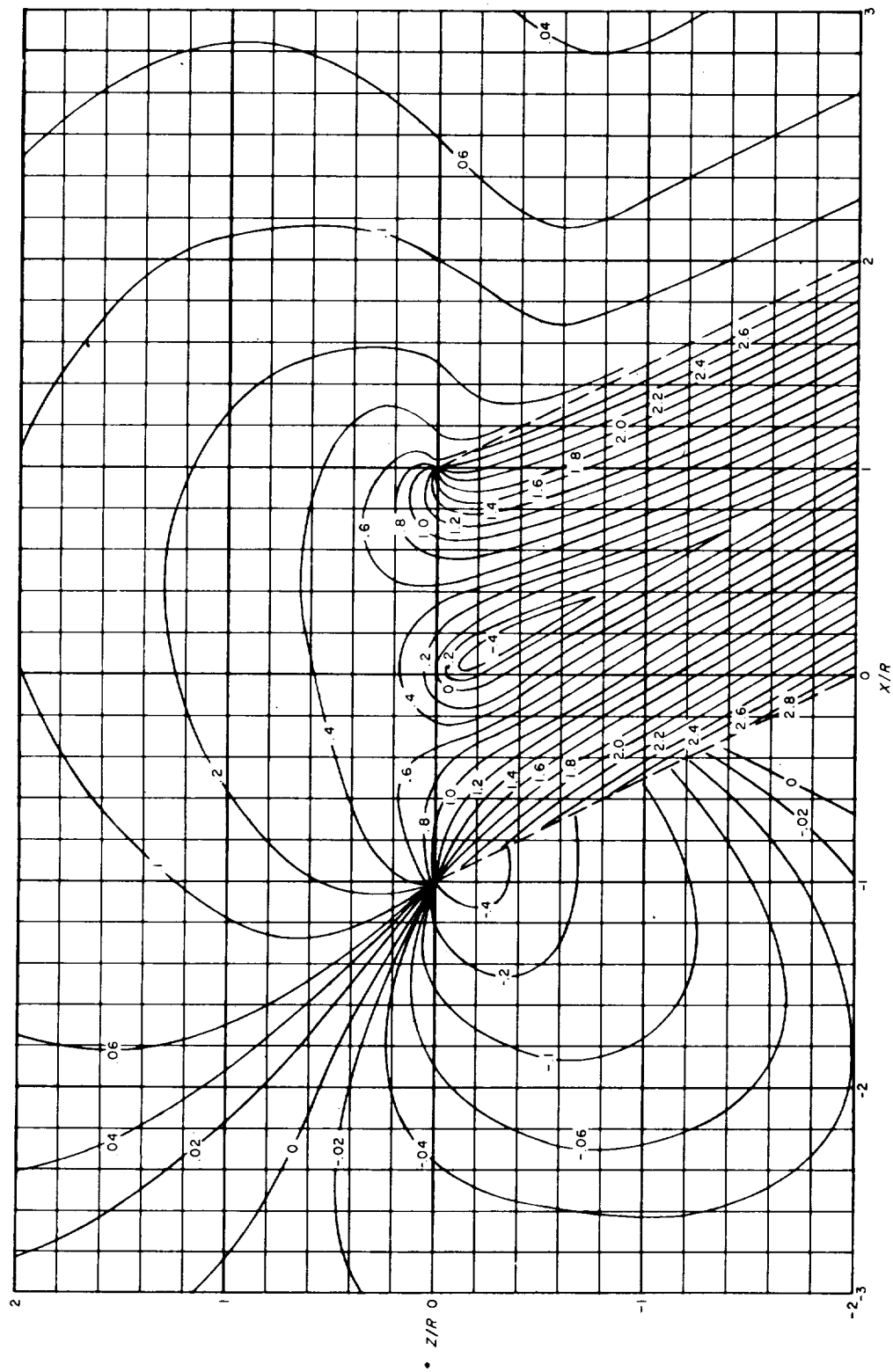

(b) Triangular disk loading (from ref. 9).

Figure 5.- Concluded.

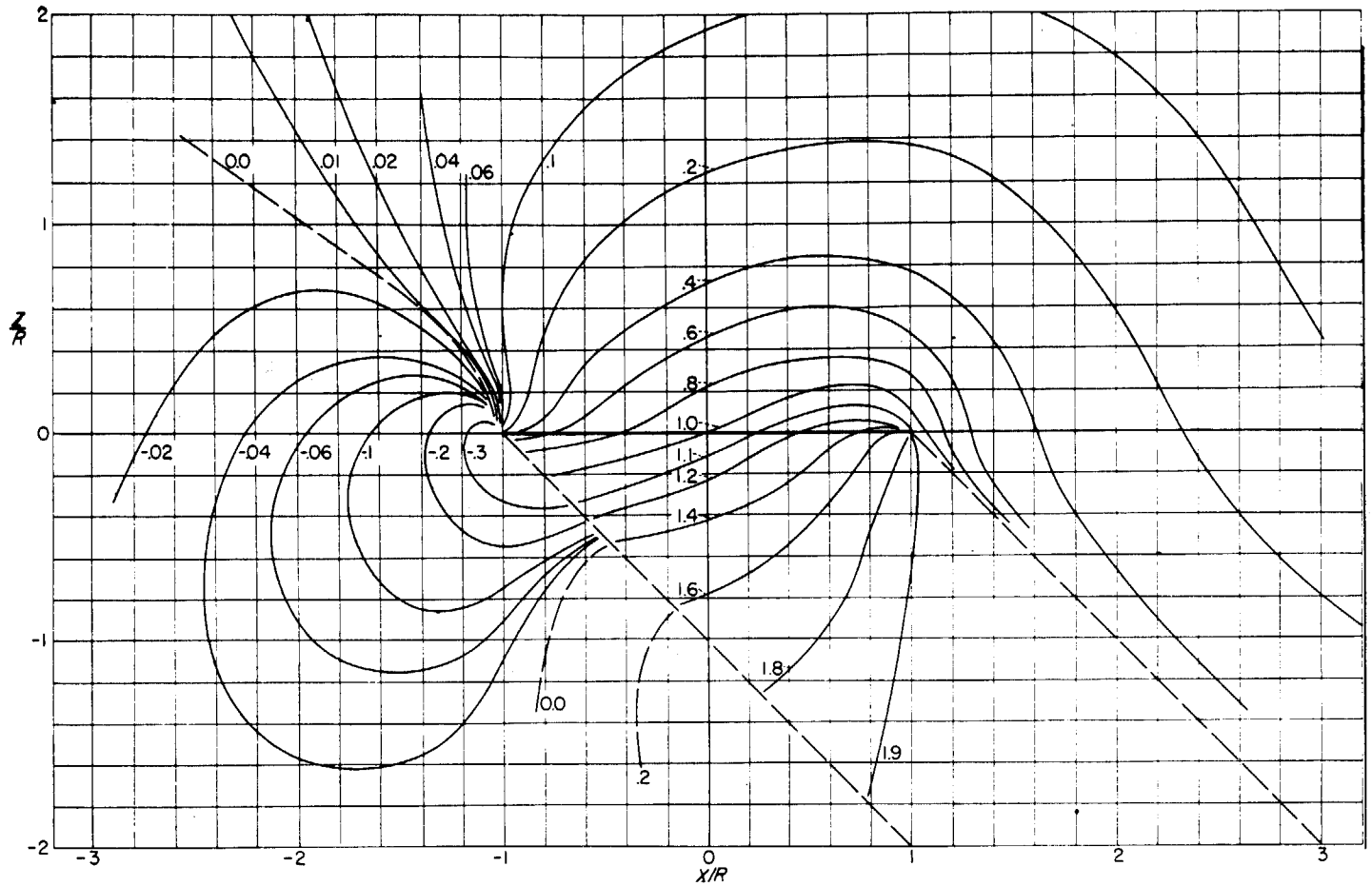

(a) Uniform disk loading (from ref. 5).

Figure 6.- Contours of induced-velocity ratio v/v_o in the longitudinal plane of the rotor for $\chi = \tan^{-1} 1 = 45.00^{\circ}$.

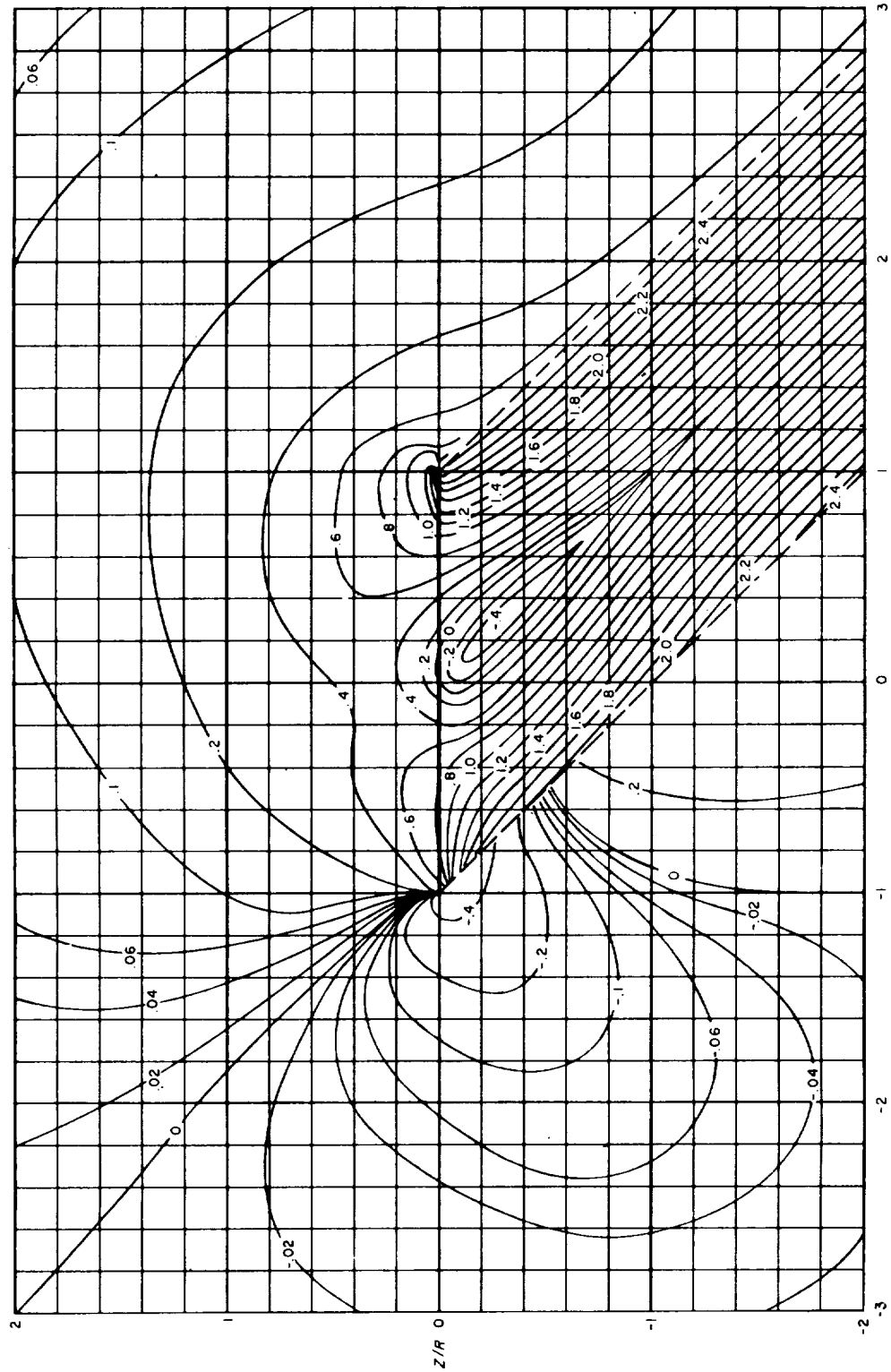

(b) Triangular disk loading (from ref. 9).

Figure 6.- Continued.

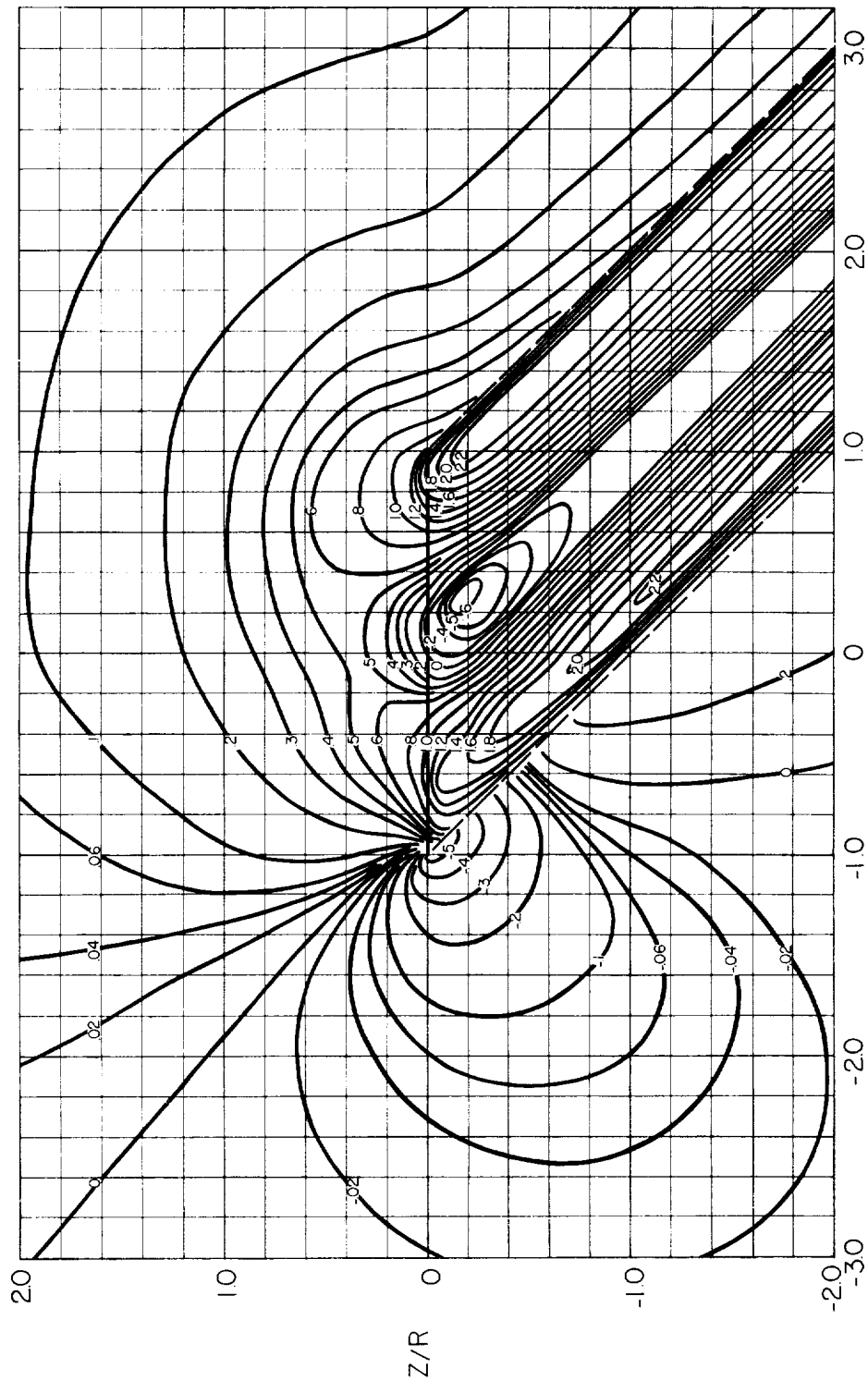

(c) Typical disk loading.

Figure 6.- Concluded.

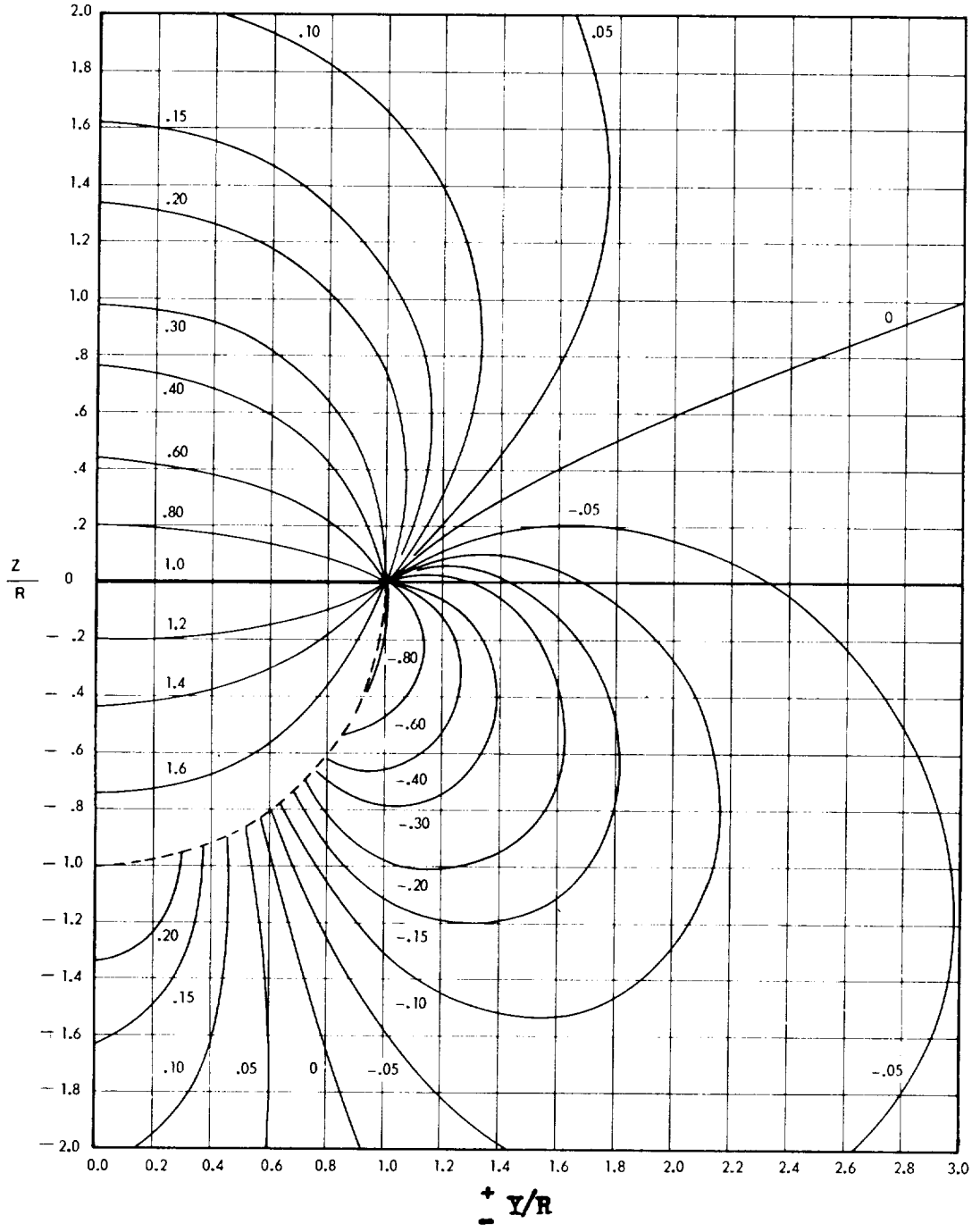

(a) Uniform disk loading (from ref. 6).

Figure 7.- Contours of induced-velocity ratio v/v_o in the lateral plane of the rotor for $\chi = \tan^{-1} l = 45.00°$.

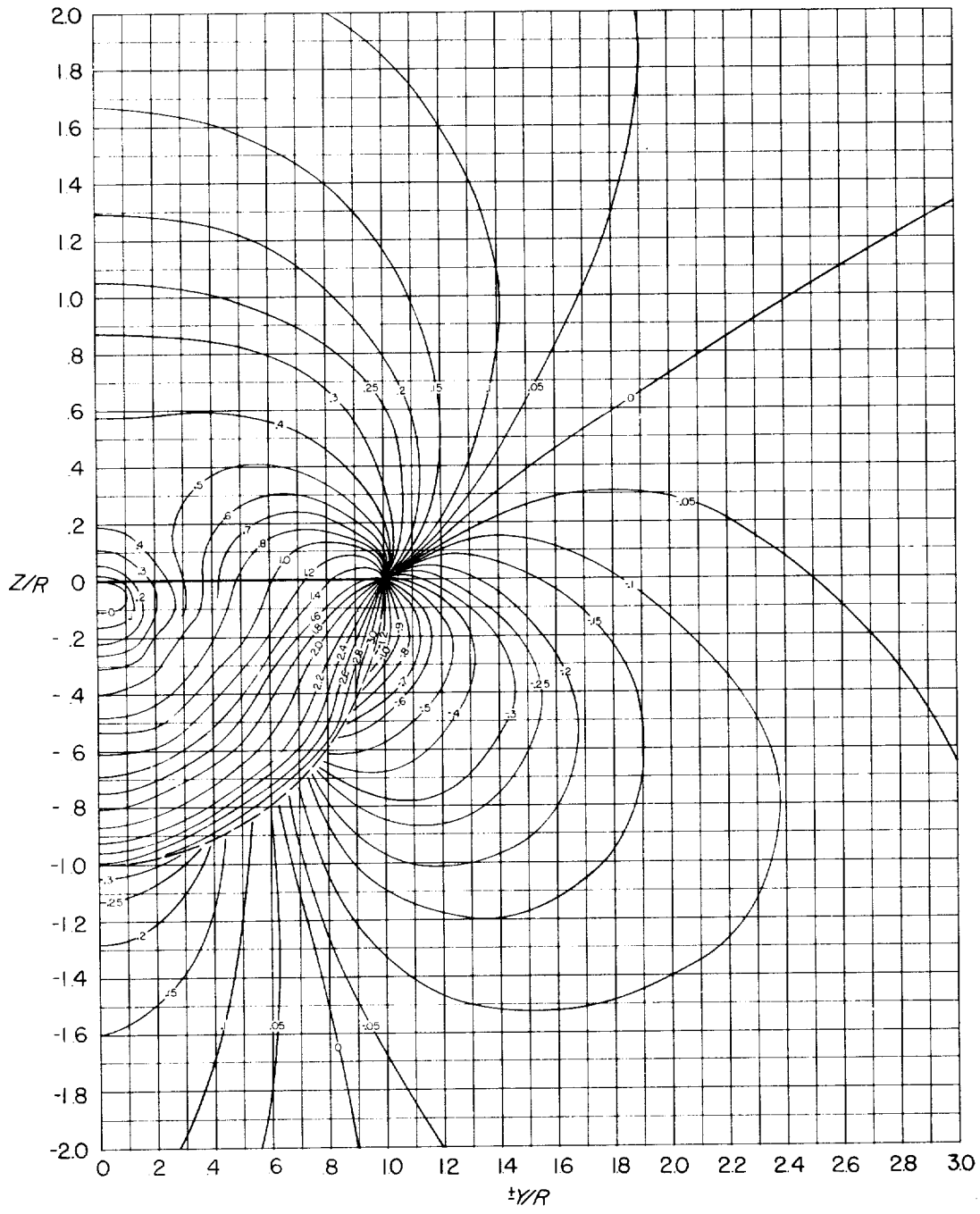

(b) Triangular disk loading.

Figure 7.- Continued.

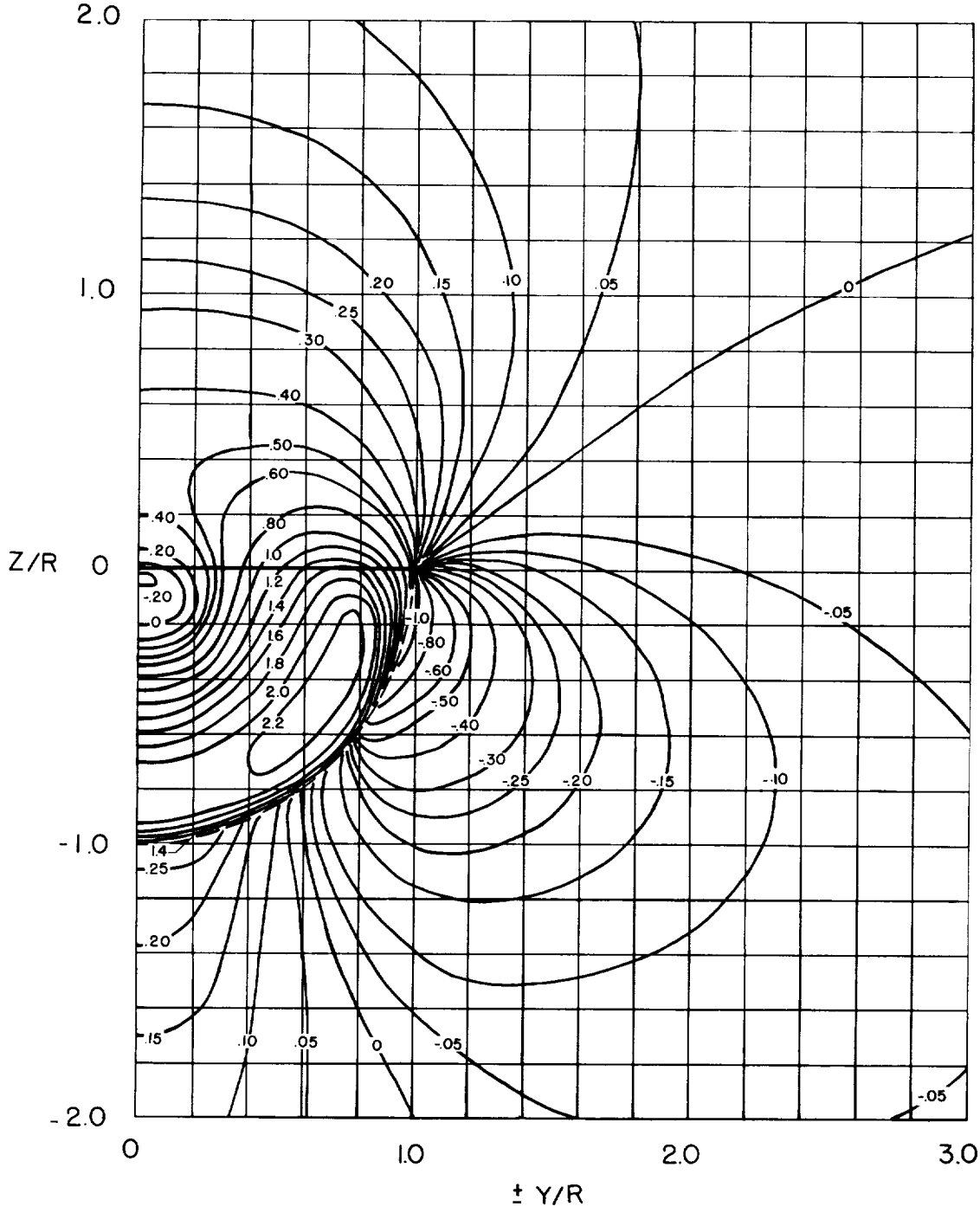

(c) Typical disk loading.

Figure 7.- Concluded.

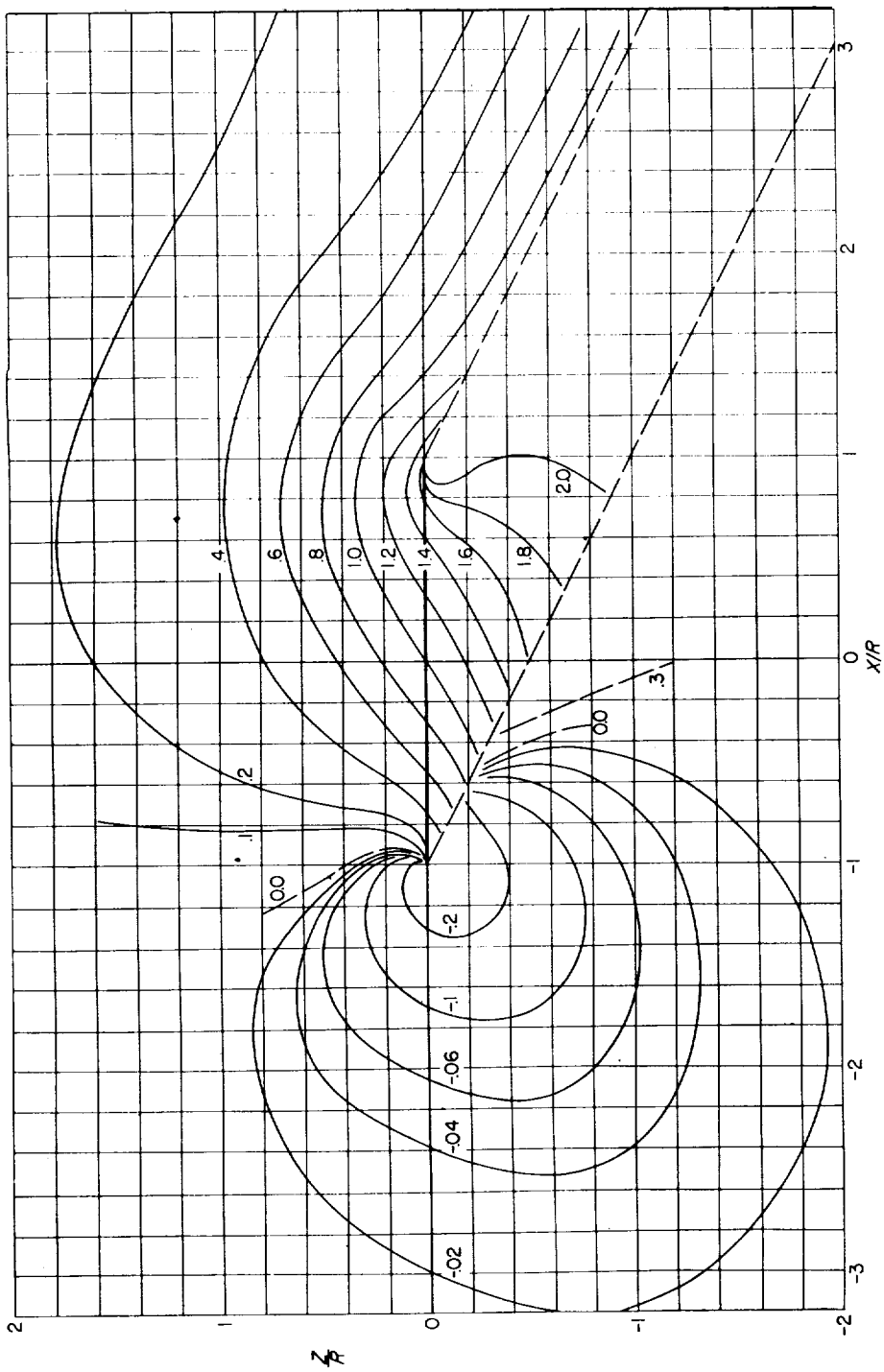

(a) Uniform disk loading (from ref. 5).

Figure 8.- Contours of induced-velocity ratio v/v_o in the longitudinal plane of the rotor for $\chi = \tan^{-1} 2 = 63.43^{\circ}$.

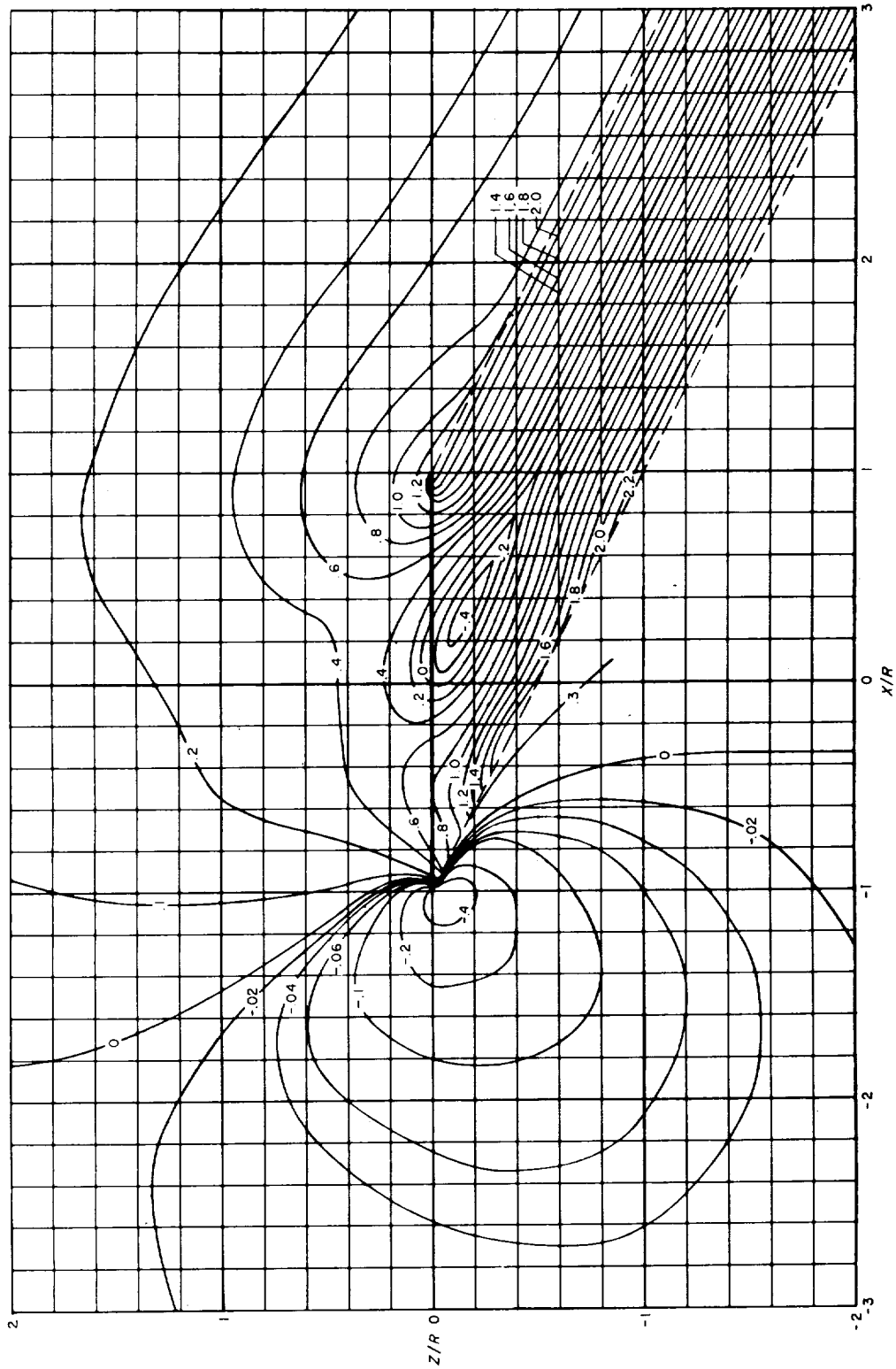

(b) Triangular disk loading (from ref. 9).

Figure 8.- Continued.

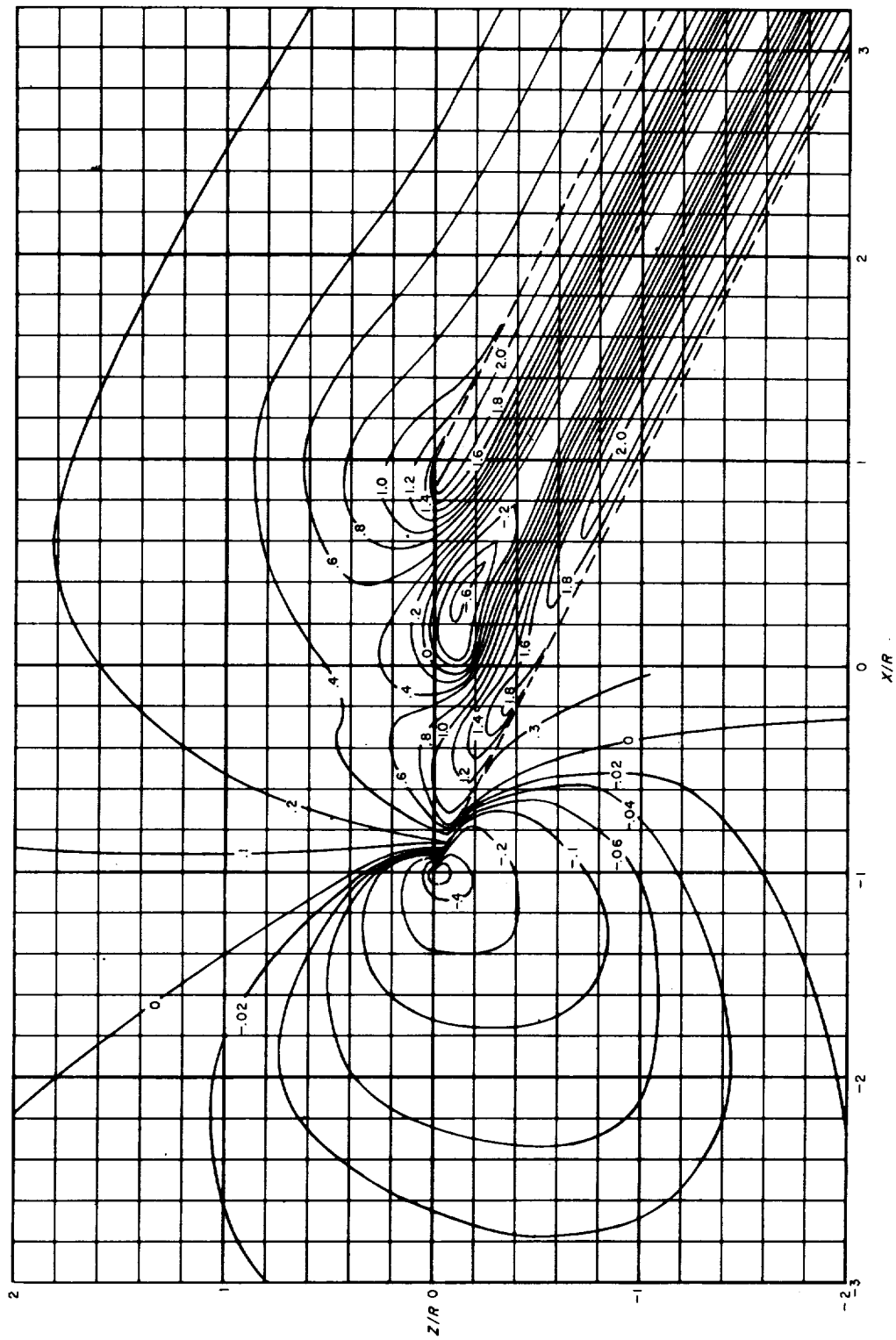

(c) Typical disk loading (from ref. 9).

Figure 8.- Concluded.

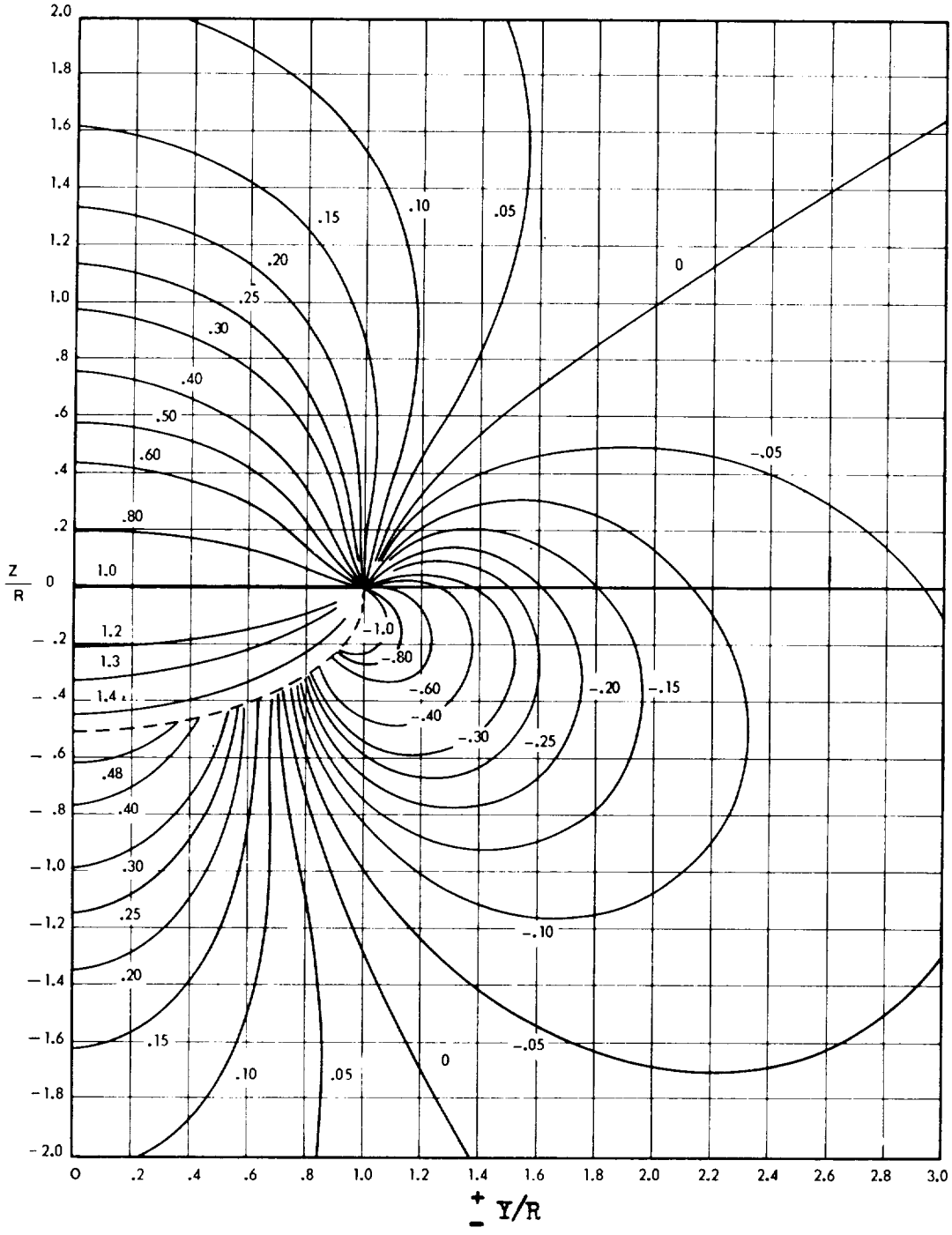

(a) Uniform disk loading (from ref. 6).

Figure 9.- Contours of induced-velocity ratio v/v_o in the lateral plane of the rotor for $\chi = \tan^{-1} 2 = 63.43^\circ$.

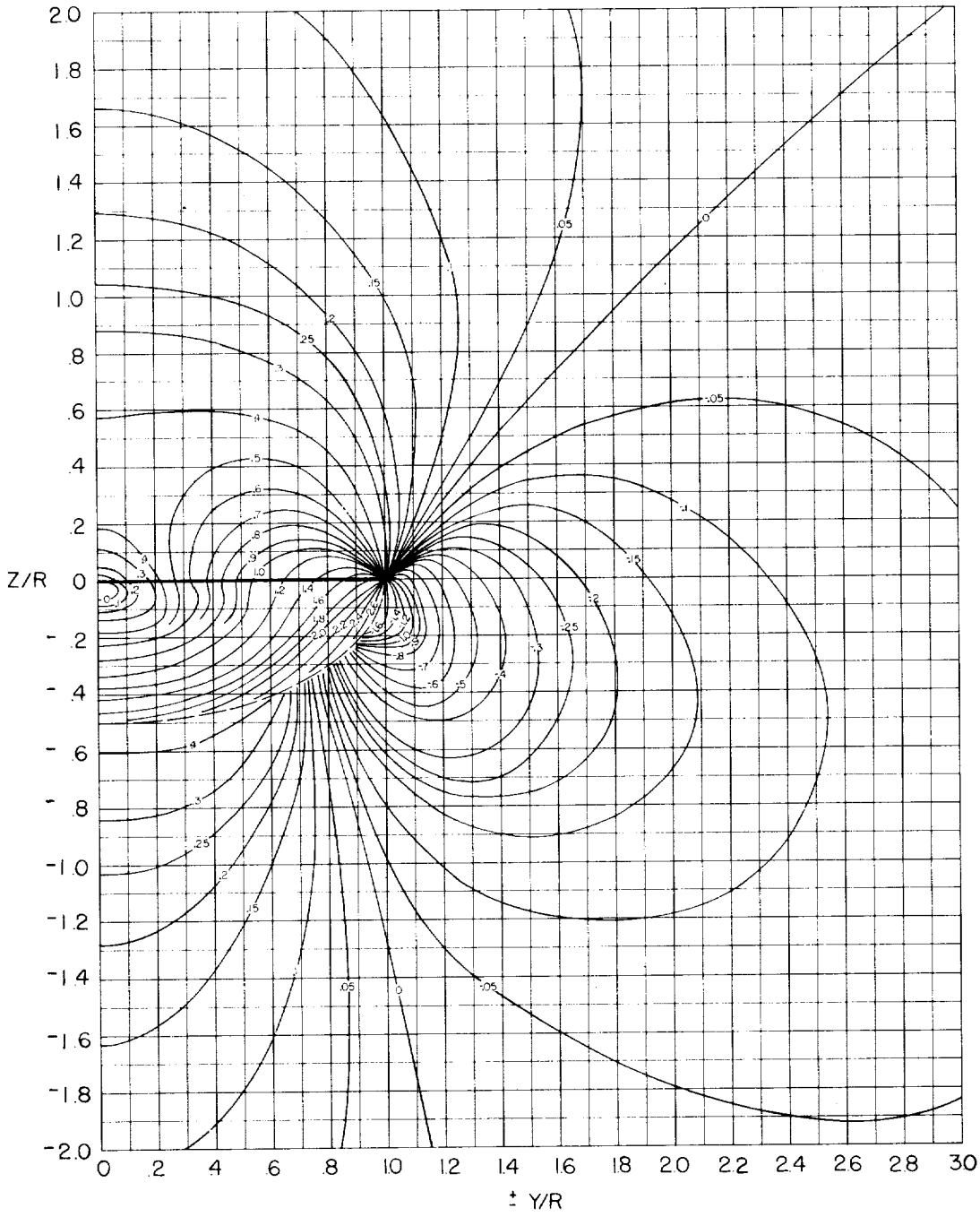

(b) Triangular disk loading.

Figure 9.- Continued.

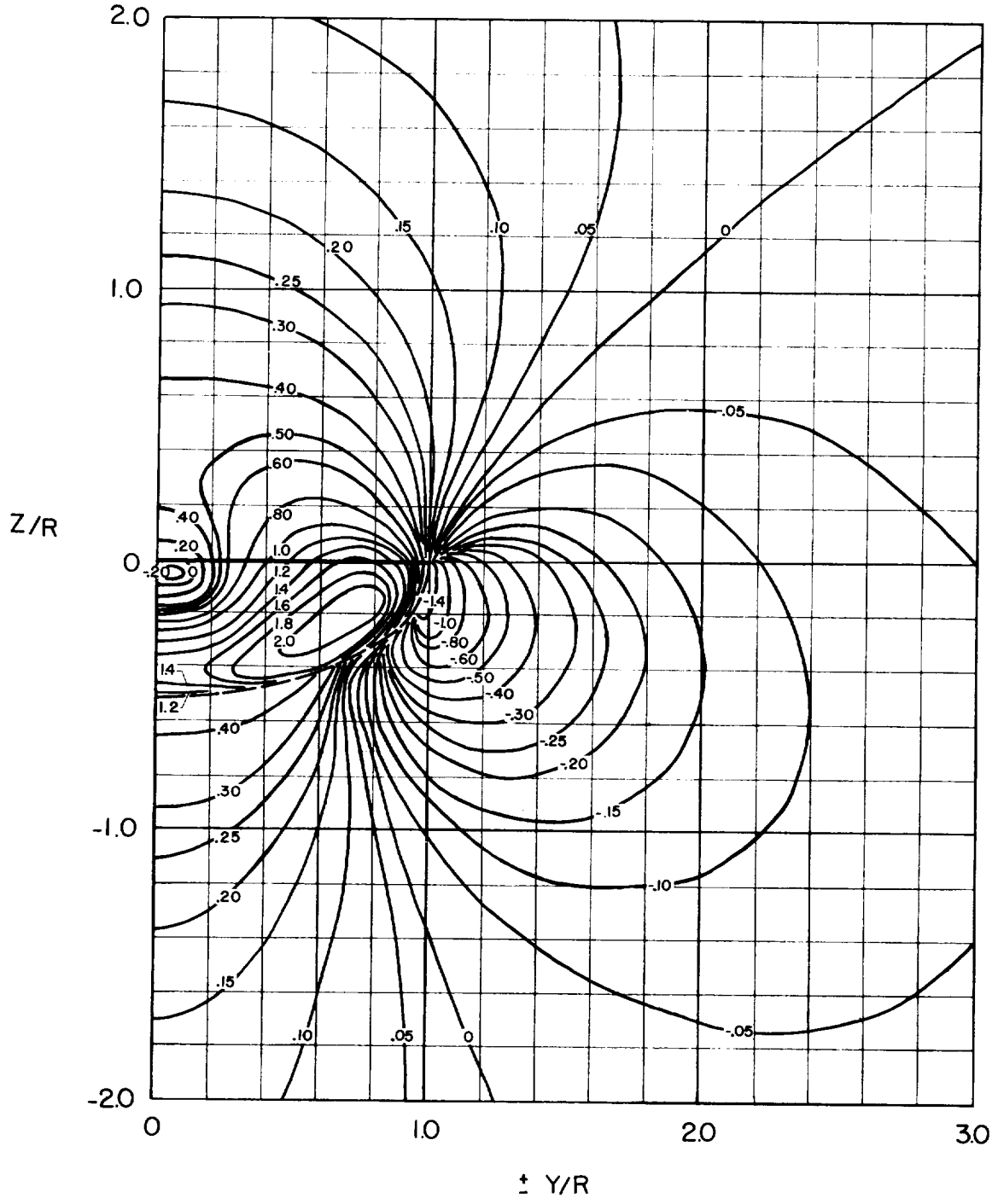

(c) Typical disk loading.

Figure 9.- Concluded.

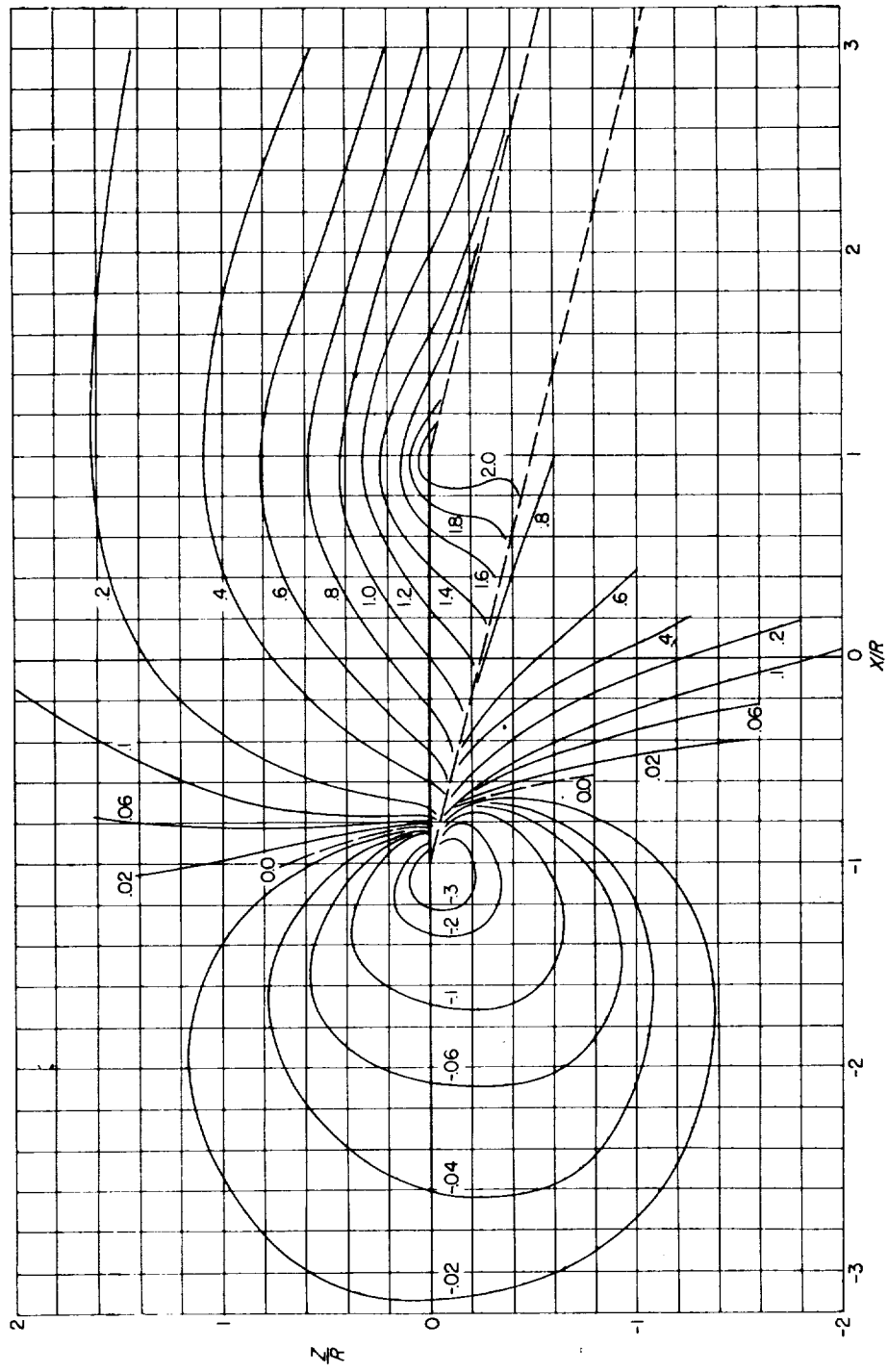

(a) Uniform disk loading (from ref. 5).

Figure 10.- Contours of induced-velocity ratio v/v_o in the longitudinal plane of the rotor for $\chi = \tan^{-1} 4 = 75.97°$.

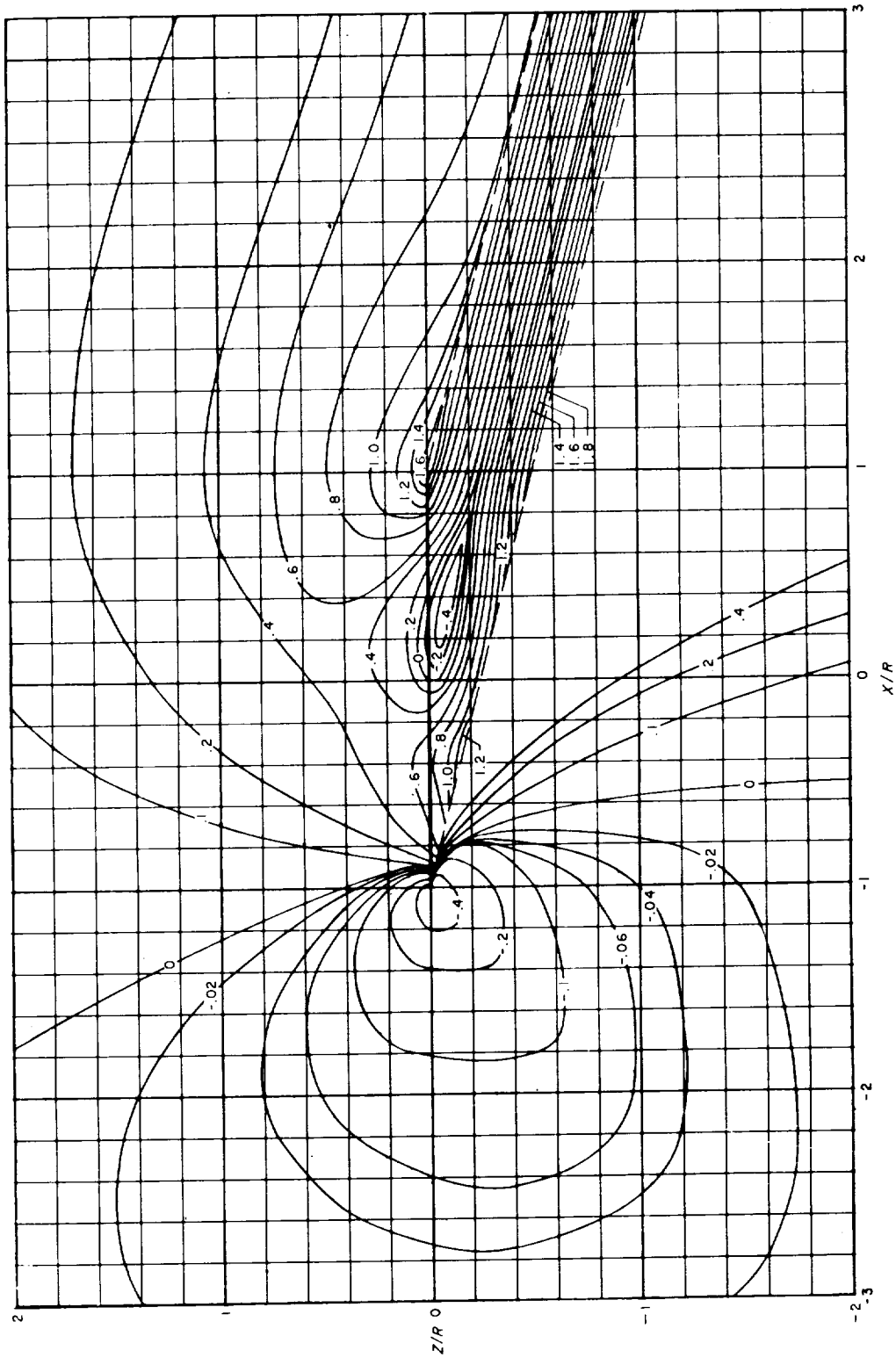

(b) Triangular disk loading (from ref. 9).

Figure 10.- Continued.

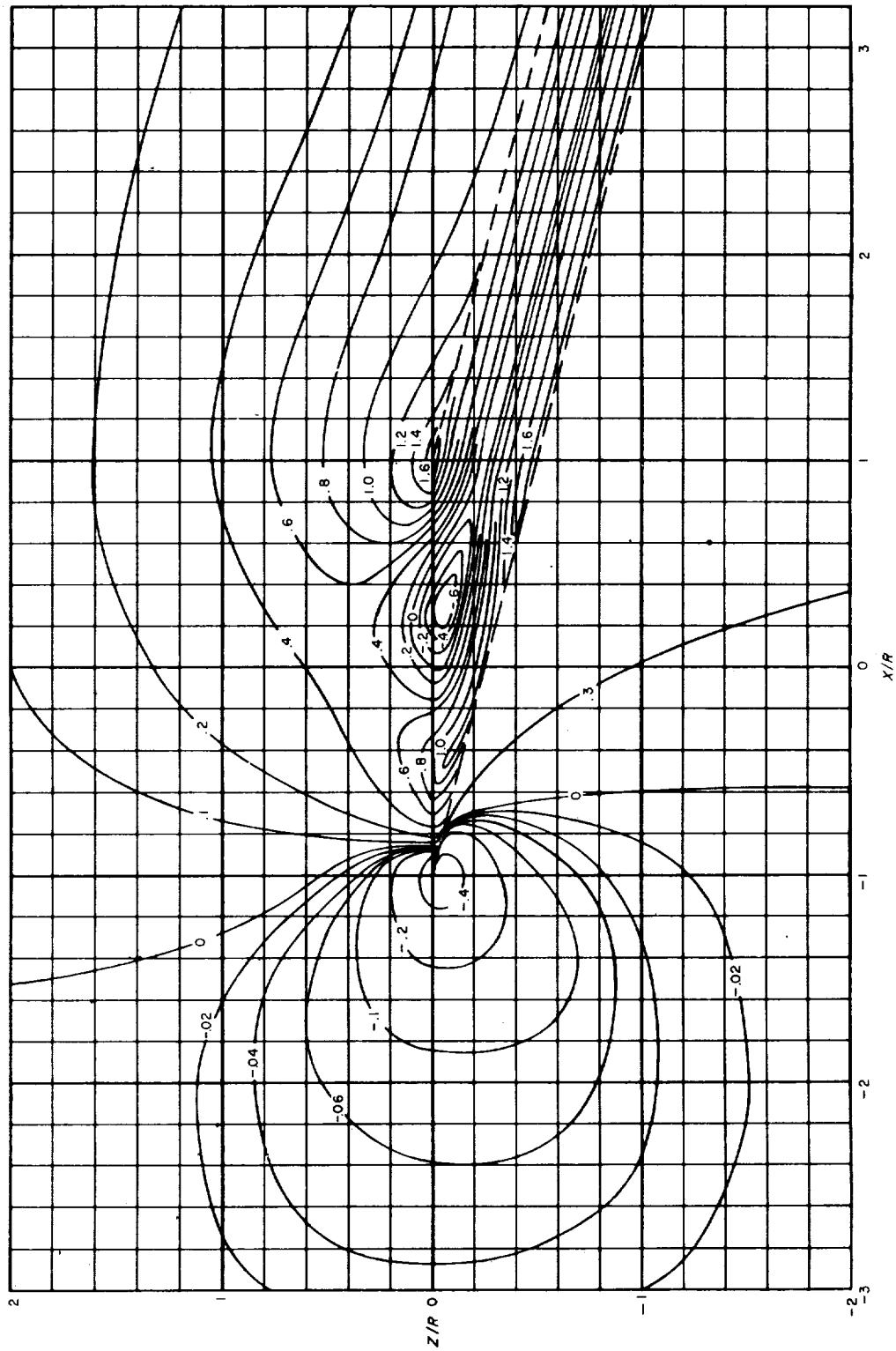

(c) Typical disk loading (from ref. 9).

Figure 10.- Concluded.

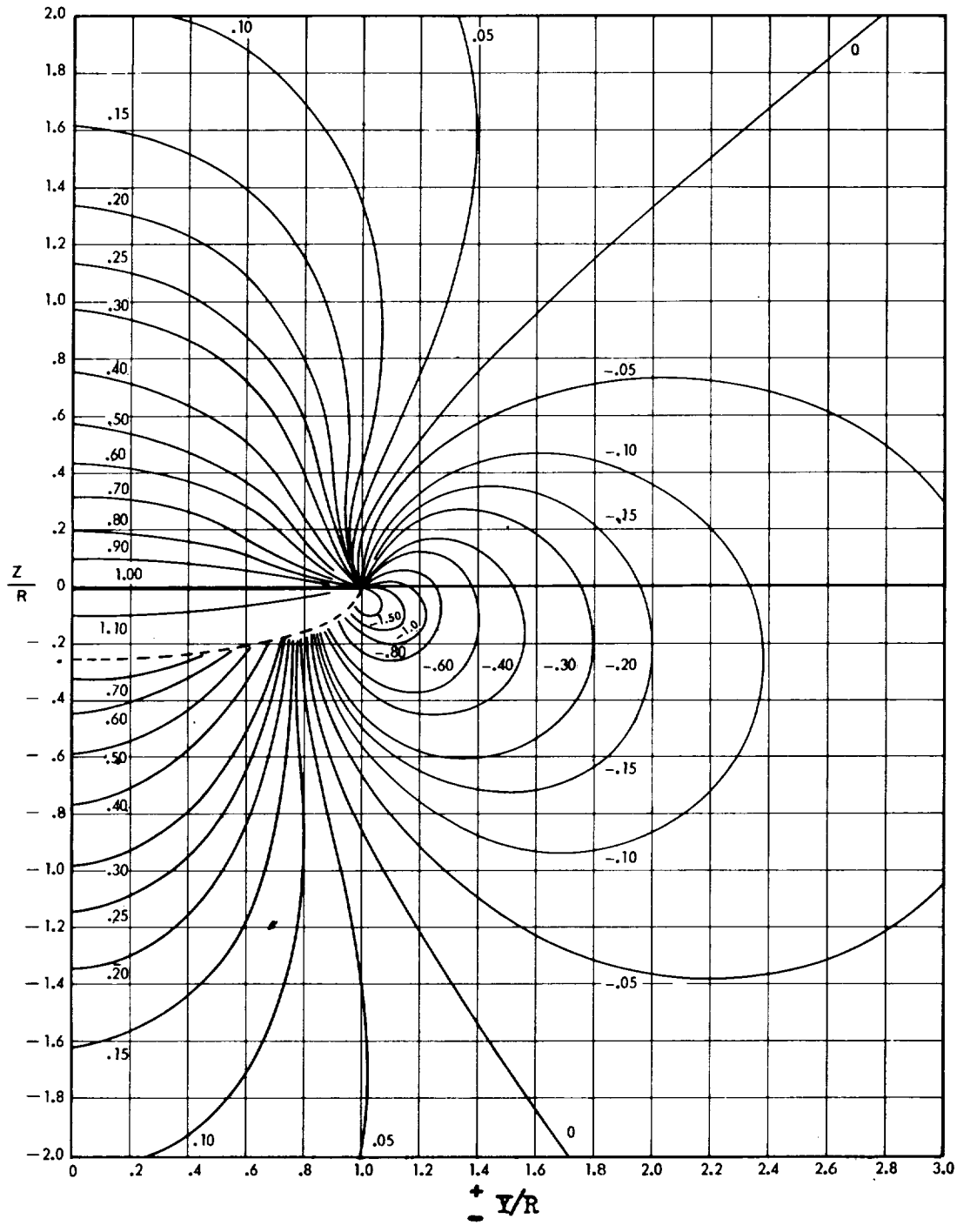

(a) Uniform disk loading (from ref. 6).

Figure 11.- Contours of induced-velocity ratio v/v_o in the lateral plane of the rotor for $\chi = \tan^{-1} 4 = 75.97^{\circ}$.

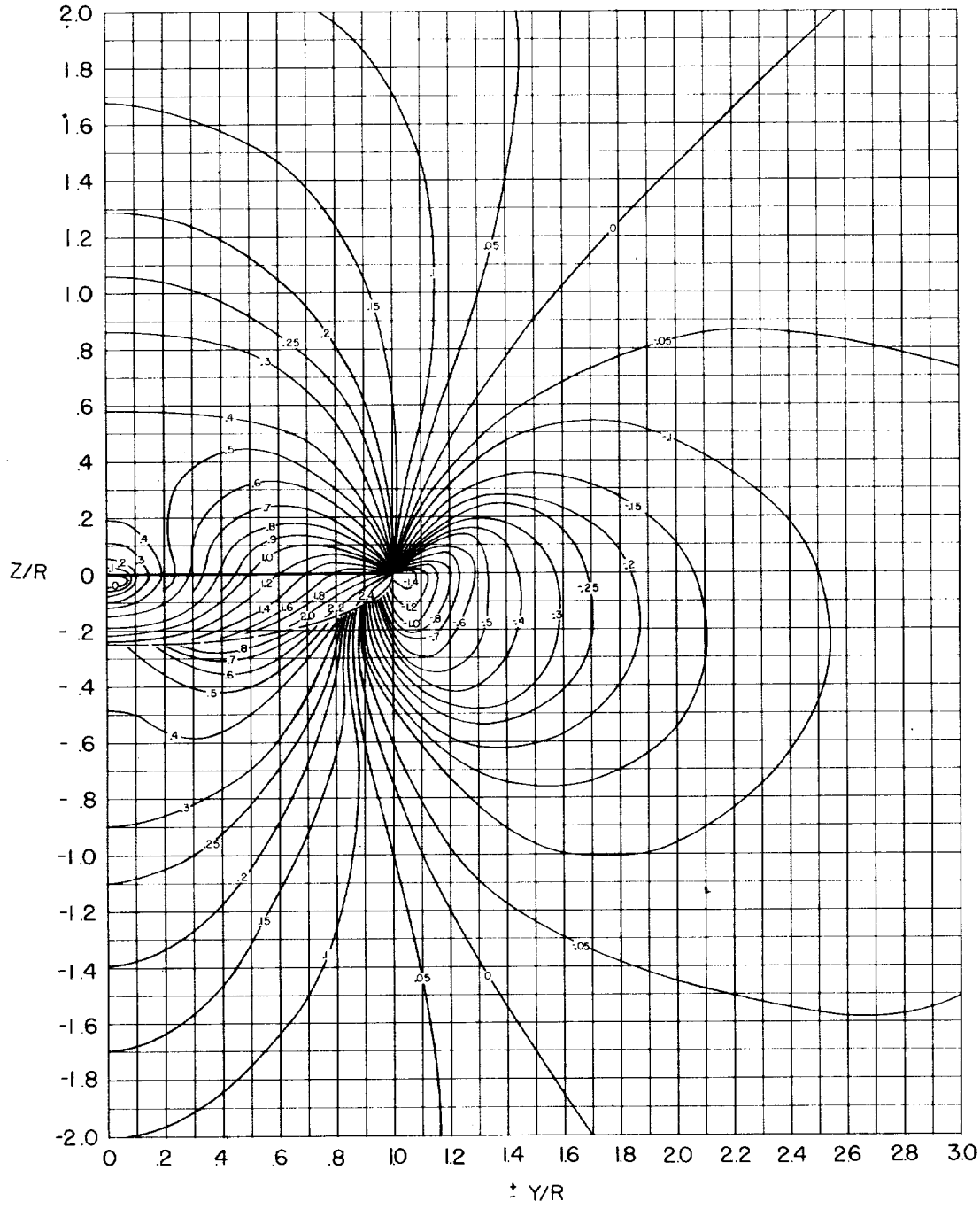

(b) Triangular disk loading.

Figure 11.- Continued.

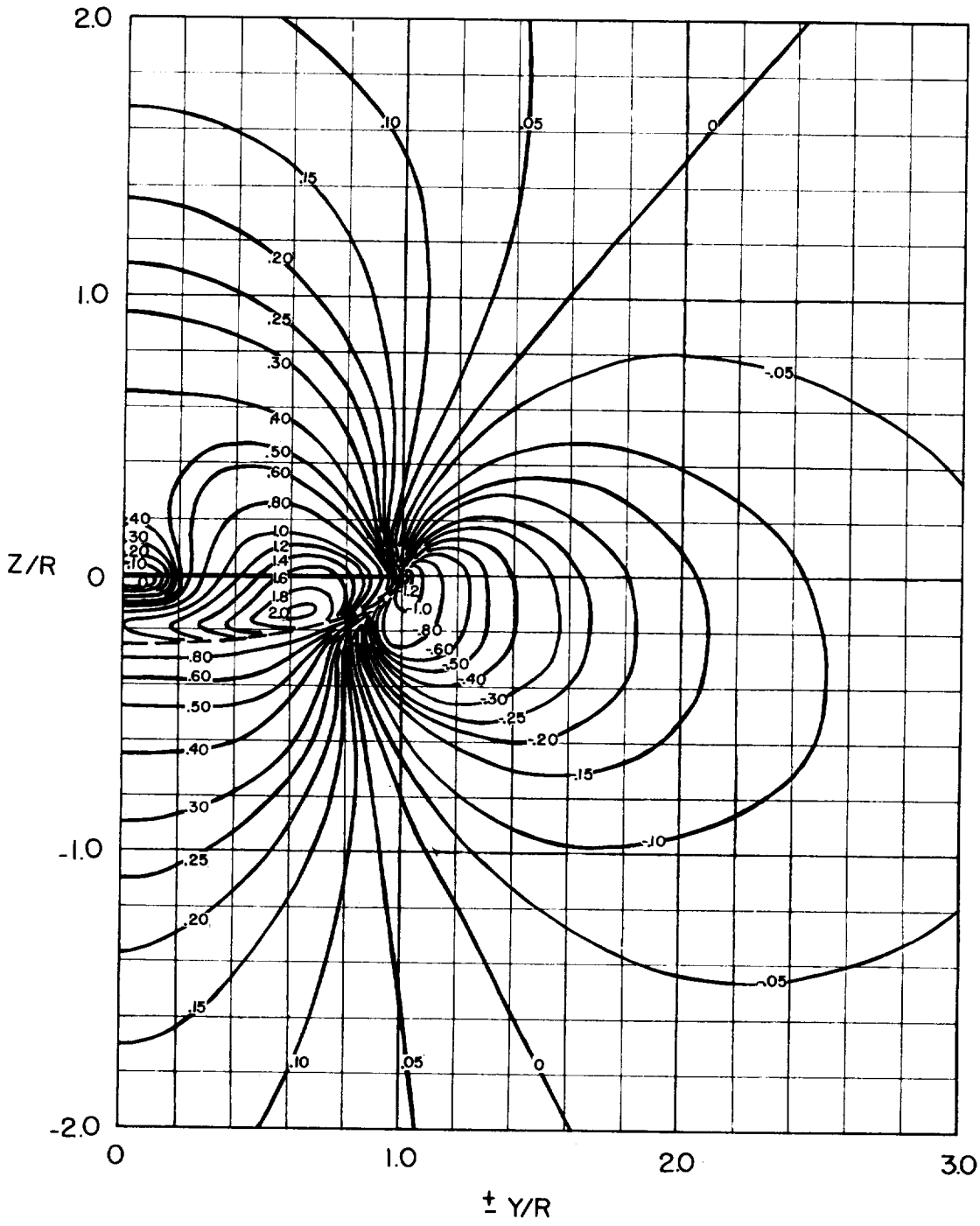

(c) Typical disk loading.

Figure 11.- Concluded.

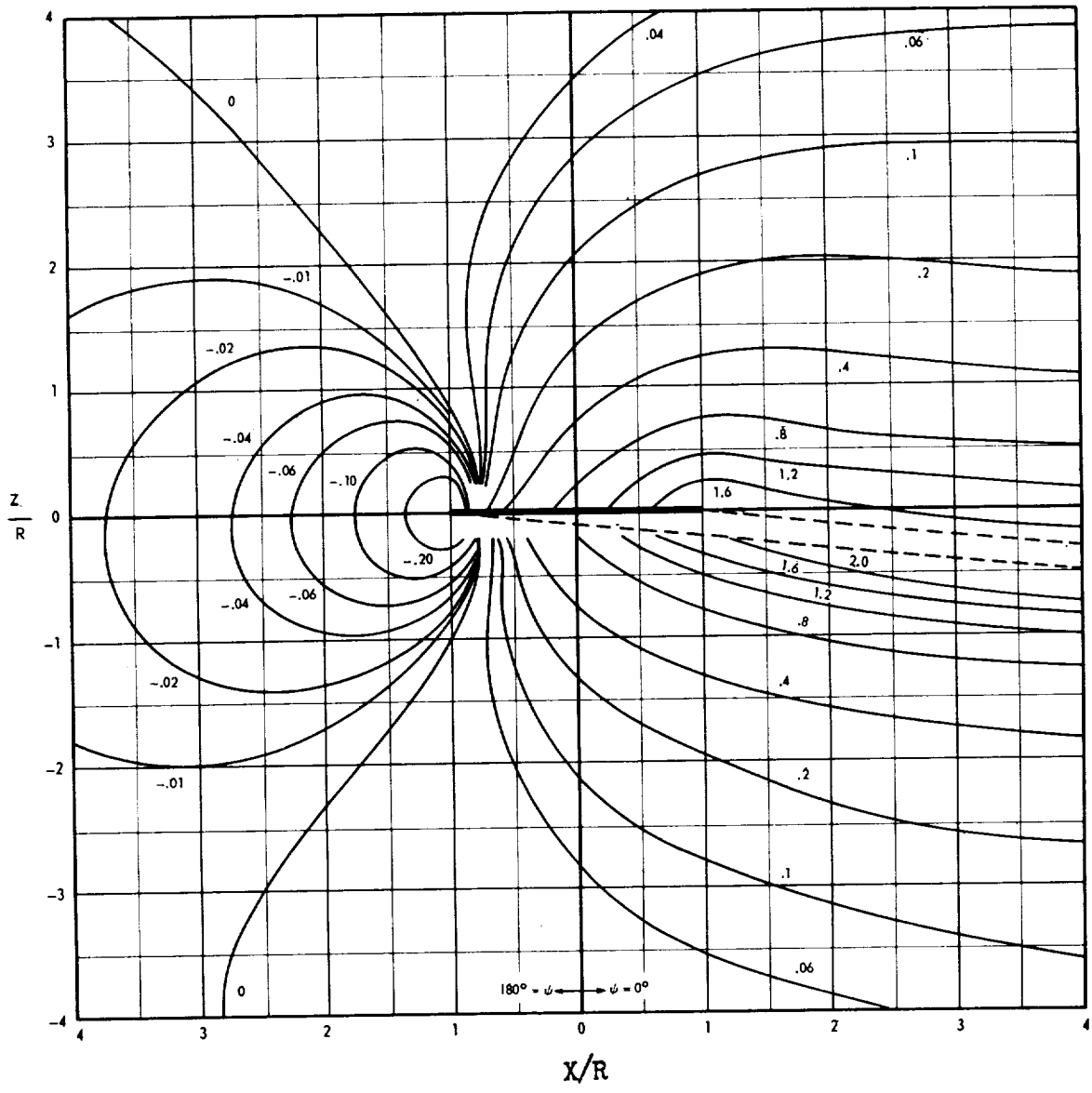

(a) Uniform disk loading (from ref. 7).

Figure 12.- Contours of induced-velocity ratio v/v_o in the longitudinal plane of the rotor for $\chi = \tan^{-1} 10 = 84.29^{\circ}$.

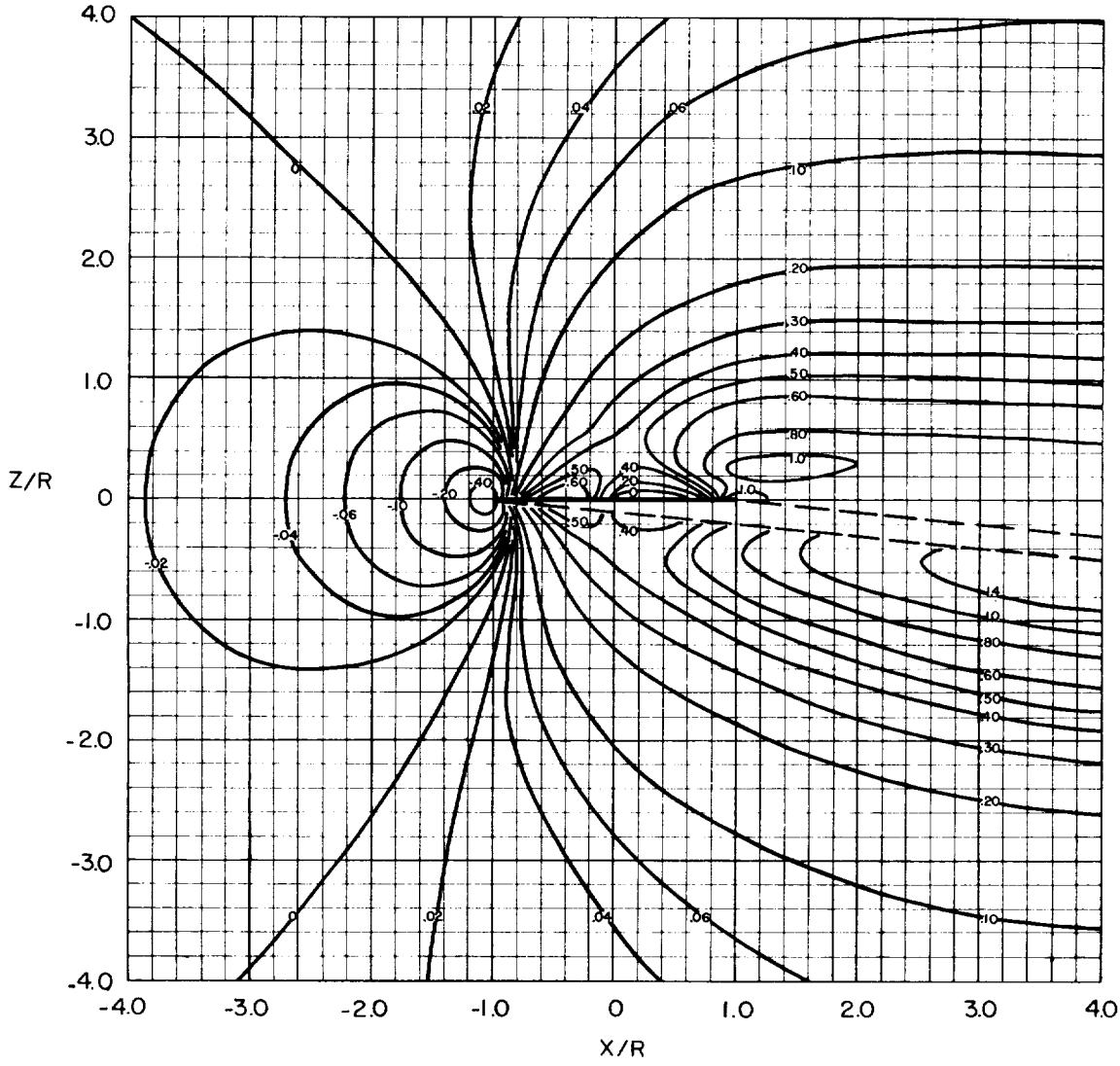

(b) Triangular disk loading.

Figure 12.- Continued.

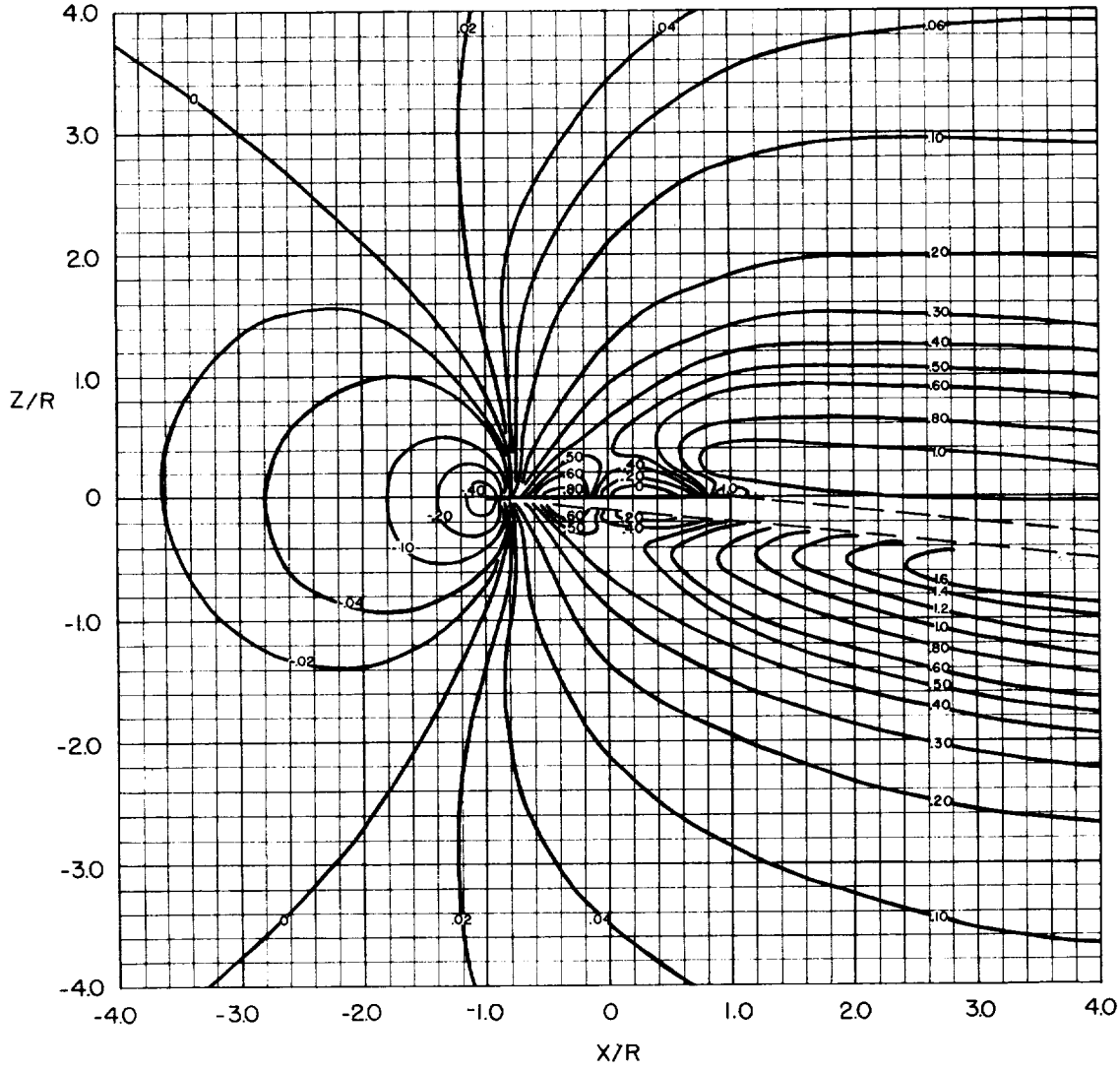

(c) Typical disk loading.

Figure 12.- Concluded.

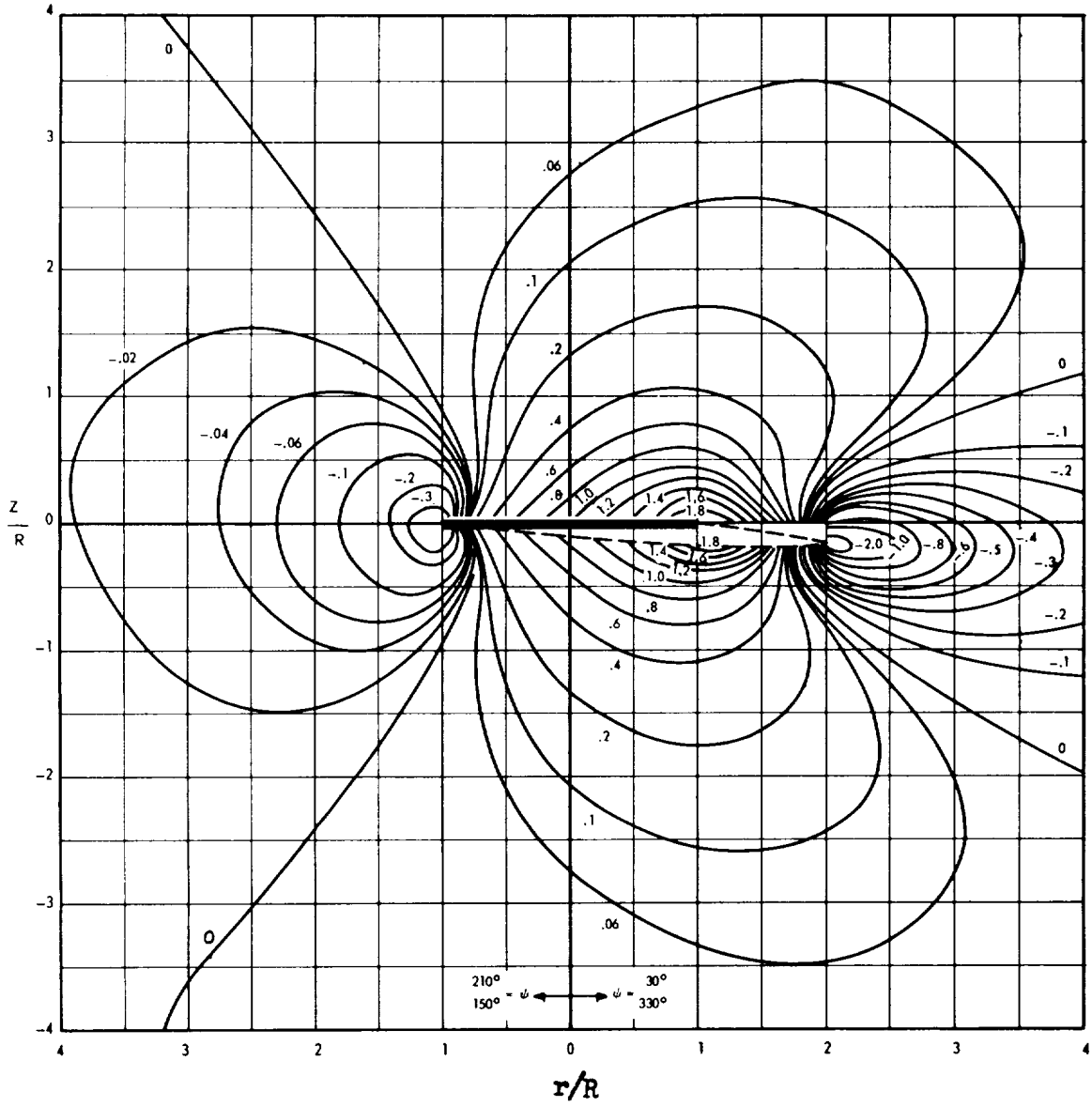

(a) Uniform disk loading (from ref. 7).

Figure 13.- Contours of induced-velocity ratio v/v_o in the radial planes $\psi = 30^\circ$, 150°, 210°, and 330° of the rotor. $\chi = \tan^{-1} 10 = 84.29^\circ$.

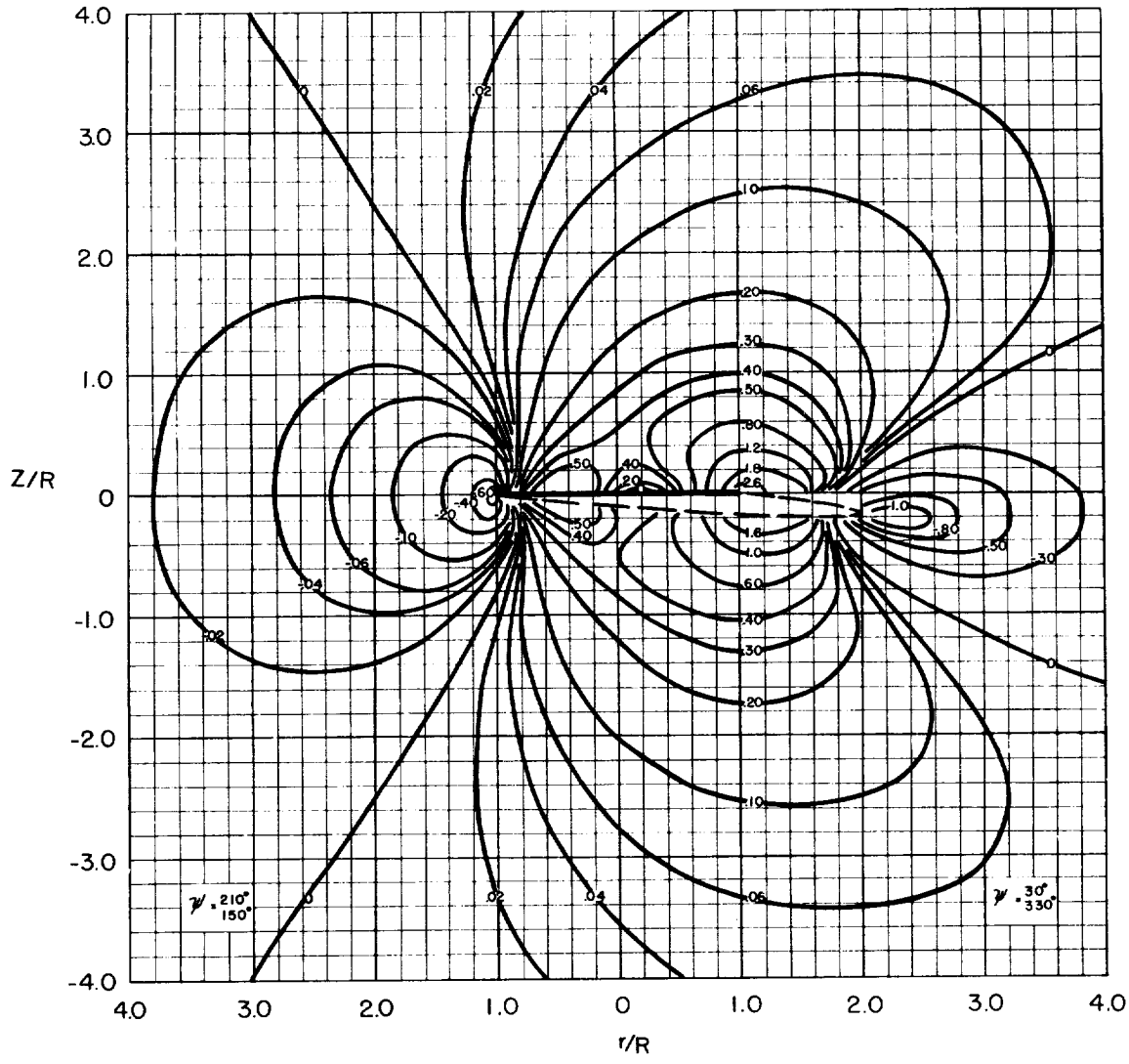

(b) Triangular disk loading.

Figure 13.- Continued.

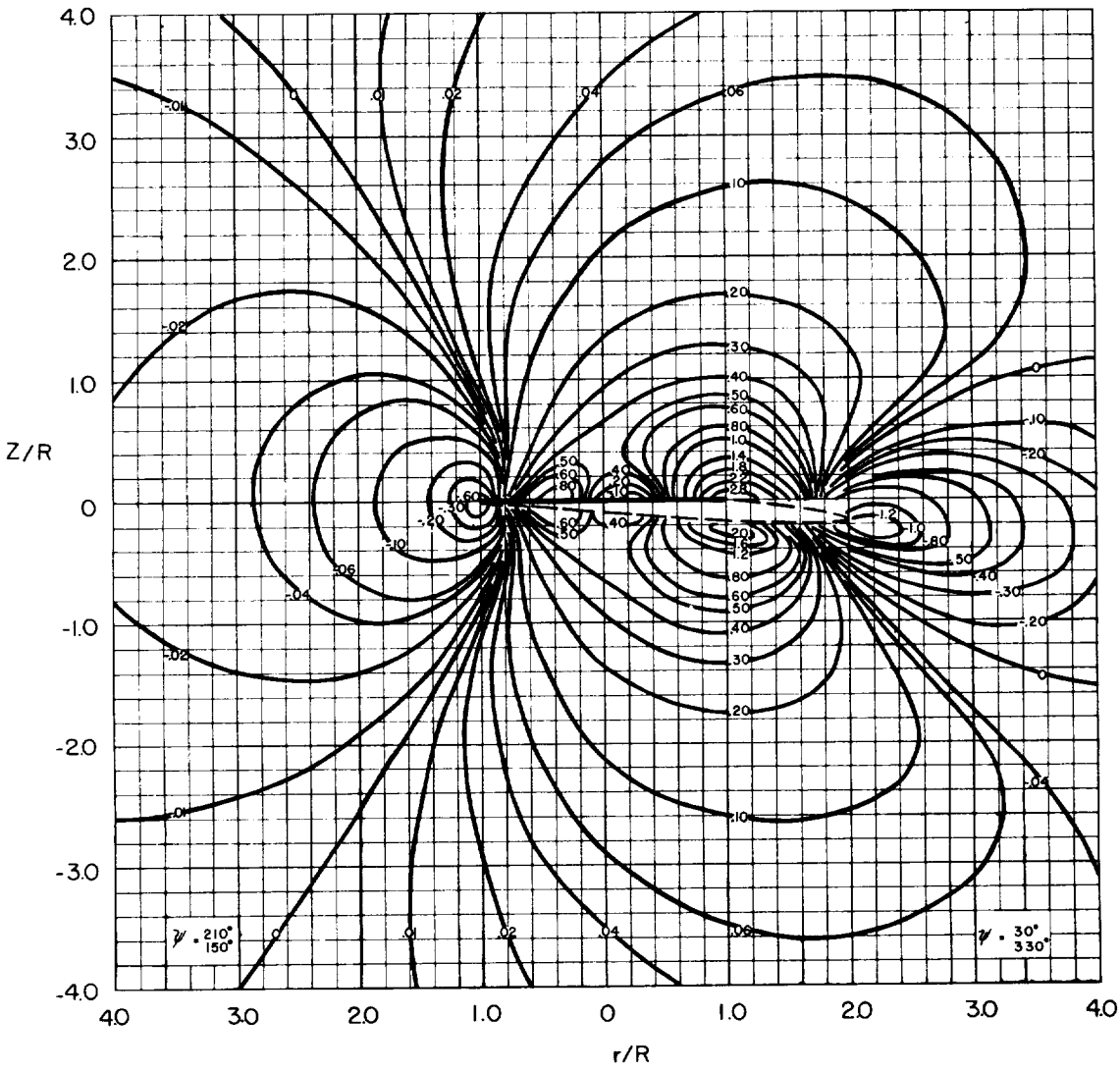

(c) Typical disk loading.

Figure 13.- Concluded.

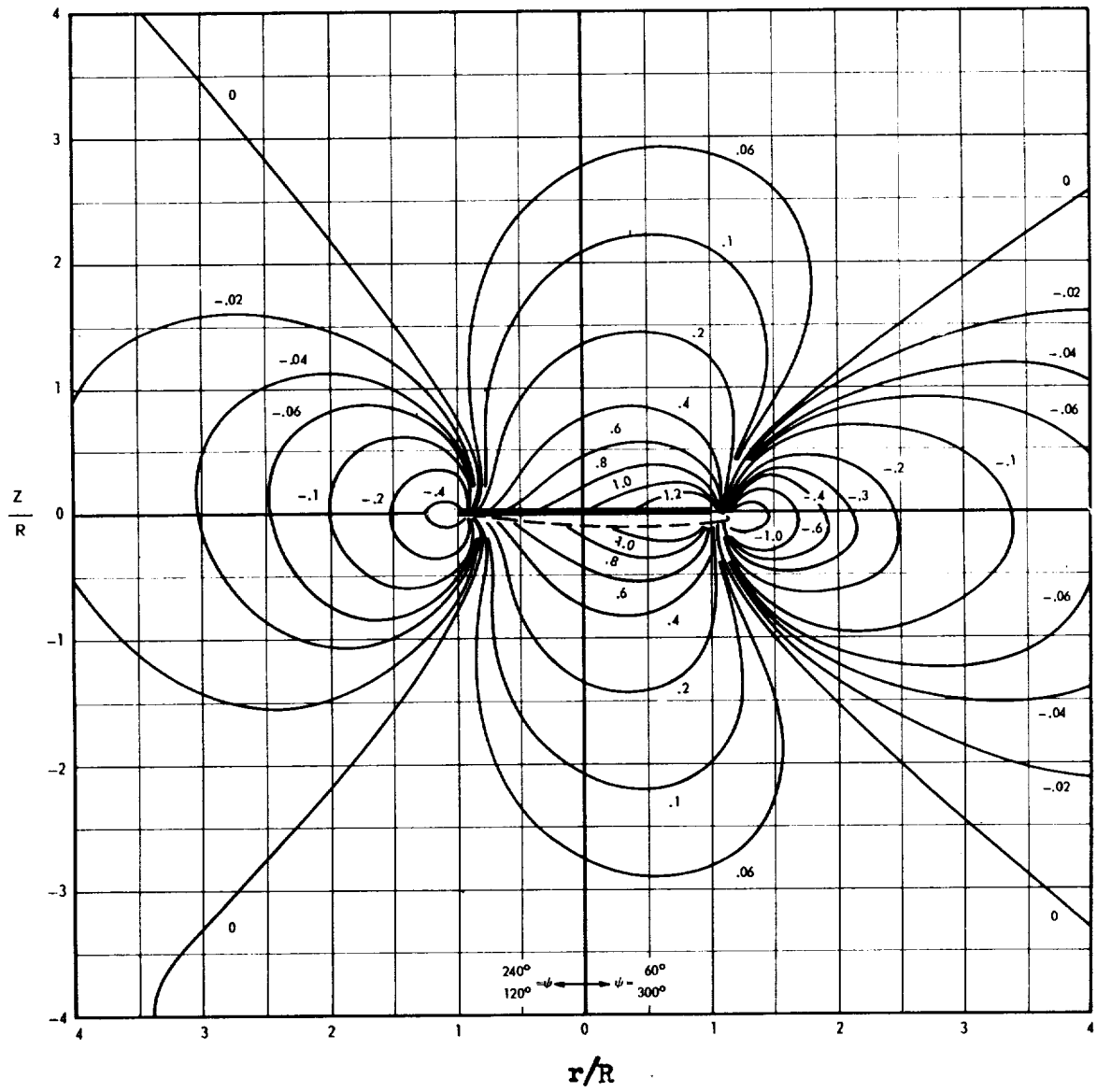

(a) Uniform disk loading (from ref. 7).

Figure 14.- Contours of induced-velocity ratio v/v_o in the radial planes $\psi = 60^\circ$, 120°, 240°, and 300° of the rotor. $\chi = \tan^{-1} 10 = 84.29^\circ$.

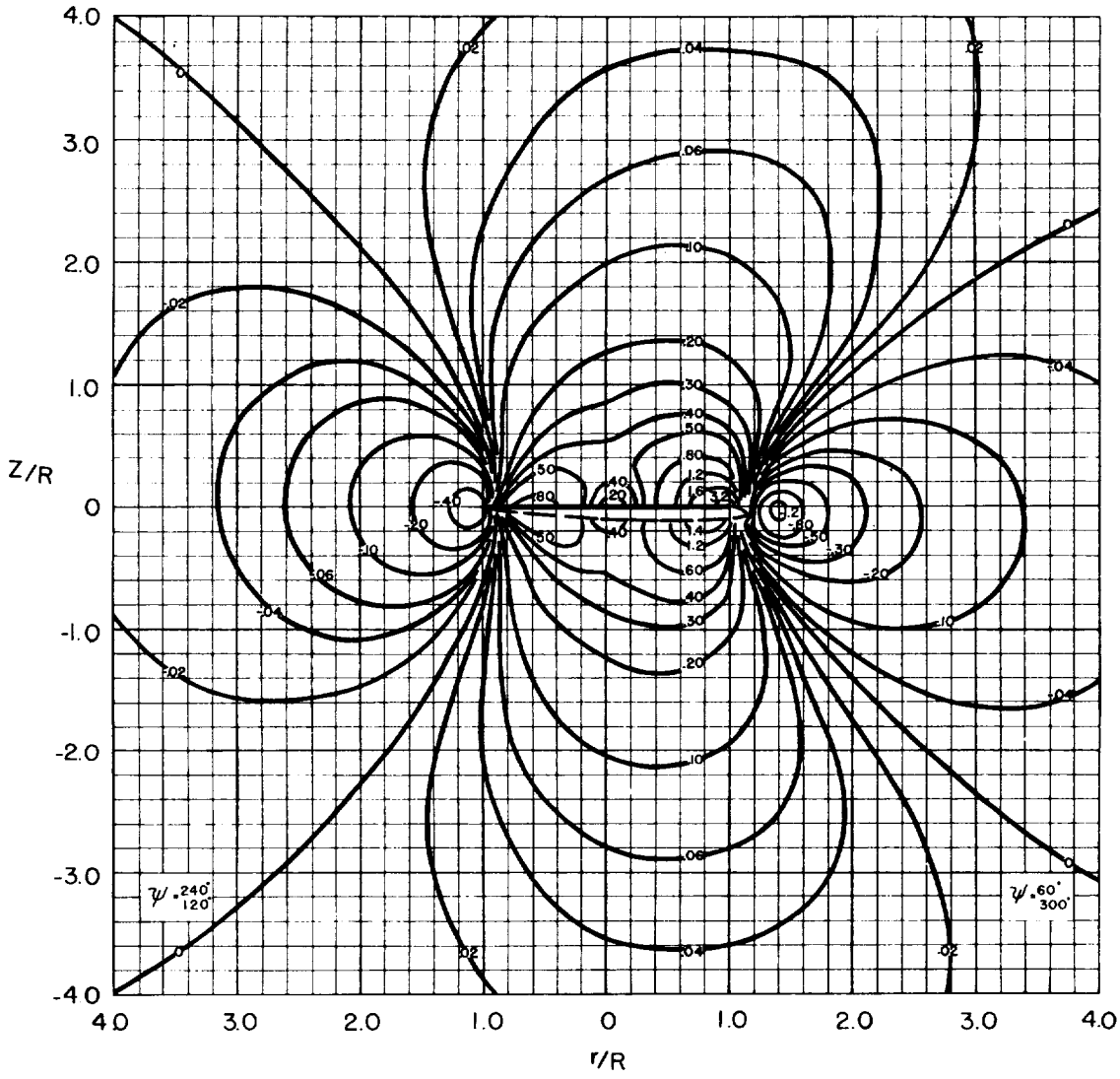

(b) Triangular disk loading.

Figure 14.- Continued.

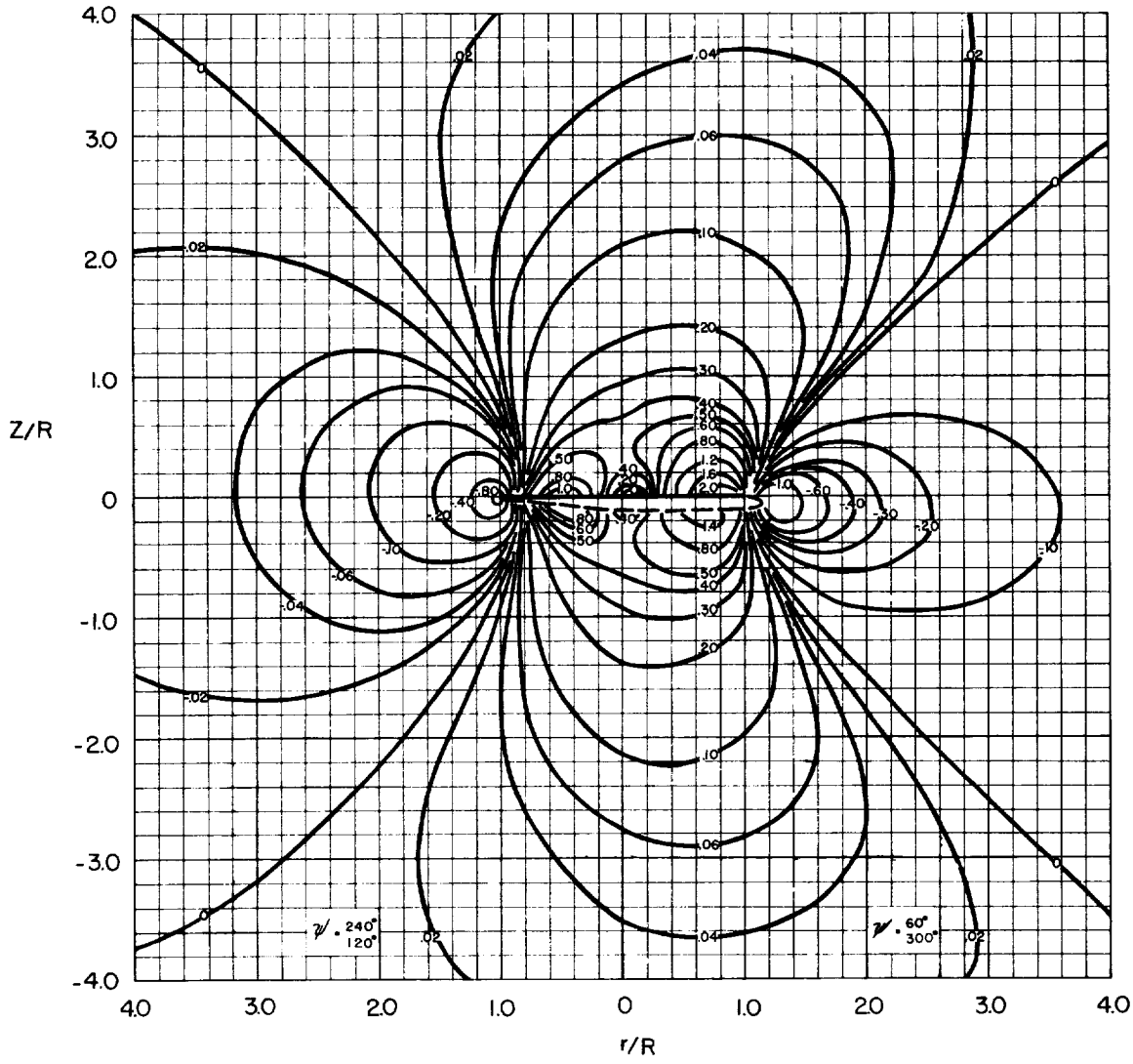

(c) Typical disk loading.

Figure 14.- Concluded.

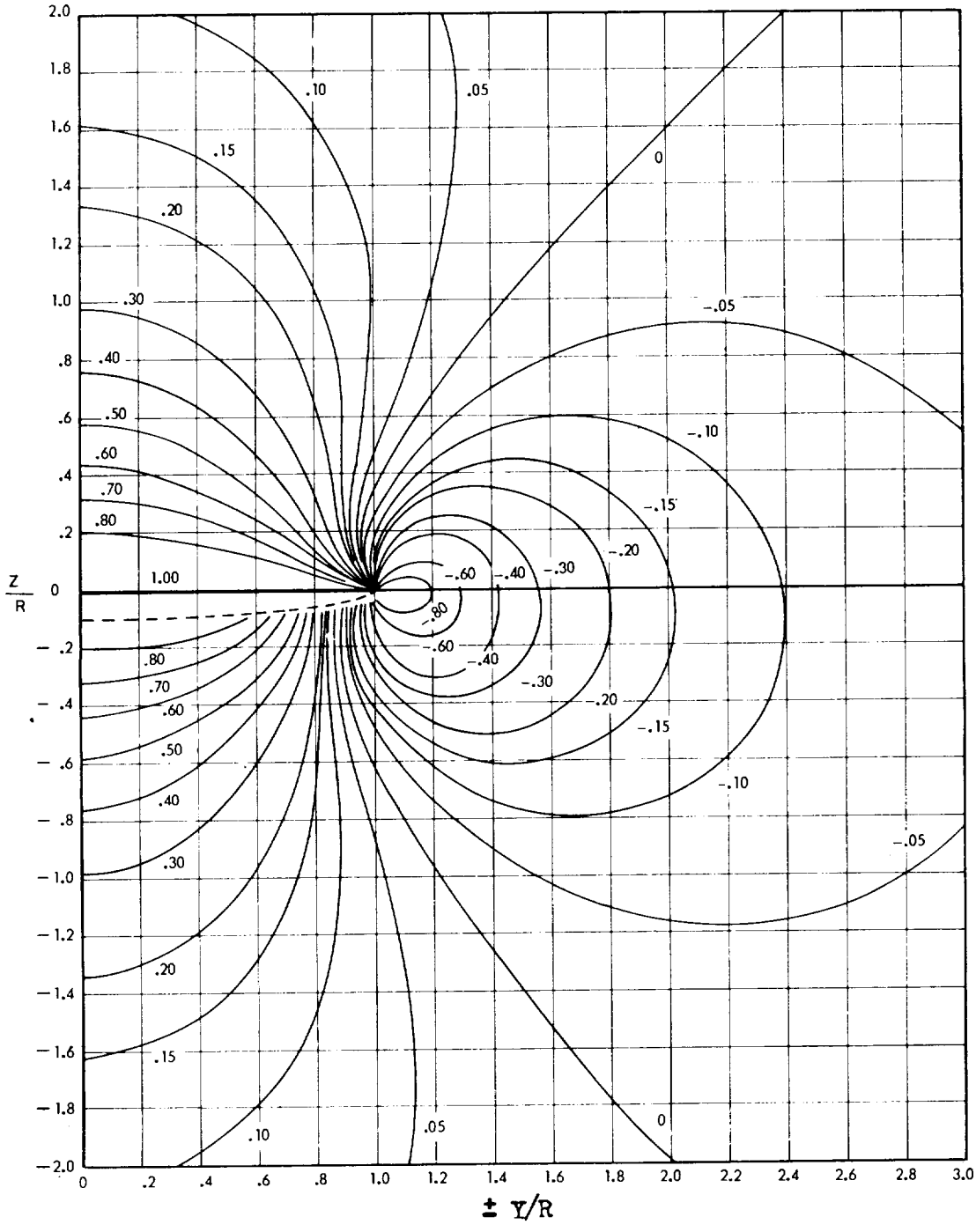

(a) Uniform disk loading (from ref. 6).

Figure 15.- Contours of induced-velocity ratio v/v_o in the lateral plane of the rotor for $\chi = \tan^{-1} 10 = 84.29^{\circ}$.

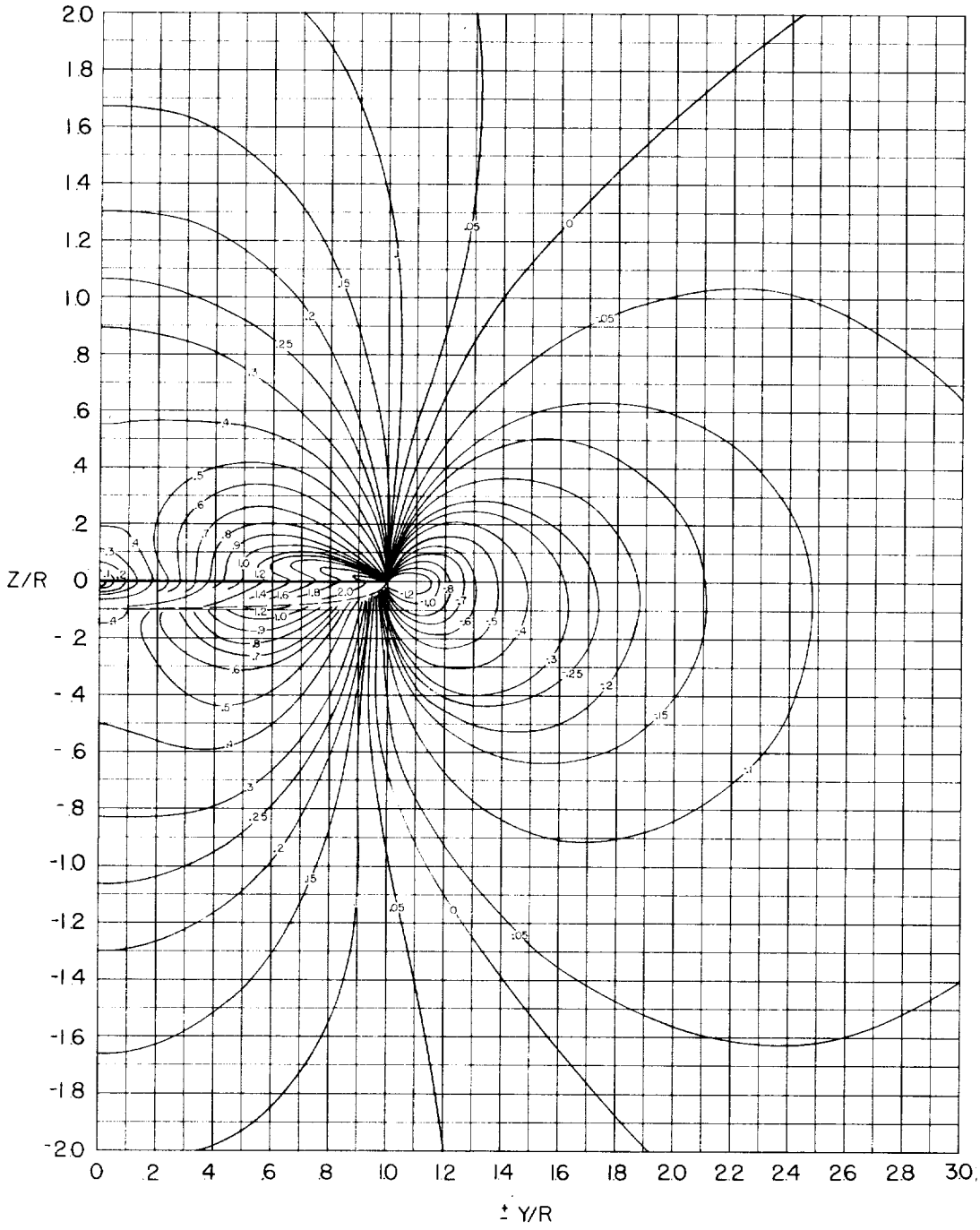

(b) Triangular disk loading.

Figure 15.- Continued.

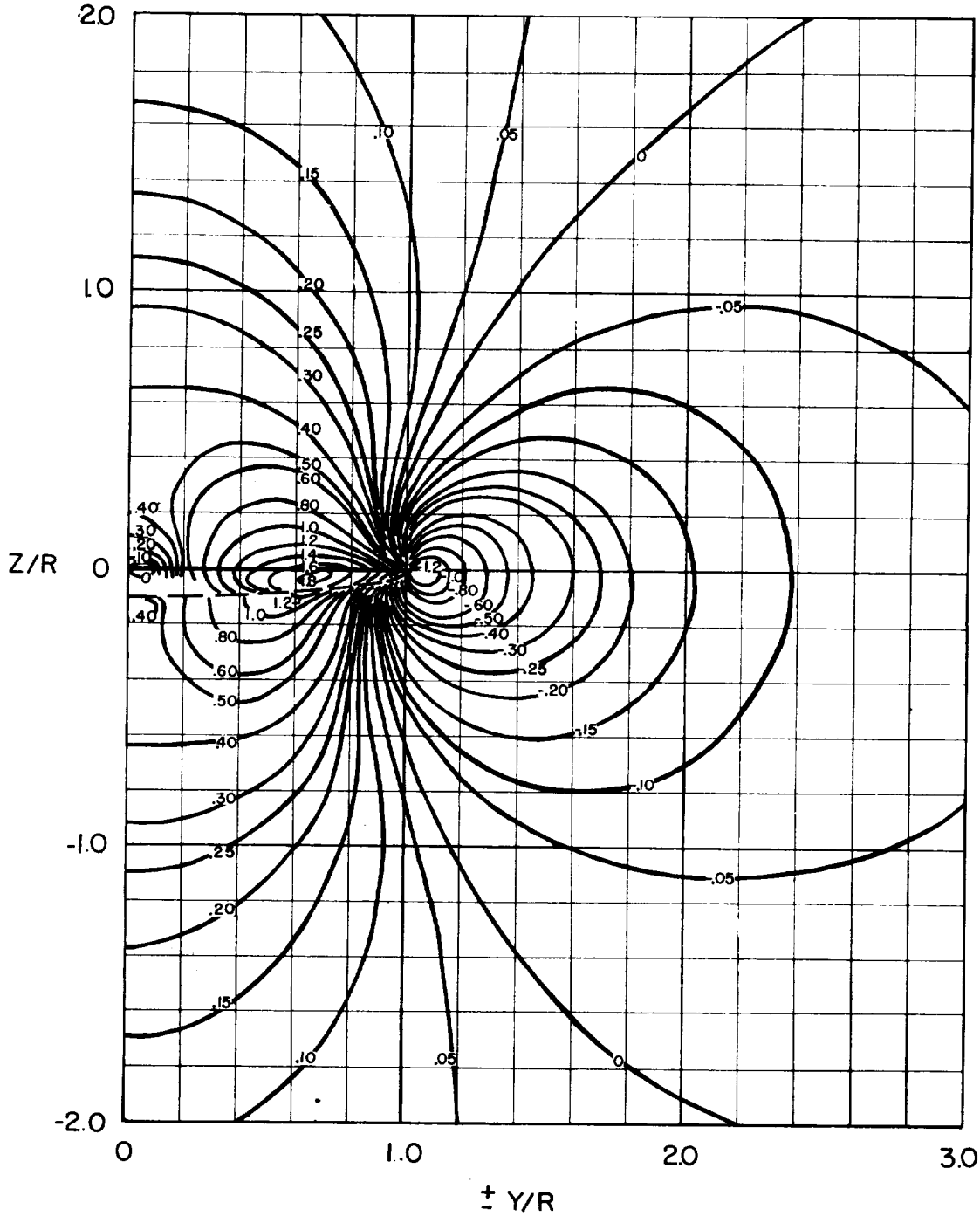

(c) Typical disk loading.

Figure 15.- Concluded.

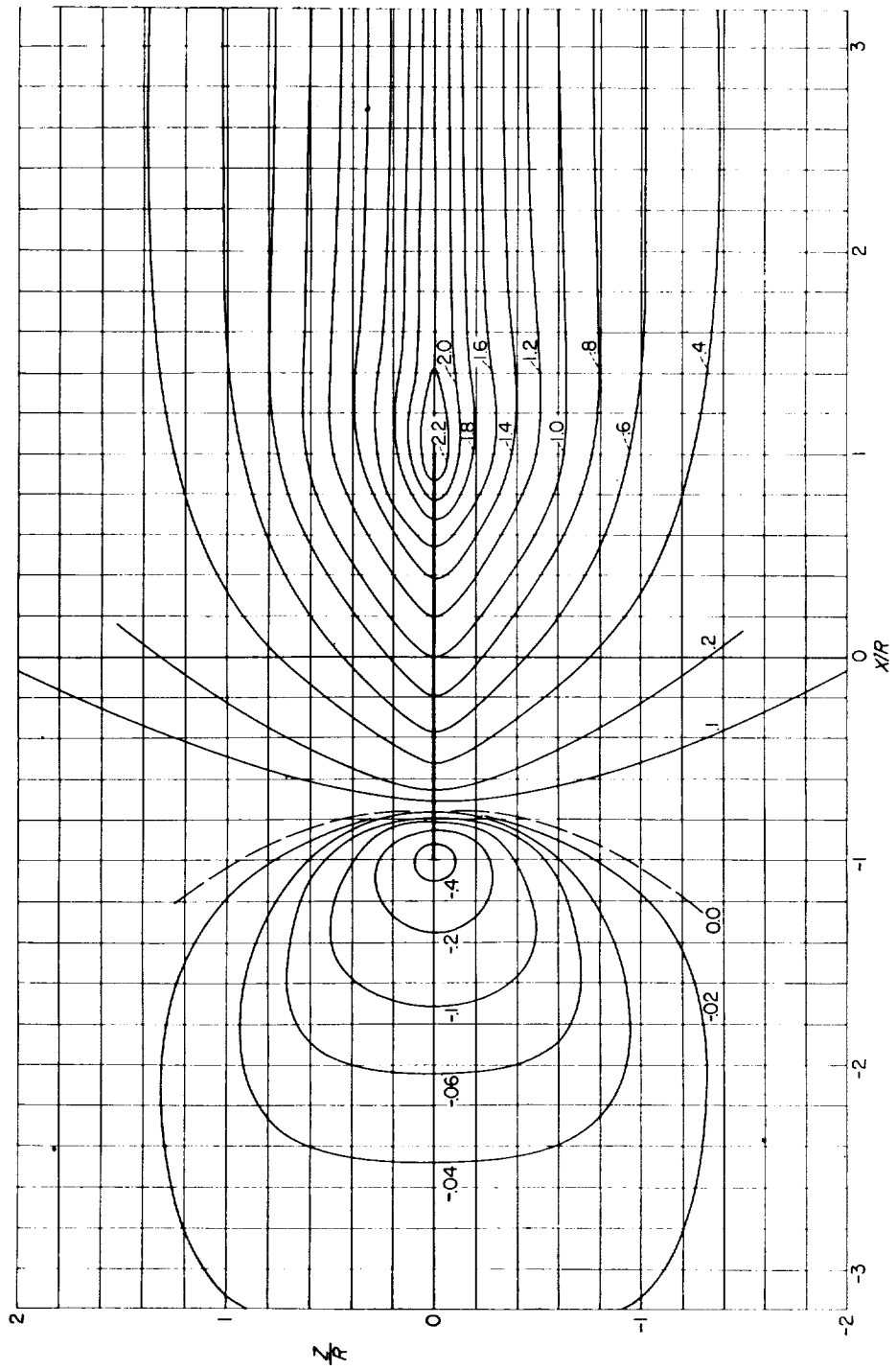

(a) Uniform disk loading (from ref. 5).

Figure 16.- Contours of induced-velocity ratio v/v_o in the longitudinal plane of the rotor for $\chi = \tan^{-1} \infty = 90.00^\circ$.

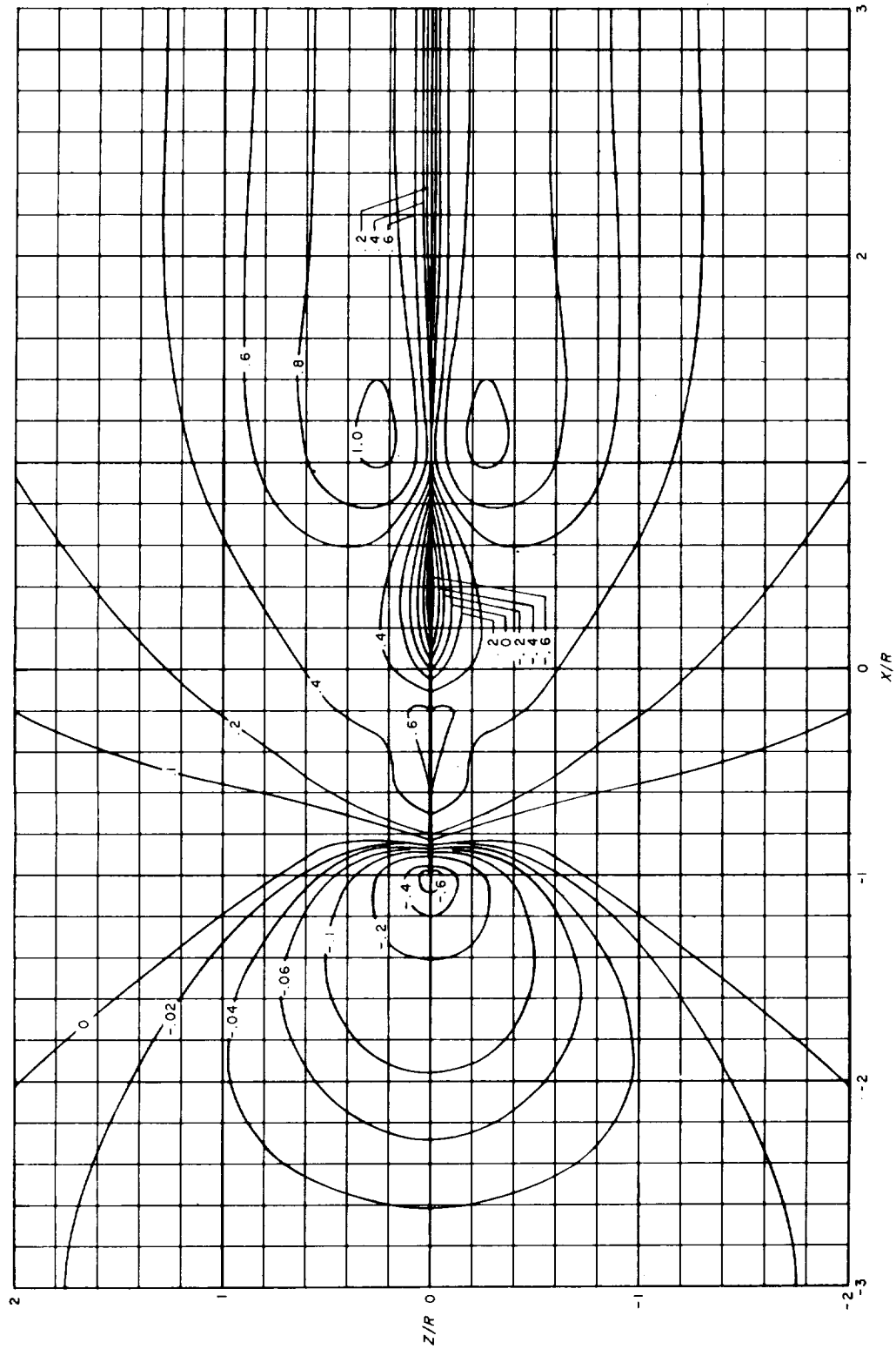

(b) Triangular disk loading (from ref. 9).

Figure 16.- Continued.

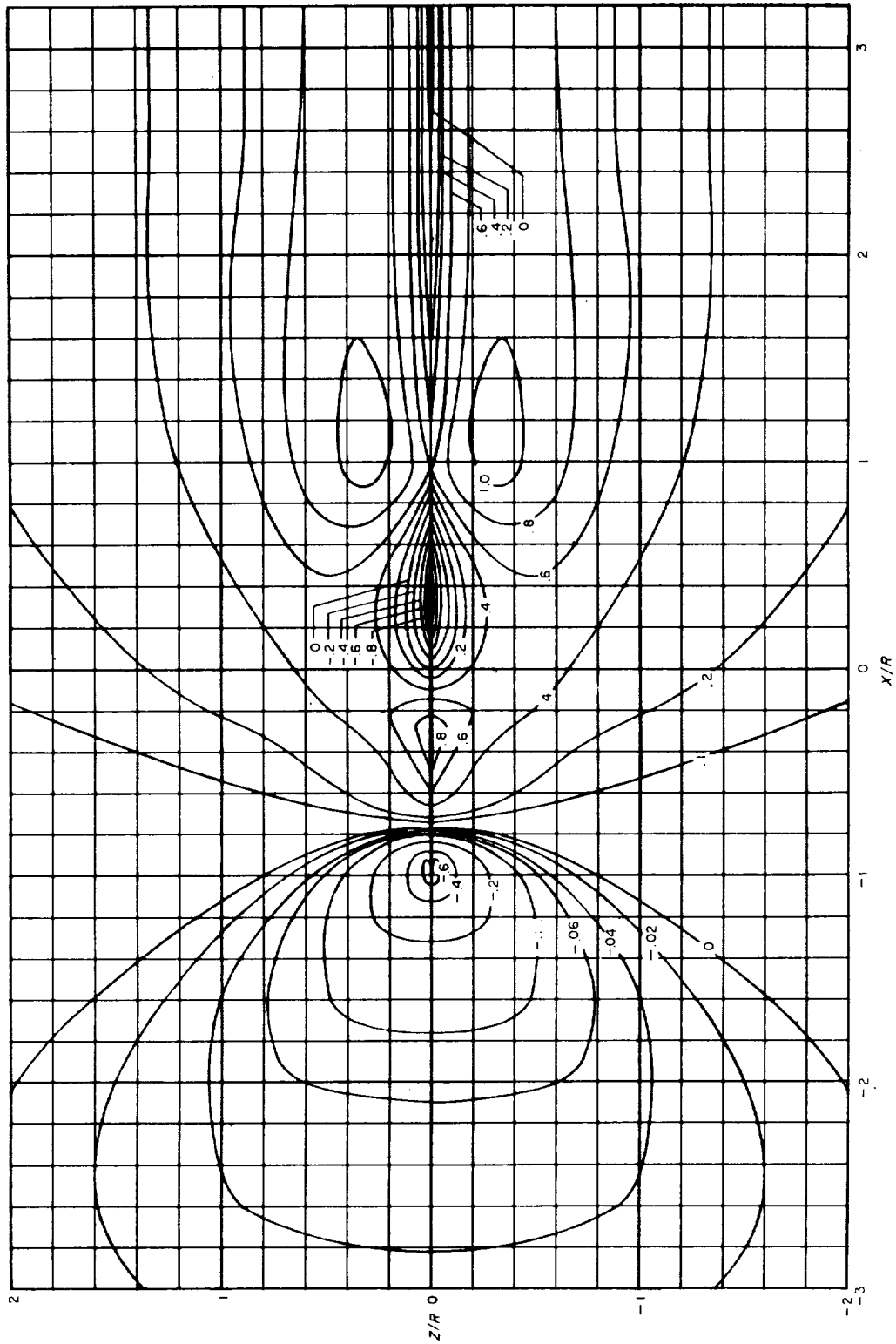

(c) Typical disk loading (from ref. 9).

Figure 16.- Concluded.

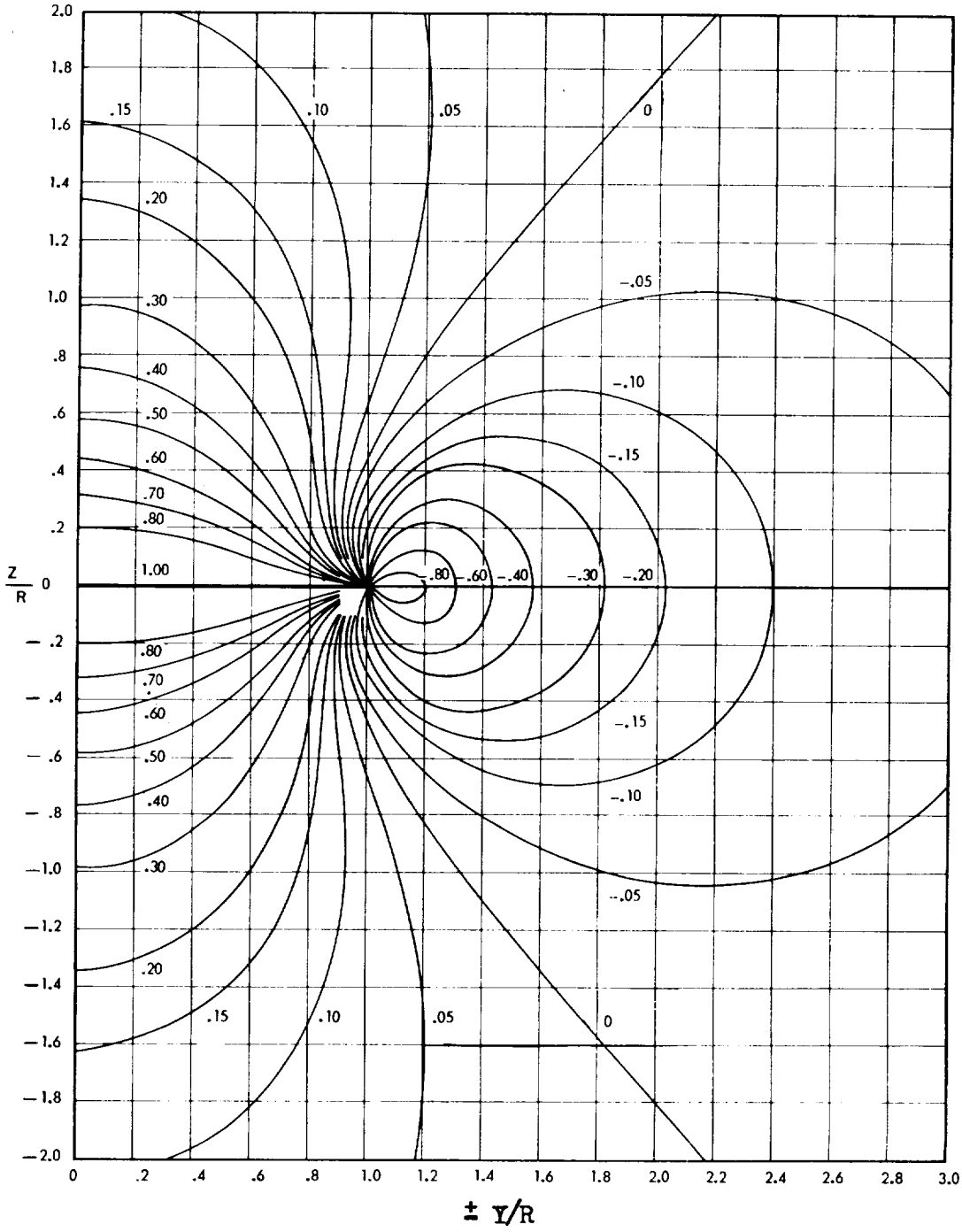

(a) Uniform disk loading (from ref. 6).

Figure 17.- Contours of induced-velocity ratio v/v_o in the lateral plane of the rotor for $\chi = \tan^{-1} \infty = 90.00^{\circ}$.

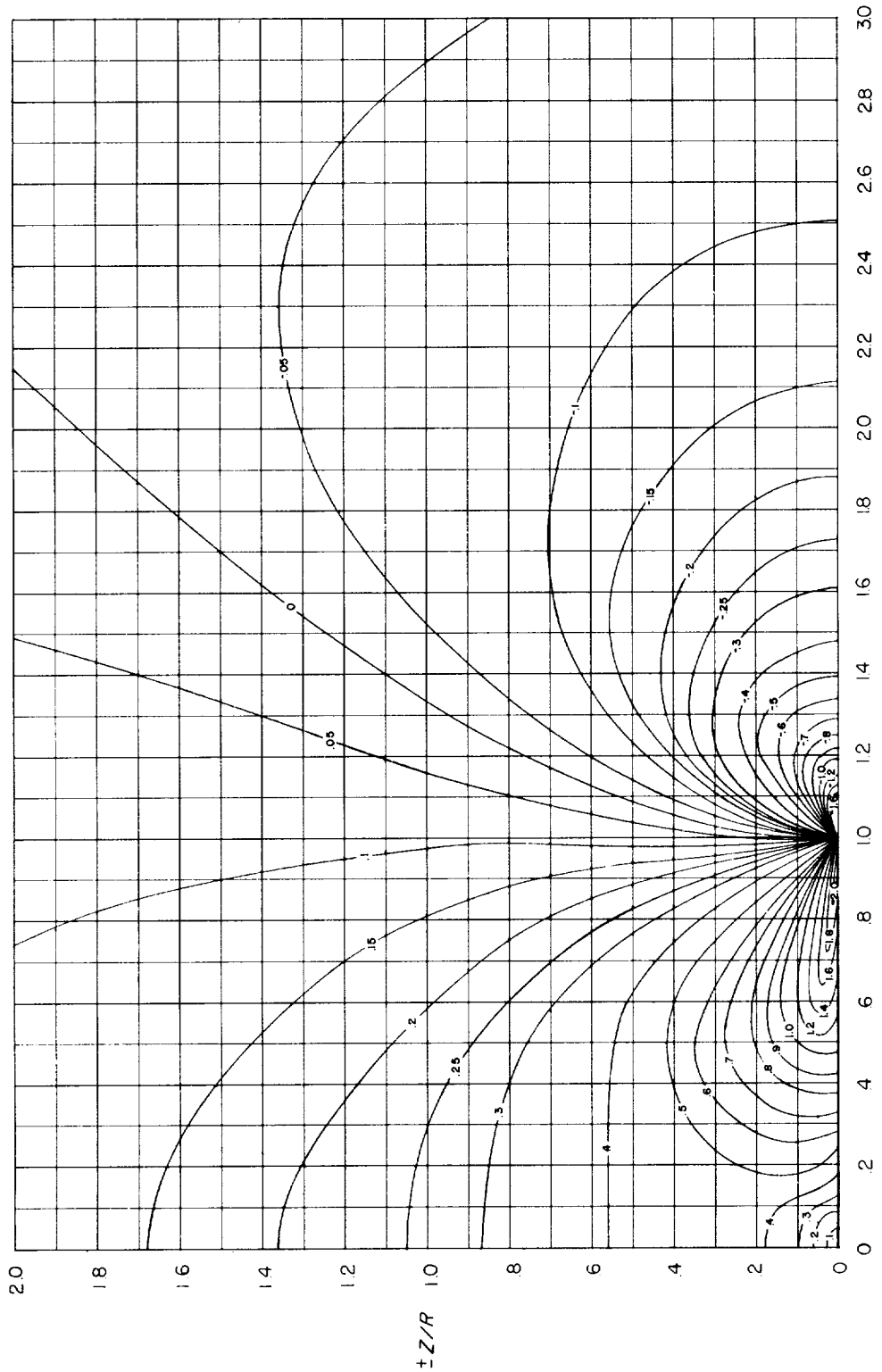

(b) Triangular disk loading.

Figure 17.- Continued.

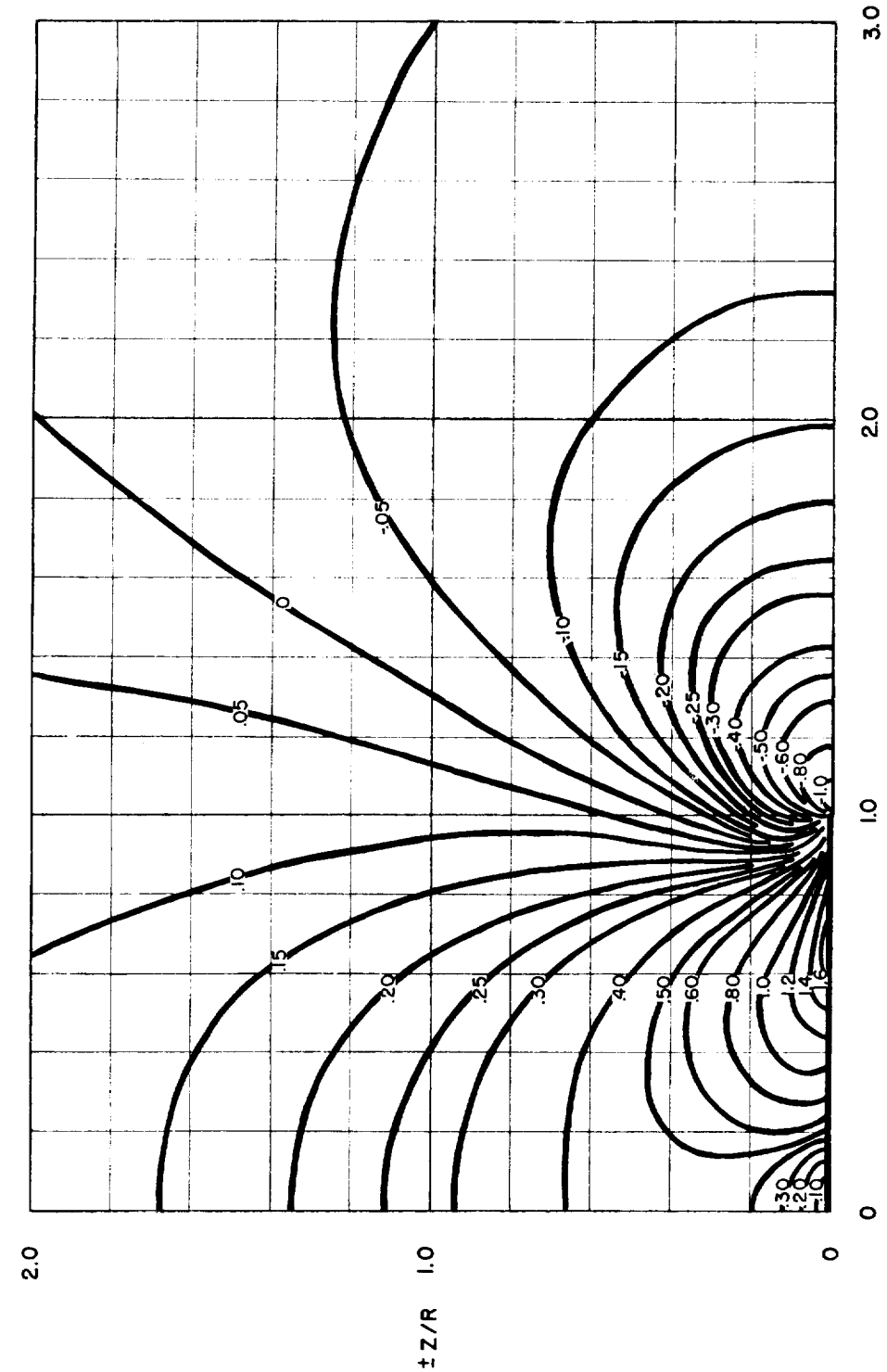

(c) Typical disk loading.

Figure 17.- Concluded.

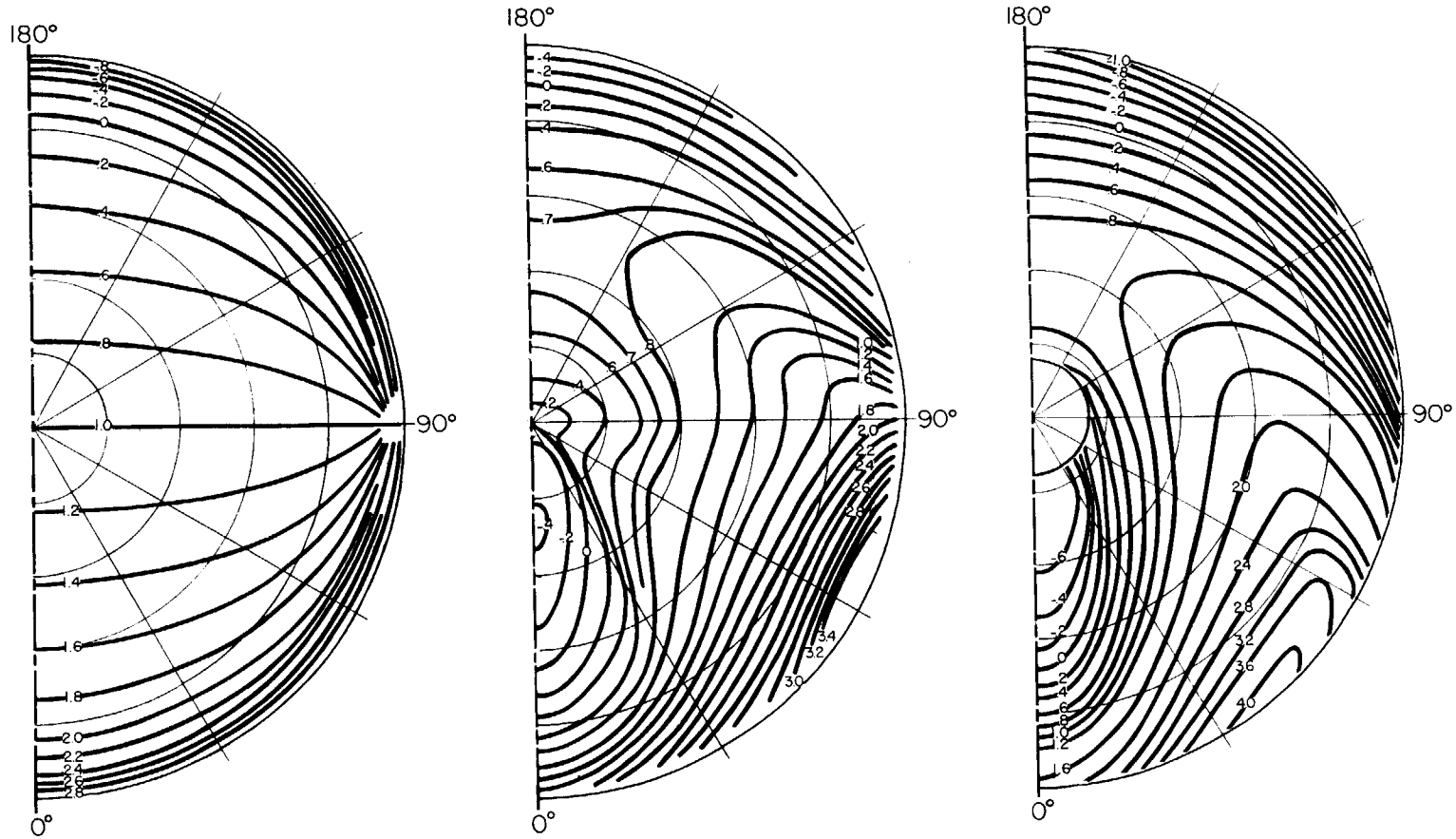

(a) Uniform disk loading. (b) Triangular disk loading. (c) Typical disk loading.

Figure 18.- Contours of induced-velocity ratio v/v_o in the plane of the rotor. $\chi = \tan^{-1} 10 = 84.29°$.

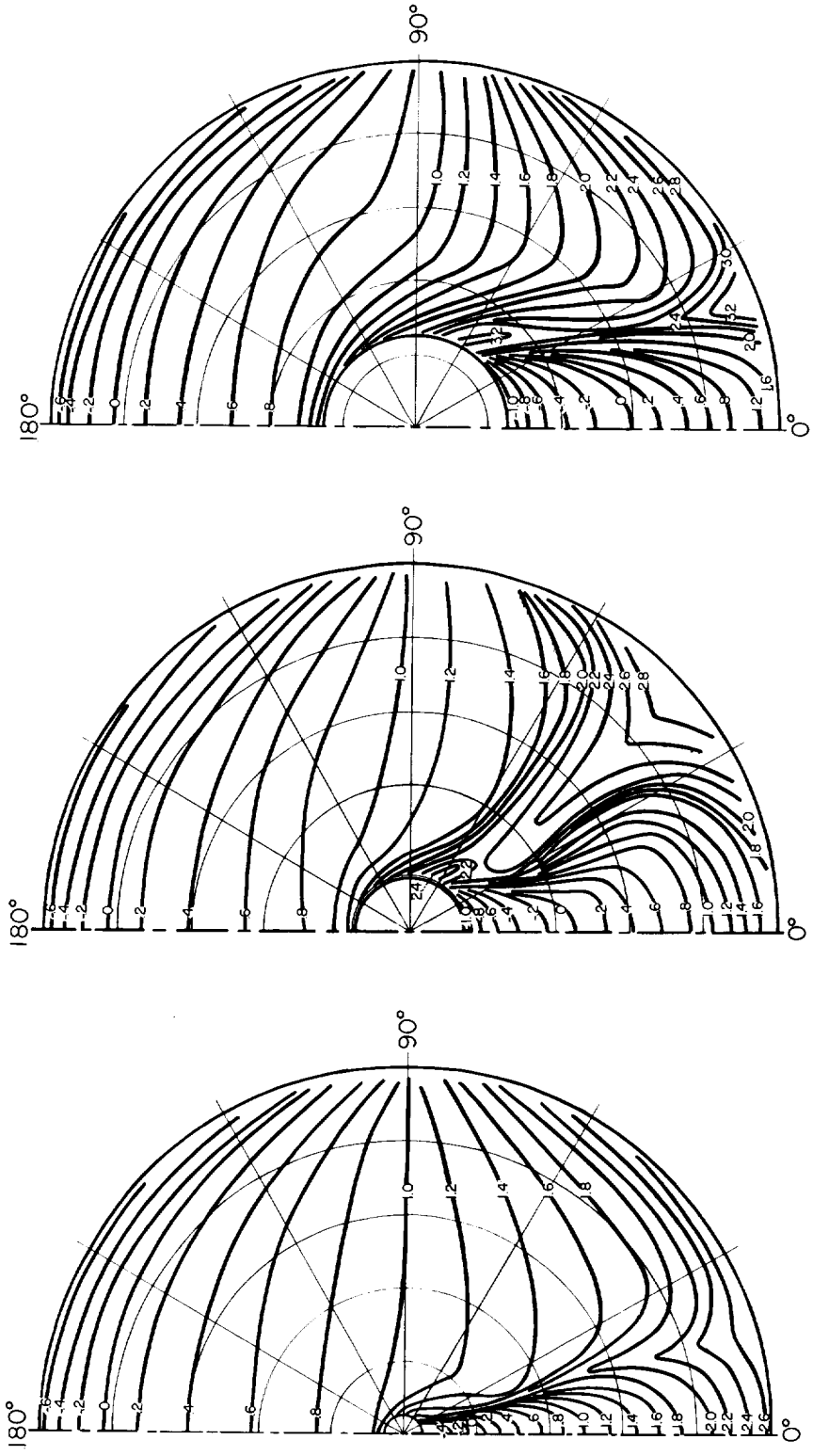

(d) Uniform disk loading with cutout of 5 percent R.

(e) Uniform disk loading with cutout of 15 percent R.

(f) Uniform disk loading with cutout of 25 percent R.

Figure 18.- Concluded.

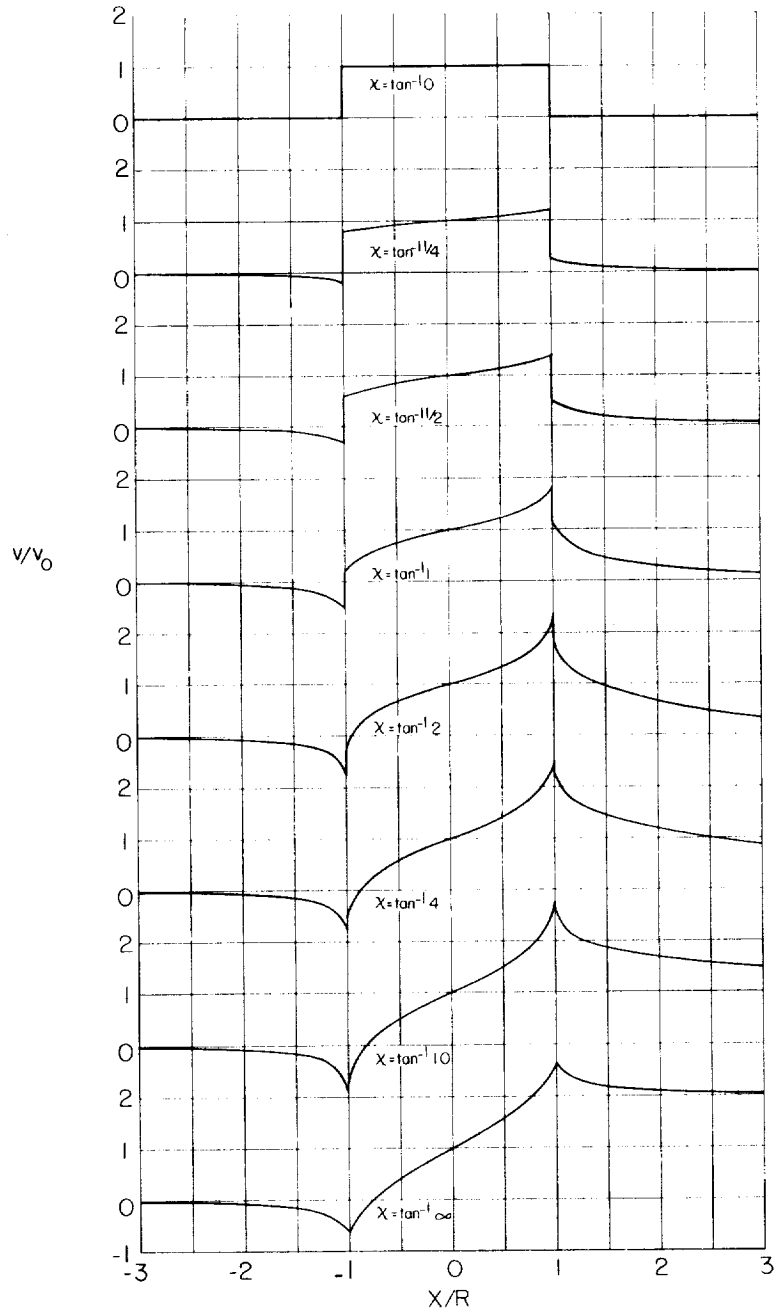

(a) Uniform disk loading (from refs. 5 and 7).

Figure 19.- Induced-velocity distribution along the longitudinal axis (X-axis) of the rotor.

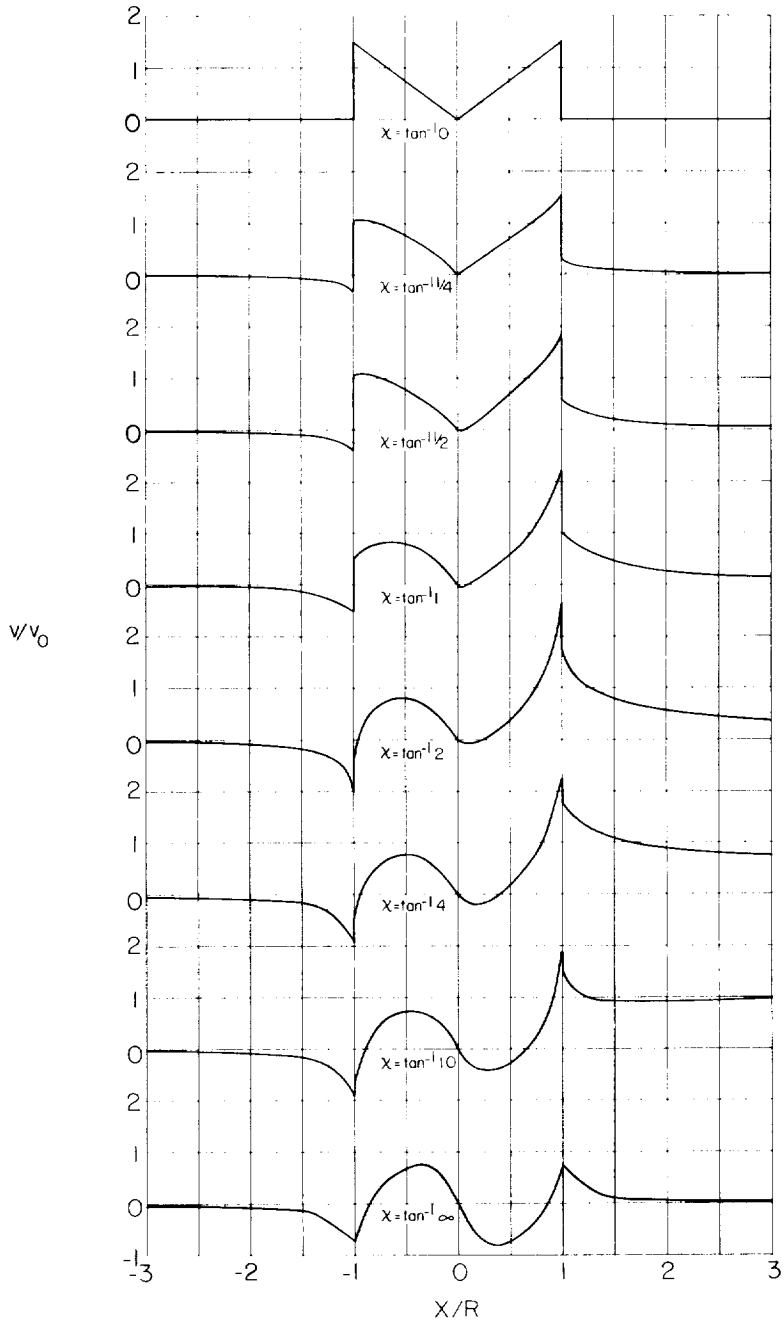

(b) Triangular disk loading (portions of this figure from ref. 9).

Figure 19.- Continued.

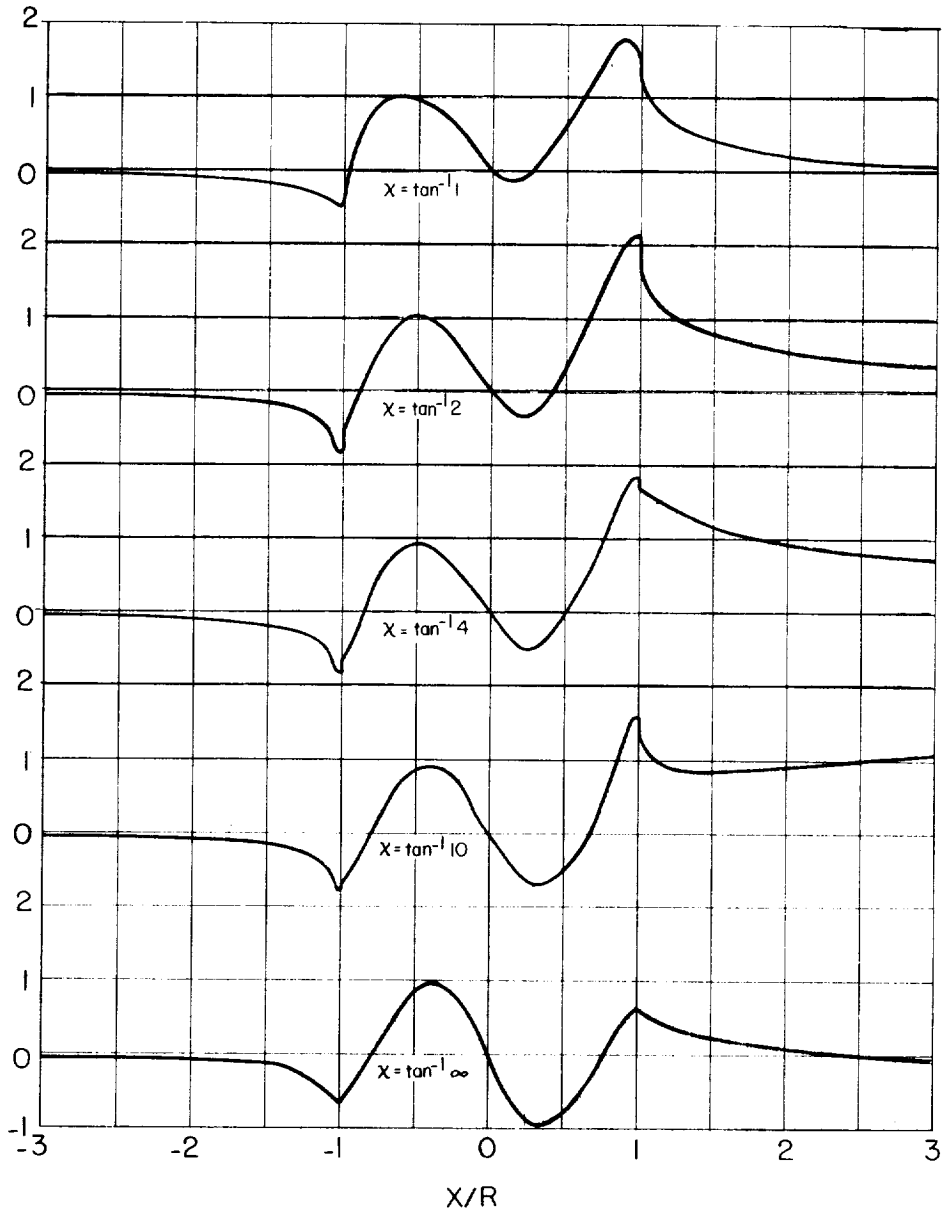

(c) Typical disk loading (portions of this figure from ref. 9).

Figure 19.- Concluded.

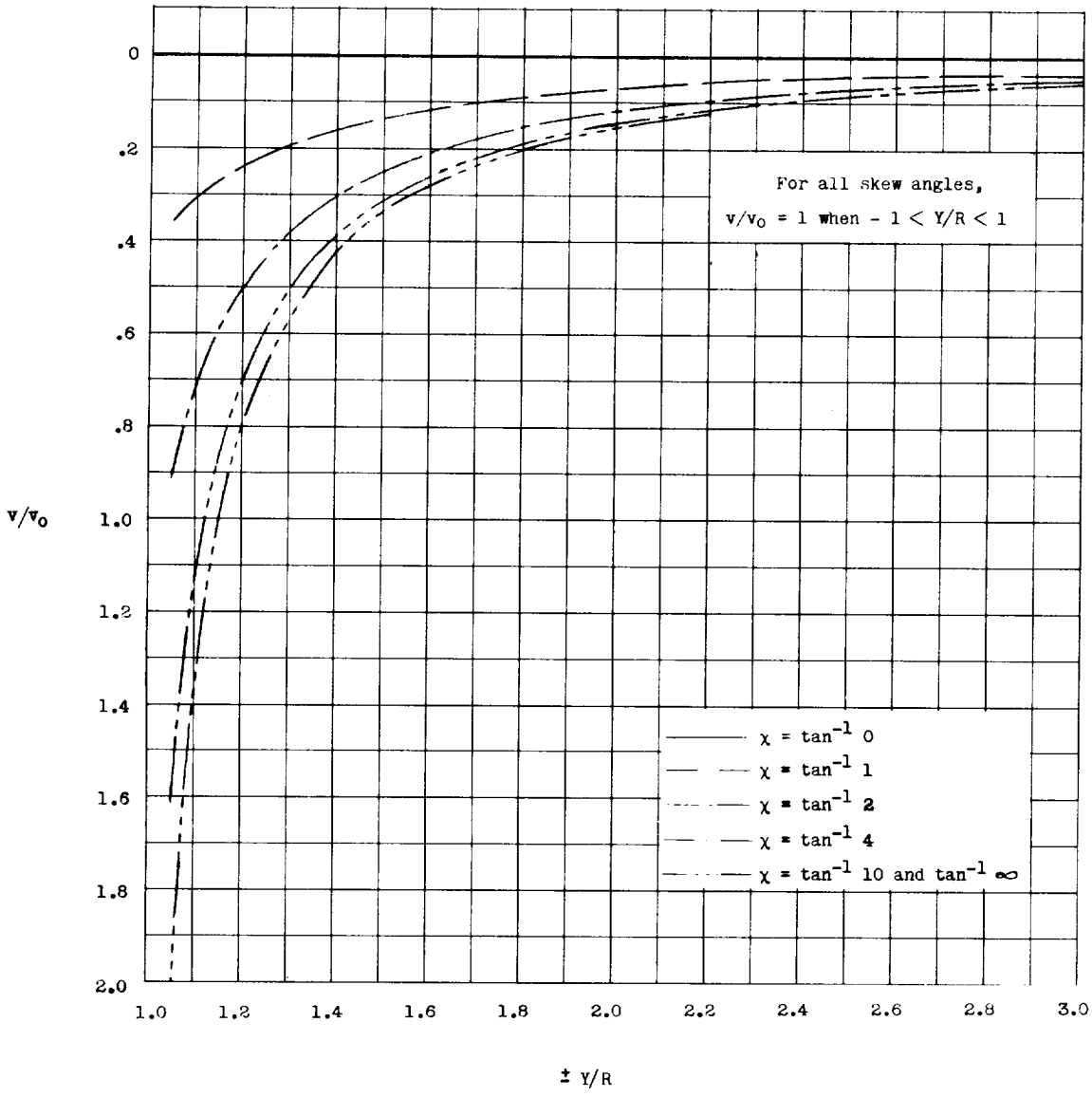

(a) Uniform disk loading (from ref. 6).

Figure 20.- Induced-velocity distribution along the lateral axis (Y-axis) of the rotor.

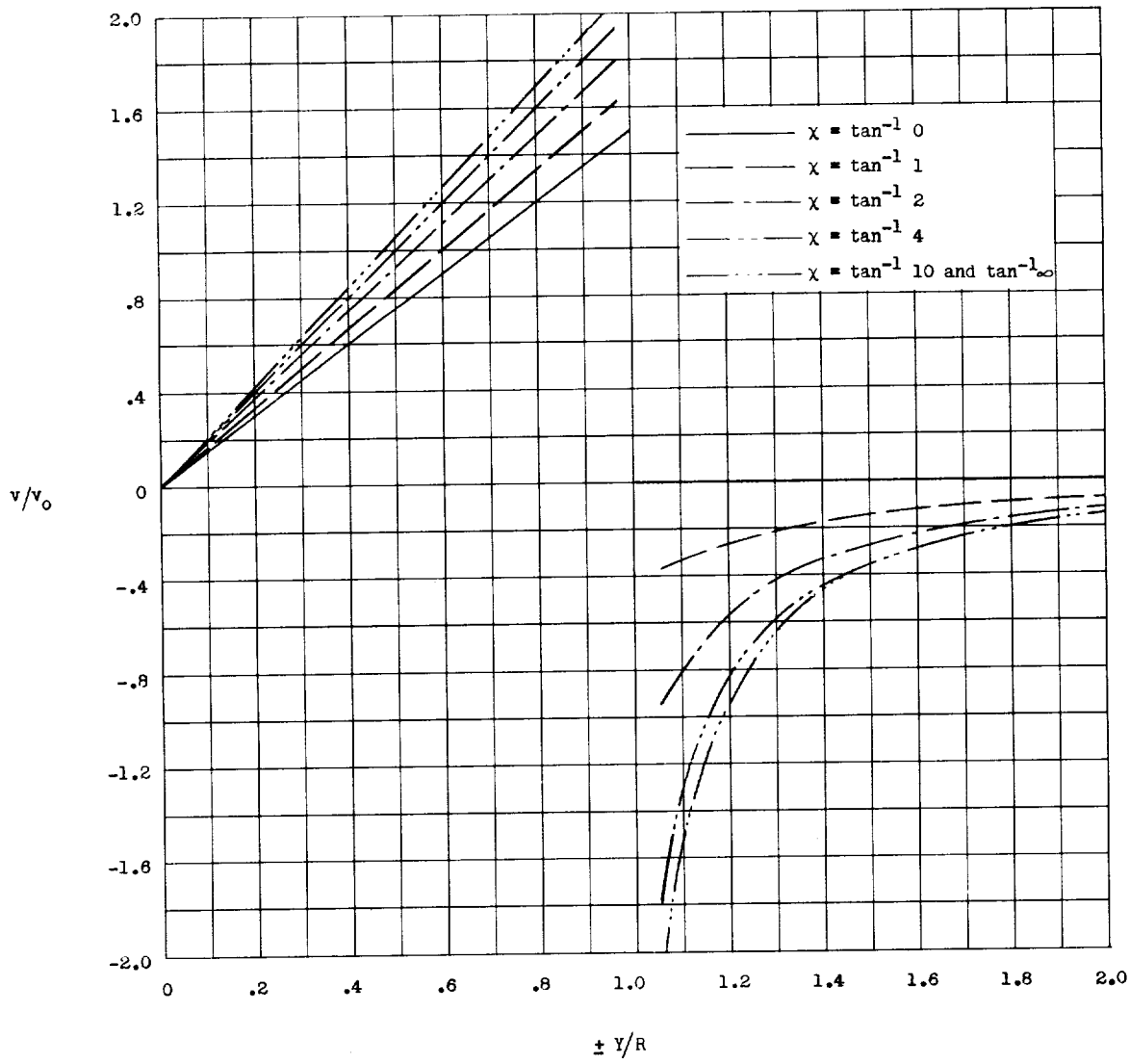

(b) Triangular disk loading (portions of this figure from ref. 9).

Figure 20.- Continued.

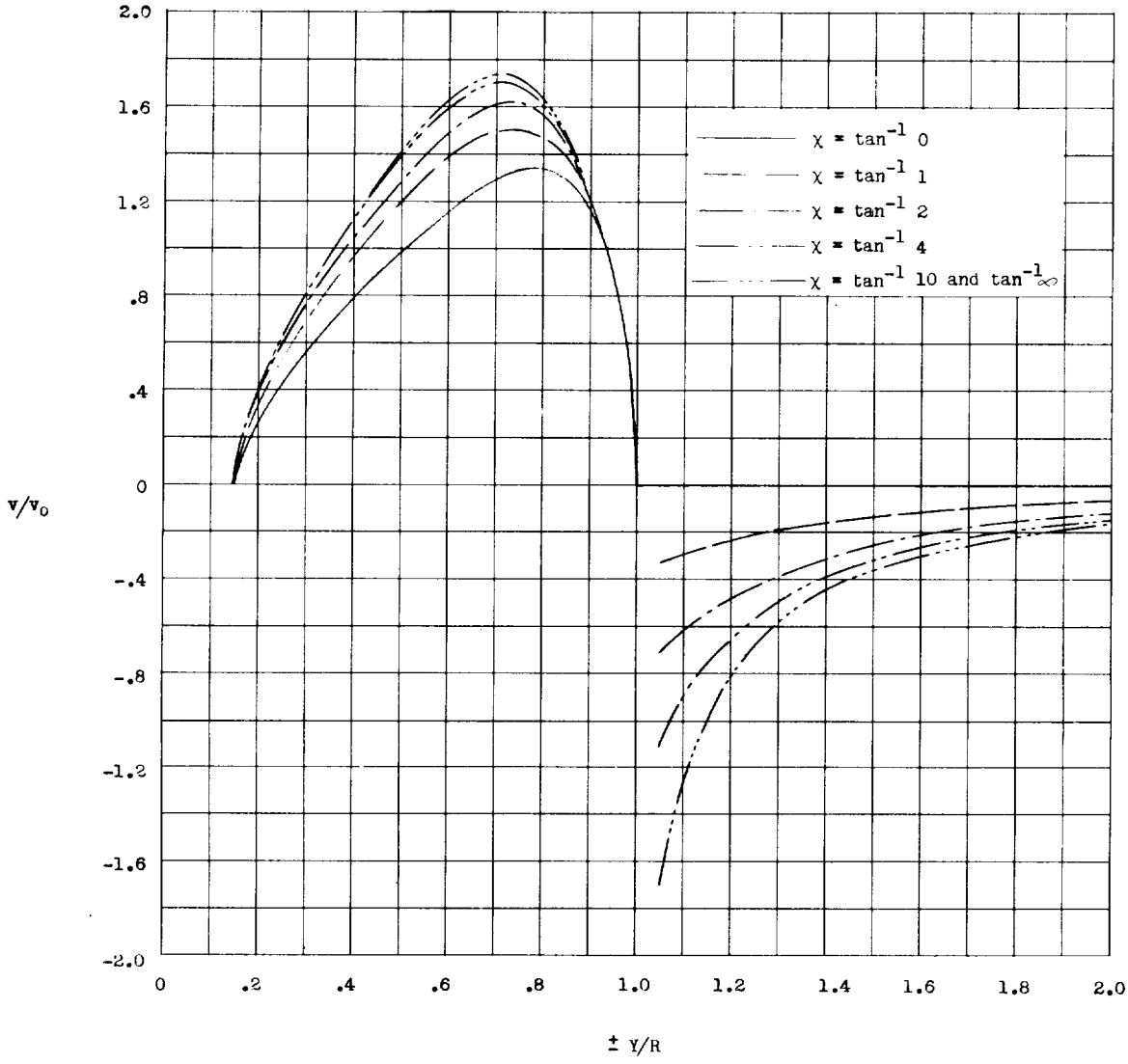

(c) Typical disk loading (portions of this figure from ref. 9).

Figure 20.- Concluded.

NASA MEMO 4-15-59L
National Aeronautics and Space Administration.
CHARTS OF THE INDUCED VELOCITIES NEAR A LIFTING ROTOR. Joseph W. Jewel, Jr., and Harry H. Heyson. May 1959. 63p. diagrs., tab. (NASA MEMORANDUM 4-15-59L)

This paper is a compilation of induced-velocity charts for both uniform and nonuniform loading. These charts should be applicable to several aerodynamic interference problems involving rotary-wing aircraft.

Copies obtainable from NASA, Washington

1. Slipstream - Propellers (1.5.4)
2. Wings, Rotating - Theory (1.6.1)
3. Rotating-Wing Aircraft (1.7.3)
4. Loads - Rotating Wings (4.1.1.4)
5. Vibration and Flutter - Rotating-Wing Aircraft (4.2.5)

I. Jewel, Joseph W., Jr.
II. Heyson, Harry H.
III. NASA MEMO 4-15-59L

NASA

NASA MEMO 4-15-59L
National Aeronautics and Space Administration.
CHARTS OF THE INDUCED VELOCITIES NEAR A LIFTING ROTOR. Joseph W. Jewel, Jr., and Harry H. Heyson. May 1959. 63p. diagrs., tab. (NASA MEMORANDUM 4-15-59L)

This paper is a compilation of induced-velocity charts for both uniform and nonuniform loading. These charts should be applicable to several aerodynamic interference problems involving rotary-wing aircraft.

Copies obtainable from NASA, Washington

1. Slipstream - Propellers (1.5.4)
2. Wings, Rotating - Theory (1.6.1)
3. Rotating-Wing Aircraft (1.7.3)
4. Loads - Rotating Wings (4.1.1.4)
5. Vibration and Flutter - Rotating-Wing Aircraft (4.2.5)

I. Jewel, Joseph W., Jr.
II. Heyson, Harry H.
III. NASA MEMO 4-15-59L

NASA

NASA MEMO 4-15-59L
National Aeronautics and Space Administration.
CHARTS OF THE INDUCED VELOCITIES NEAR A LIFTING ROTOR. Joseph W. Jewel, Jr., and Harry H. Heyson. May 1959. 63p. diagrs., tab. (NASA MEMORANDUM 4-15-59L)

This paper is a compilation of induced-velocity charts for both uniform and nonuniform loading. These charts should be applicable to several aerodynamic interference problems involving rotary-wing aircraft.

Copies obtainable from NASA, Washington

1. Slipstream - Propellers (1.5.4)
2. Wings, Rotating - Theory (1.6.1)
3. Rotating-Wing Aircraft (1.7.3)
4. Loads - Rotating Wings (4.1.1.4)
5. Vibration and Flutter - Rotating-Wing Aircraft (4.2.5)

I. Jewel, Joseph W., Jr.
II. Heyson, Harry H.
III. NASA MEMO 4-15-59L

NASA

NASA MEMO 4-15-59L
National Aeronautics and Space Administration.
CHARTS OF THE INDUCED VELOCITIES NEAR A LIFTING ROTOR. Joseph W. Jewel, Jr., and Harry H. Heyson. May 1959. 63p. diagrs., tab. (NASA MEMORANDUM 4-15-59L)

This paper is a compilation of induced-velocity charts for both uniform and nonuniform loading. These charts should be applicable to several aerodynamic interference problems involving rotary-wing aircraft.

Copies obtainable from NASA, Washington

1. Slipstream - Propellers (1.5.4)
2. Wings, Rotating - Theory (1.6.1)
3. Rotating-Wing Aircraft (1.7.3)
4. Loads - Rotating Wings (4.1.1.4)
5. Vibration and Flutter - Rotating-Wing Aircraft (4.2.5)

I. Jewel, Joseph W., Jr.
II. Heyson, Harry H.
III. NASA MEMO 4-15-59L

NASA